Green Chemistry

ROYAL SOCIETY OF CHEMISTRY

CRITICAL REVIEW

View Article Online
View Journal | View Issue

Cite this: *Green Chem.*, 2021, **23**, 9747

Direct and oxidative dehydrogenation of propane: from catalyst design to industrial application

James H. Carter,*[a] Takudzwa Bere,[a] Jack R. Pitchers,[a] Daniel G. Hewes,[a] Bart D. Vandegehuchte,[b] Christopher J. Kiely,[c] Stuart H. Taylor [a] and Graham J. Hutchings *[a]

The direct formation of propene from propane is a well-established commercial process, which on the basis of energy consumption, is environmentally preferred to the current large-scale sources of propene from steam cracking and fluid catalytic cracking. Propene is a major platform chemical with applications in the polymer and chemical industry and its place in modern society is guaranteed over the coming decades. At present, sources of propane are mostly non-renewable, but the development of technologies to produce renewable "green" propane are gaining traction, which coupled with new catalytic processes will provide the platform to produce green propene. In this critical review, we examine the significant advances made in the development of dehydrogenation catalysts, evaluating the technological and environmental merits. Currently, non-oxidative direct dehydrogenation (DDH) is the only commercialised process, and this is reflected in the high space–time yield commonly reported over the most active catalysts which are typically Pt or Cr based. However, the formation of coke over even the most selective catalysts necessitates multi-reactor cycling to facilitate regeneration. Oxidative dehydrogenation using O_2 (ODH-O_2) does not suffer from coke formation, but can lead to overoxidation, limiting the yield of propene. While no commercial processes have yet been developed, a promising new class of ODH-O_2 catalysts has emerged in recent years which use boron as the active component. These catalysts are amongst the most active and selective reported to date for this reaction. The use of CO_2 as a soft oxidant (ODH-CO_2) has also gained interest due to the environmental advantages of utilising CO_2. Although this is an attractive prospect with considerable potential, the propene yields reported over these catalysts are an order of magnitude lower than the most active DDH and ODH-O_2 catalysts. Despite significant advances in the past decade, current ODH-CO_2 catalysts remain far from displaying the activity levels necessary to be considered for commercial application. The specific requirements of catalyst design for each sub-reaction are discussed and we identify that, regardless of the method of dehydrogenation, the balance of acid and base sites on the catalyst surface is of paramount importance. Future catalyst design in DDH and ODH-O_2 should focus on improving selectivity to propene, while ODH-CO_2 catalysts are limited by their low intrinsic activity with respect to CO_2. The scarcity of some common catalytic elements is also discussed, with recommendations focusing on more abundant chemical elements. Future research should focus on the low temperature activation of CO_2 as a priority. With further research and development of lower energy routes to propene based on the dehydrogenation of green propane, it should be possible to transform the manufacturing landscape of this key chemical intermediate.

Received 7th October 2021,
Accepted 14th November 2021

DOI: 10.1039/d1gc03700e

rsc.li/greenchem

1. Introduction

1.1. The importance of propene in modern society

Propene is a major platform chemical with a myriad of uses in the manufacturing and chemical industry. The majority of propene is used to manufacture polypropene, a recyclable thermoplastic polymer which is second only to polyethene in the scale of production. Polypropene has favourable physical properties such as high chemical resistance and good elasticity, which makes it useful in a broad range of applications, includ-

[a]*Cardiff Catalysis Institute, Cardiff University, Main Building, Park Place, Cardiff, CF10 3AT, UK. E-mail: carterj5@cf.ac.uk, hutch@cf.ac.uk*
[b]*TotalEnergies One Tech Belgium, Seneffe B-7181, Belgium*
[c]*Department of Materials Science and Engineering, Lehigh University, Bethlehem, PA 18015, USA*

ing packaging, manufacturing and in construction materials. Propene is also the precursor to many other polymer-related chemicals, including propene oxide (used to make polyurethane), acrylic acid (used to make acrylic polymers) and acrylonitrile (used to make polypropenonitrile). Additionally, large scale chemicals such as isopropanol and cumene (used to manufacture phenol and acetone) are made from propene. Annual propene production was around 130 megatonnes in 2019[1] and is predicted to increase to 191 megatonnes by 2030. Significantly, the expected growth in propane demand cannot be met by existing processes, which are based on steam-cracking (SC) and fluid catalytic cracking (FCC). Instead, direct or on-purpose processes are being developed to fill the so-called '*propene gap*'. The focus of this critical review is on the dehydrogenation of propane.

Direct dehydrogenation can be performed either with or without an oxidant present, and O_2, CO_2 and N_2O can all participate as oxidants to form propene from propane. The discovery of active and selective catalysts is central to the development of these on-purpose technologies and is the focus of the current review. Research into propane dehydrogenation is an ever-growing field and to date there are several review articles available on direct dehydrogenation (DDH) (Sattler,[2] 2013), soft oxidation with CO_2 (ODH-CO_2) (Atanga,[3] 2018) and oxidative dehydrogenation (ODH-O_2) (Carrero,[4] 2014 and Shi,[5] 2018). Otroshchenko *et al.* recently reviewed the literature on metal oxide catalysts for each dehydrogenation reaction, including reaction-engineering and catalyst design, but omitted supported nanoparticle catalysts. To our knowledge there are no comprehensive literature reviews that compare and contrast non-oxidative and oxidative dehydrogenation reactions.

The scope of this article is to critically review the literature on DDH, ODH-CO_2 and ODH-O_2 to identify over-arching themes and common rules for catalyst design. We do not try to capture aspects of reaction design and engineering, which itself is a vibrant field of research. We attempt to compare the performance of catalysts in the different sub-reactions by calculating a space time yield (STY), (measured in $mol_{C_3H_6}$ kg_{cat}^{-1} h^{-1}), which is based on the initial activity of the catalysts. This enables a meaningful comparison between different research groups and reaction conditions. Additionally, we emphasise the environmental and industrial perspectives of each reaction and the prospects for industrial application.

1.2. Propene production processes – an environmental perspective

Traditionally, the industrial production of light alkenes, such as propene, has been carried out *via* either SC, or FCC of naphtha and diesel feedstocks. These methods typically provide a range of products including ethene, propene and gasoline, amongst others.[6] As of 2016, these routes accounted for 81% of propene production in industry, with 50% coming from SC and 31% from FCC. The remaining 19% was from newer technologies, such as direct dehydrogenation.[6]

SC, which involves the heating of fossil-fuels in the absence of oxygen to produce alkenes, requires temperatures up to 750–875 °C.[7] As an established process, naphtha SC has a high carbon efficiency, producing almost no CO_2 from the cracking process itself.[7] Although naphtha SC has an effective carbon efficiency, the process still relies on high temperatures for alkene production, which itself produces a significant amount of CO_2 from energy consumption.[7,8] These factors taken together result in steam cracking being responsible for the global emission of more than 300 million tonnes of CO_2 per year, as well as naphtha SC producing ozone-depleting CFCs.[7] FCC provides a way of producing light alkenes at lower temperatures compared to SC, by employing a catalyst into the process. However, despite its modestly lower operating temp-

James H. Carter

James H. Carter obtained his PhD under the supervision of Professors Graham Hutchings and Stan Golunski, and currently works as a Post-Doctoral Research Associate at Cardiff Catalysis Institute in the Hutchings group. His research focuses on the synthesis, characterisation and evaluation of novel heterogenous catalysts for wide-ranging applications, including carbon-free energy, environmental catalysis, sustainable manufacturing and selective oxidation. His research is centred on advancing the fundamental understanding of the chemistry and materials, and involves collaboration with universities and industry nationally and internationally.

Takudzwa Bere

Takudzwa Bere is a PhD candidate at Cardiff Catalysis Institute under the supervision of Professor Graham Hutchins and Professor Stuart Taylor. His primary research encompasses building fundamental structure–activity relationships through catalyst design and advanced characterisation with a focus on the design, synthesis and functionalization of novel amorphous catalytic materials, synthesised using the supercritical antisolvent (SAS) precipitation method. Target reactions include non-oxidative propane dehydrogenation reaction and alcohol dehydration for alternative fuels.

Table 1 Summary of various propene production processes from a green chemistry perspective

Feedstock	Processes	Atom economy	Toxic reactants	Renewability of feedstock	GWP (kg CO_2 per kg C_3H_6)[a]	Resource scarcity (USD per kg C_3H_6)[a]	Human health (DALY per kg C_3H_6)[a]	Ecosystem (species year per kg C_3H_6)[a]
Naphtha	SC	Low	Crude oil/ naptha streams	Non-renewable	1.8	0.61	0.25	0.05
Coal	*Syn* gas, methanol synthesis, MTO	Low	Methanol	Non-renewable	16.5	0.60	4.0	1.1
Natural gas	*Syn* gas, methanol synthesis, MTO	Low	Methanol	Mostly non-renewable	4.5	1.10	0.8	0.2
Propane	DH	High	None	Mostly non-renewable	2.5	0.55	0.4	0.1

SC = steam cracking, GWP = global warming potential, DALY = disability-adjusted life years, MTO = methanol to olefins. [a] Values from ref. 11.

eratures, the FCC process produces many by-products. Many reduced S and N species are formed, as well as significant CO and HCN, which start forming at as low as 450 °C. Partial burn FCC reactors, (*i.e.*, reactors which form CO, rather than CO_2) will incorporate a CO burner downstream.[9] Feedstocks involved in FCC processes typically include high molecular weight hydrocarbons, breaking them down into more valuable light alkenes; however, it often struggles to process lighter feedstocks such as naphtha.[9] Both processes are designed to produce a wide array of products, as well as often generating by-products that require additional energy to process. In addition, while propene demand is increasing, processing plants are tending towards higher ethene production due to shale gas production, leading towards a global shortage of propene.[6,10] Overall, cracking of naptha and other petrochemical feedstocks to produce propene is unsustainable and leads to significant CO_2 emissions. Alternative indirect routes to propene, from *syn* gas and *via* methanol, has also gained interest in recent years.[7] The feedstock for this process can be biomass, shale gas or coal. Using coal as a feedstock has gained widespread use in China but poses a huge environmental burden.

The environmental and economic aspects of different existing propene production technologies are important considerations when reviewing the feasibility of newer technologies based on dehydrogenation. Green chemistry principles, such as atom economy, the use of toxic chemicals and the renewability of the feedstock, are especially relevant. This is summarised in Table 1, which compares steam cracking, MTO (from coal and natural gas) and dehydrogenation. Atom economy is a measurement of the percentage of atomic mass in the starting reagents that ends up in the final product. It serves as a useful indicator of how chemically efficient a process *could* be. It is important to remember that in practice, the real atom economy is determined by the selectivity of the catalyst, and the prevalence of side-reactions. Although it is not possible to precisely calculate the atom economy of SC or MTO due to the complexity of the process and uncertainty in the composition of the feedstock, it is apparent that both of these technologies are inferior to dehydrogenation. In the case of SC a wide range of chemicals are made, and while these are ultimately utilised in the production of other chemicals, the % of propene formed from such a process is low. Equally, in the MTO process from coal or natural gas, the atom economy is limited by the generation of H_2O as a by-product. In contrast, in the case of dehydrogenation only H_2 is generated as a by-product, meaning an atom economy of 95% is possible. With respect to the toxicity of the chemicals,

Jack R. Pitchers

Jack Pitchers is a PhD candidate at the Cardiff Catalysis institute, based at Cardiff university, under the supervision of Dr Graham Hutchings and Dr Stuart Taylor. Jack acquired a MSci in natural sciences at Lancaster university in 2018 and subsequently acquired a MRes as part of the catalysis CDT programme at Cardiff University. His primary interests are focused on the design, synthesis, and characterisation of novel metal oxide catalysts for selective oxidation.

Daniel G. Hewes

Daniel Hewes is a postgraduate PhD student at Cardiff Catalysis institute under the supervision of Professor Graham Hutchings and Professor Chris Kiely. His primary research focuses on the advanced characterisation techniques relating to Electron Microscopy and X-ray Absorption Spectroscopy, and how these techniques apply to the structure–activity relationships of novel catalytic materials.

SC forms various carcinogenic compounds, and the toxicity of methanol is well-established. In contrast, propane is non-hazardous. At present each of the feedstocks used in the main methods of propene production tend to be non-renewable. In the case of SC and coal-based MTO, this is unavoidable due to the nature of the feedstock. However, natural gas and propane can be produced from biomass. In these cases, the feedstock is renewable and so these processes are potentially much more sustainable than when using fossil fuels. Rodríguez-Vallejo *et al.* carried out life cycle analyses of naphtha cracking, propane dehydrogenation and MTO (using coal or natural gas as feedstocks).[11] In this analysis, the global warming potential (GWP), resource scarcity, impact on human health and the impact on the ecosystem was considered and quantified as a cost per kg of C_3H_6 produced. These data are shown in Table 1. In terms of the global warming potential of each process, the MTO based reactions are clearly worse than the naphtha cracking or direct dehydrogenation reactions, but the CO_2 emissions of the coal-based feedstock is almost an order of magnitude higher than naphtha cracking. A similar trend was observed in the ecosystem category. This was measured in terms of local species lost integrated over time and underlines the gross negative impact of utilising coal as a feedstock in this chemistry. Resource scarcity was calculated based on the monetary burden of future mineral and fossil fuel extraction and shows that natural gas has around double the cost of that associated with propane, coal and naphtha. Finally, the cost to human health was estimated in terms of disability-adjusted life years, and naphtha cracking and propane dehydrogenation came out favourably compared to the MTO processes. Based on these metrics, it is clear that MTO from coal or natural gas has a larger environmental burden than SC or dehydrogenation. Opportunities for improving the sustainability of the dehydrogenation process were recently highlighted by Agarwal *et al.* who investigated various intensification and integration strategies. It was shown that such strategies, which involved additional waste heat recovery and off-gas recycling, up to 70% reductions in CO_2 emissions were possible.[12]

The increased interest in direct propane dehydrogenation has been enhanced by the fall in propane price, which is the direct result of the discovery of vast shale gas reserves in North America. Although propane is a minor component in shale gas, it is facile to separate and therefore represents a valuable, but non-renewable source of propane. Increasing public pressure to move away from such non-renewable feedstocks continues to gain momentum and the propane production industry has responded accordingly. The production of renewable 'green' propane (also called bio-propane and bioLPG) is an emerging sector which is already being operated on a large scale. TotalEnergies operates a bio-refinery in La Mede, which has a design capacity for bio-propane of 25 000 tonnes per year.[13] Additionally, Neste recently opened a renewable propane production plant, which will produce 40 000 tonnes per year.[14] The propane generated is then sold on to be used in direct propane dehydrogenation.[15] While this is an important start, it represents less than 1% of annual propane capacity. Bio-propane can be produced from the processing of biomass, notably as a side-product in the production of biodiesel[16] as well as glycerol[17] and other substrates.[18] With increasing pressure to source chemical feedstocks sustainably, we can expect that new interest will focus on renewable and green routes to the key platform chemicals currently required by modern society, and that green propane will play an important role in this.

Overall, direct propane dehydrogenation satisfies many principles of green chemistry in comparison to SC and MTO benchmarks: it is highly atom-economic, does not use toxic

Bart D. Vandegehuchte

Bart Vandegehuchte (Ghent, Belgium, 1985) obtained his Master degree in Chemical Engineering at Ghent University in 2008. In 2014 at the same university, he obtained his PhD at the Laboratory of Chemical Technology with Prof. Joris W. Thybaut in microkinetic modeling and hydrocracking. In 2015, he joined Total Refining & Chemicals as a research engineer in the Catalysis Refining & Base Chemicals department. His initial focus was on bottom-of-the-barrel conversion and selective hydrogenation of acetylenics. Nowadays, his main research has shifted to oxidative coupling of methane, life cycle analysis, and metal-based nanocatalysis for conventional and emerging technologies.

Christopher J. Kiely

Christopher Kiely is the Harold B. Chambers Senior Professor of Materials Science and Engineering at Lehigh University, USA. He received his B.Sc and Ph.D degrees from Bristol University, UK. His research involves the development and application of analytical electron microscopy techniques for the study of nanoscale features in catalyst and other particulate materials.

reactants (or generate toxic by-products) and can in principle, utilise renewable feedstocks. However, in practice dehydrogenation will only be desirable as a means of producing propene if the reaction can operate efficiently, with minimal side-products and maximum yield. These factors are governed by the choice of catalyst, the main focus of the current review. The development of an active, selective and stable catalyst is essential for dehydrogenation to be considered as a viable process in the near- and long-term future.

2. Thermodynamics and environmental aspects of different dehydrogenation processes

Each dehydrogenation reaction has different thermodynamic, environmental and economic aspects, which are important to recognise when designing catalysts and sustainable processes. In section 1.2, the environmental implications of cracking and MTO were discussed and compared with DDH. The majority of analyses focus on well-established processes, where more information and data are available, but no such analyses were found for oxidative dehydrogenation. As a result, the environmental impact of these novel reactions can only be speculated upon. The following section focuses on the thermodynamic and environmental aspects of each sub-reaction, drawing on available literature whenever possible, and when not possible suggesting the most important aspects that could affect the sustainability of each process.

2.1 DDH

DDH is an endothermic reaction ($\Delta H^{\circ}_{298} = 124\,\mathrm{kJ\,mol^{-1}}$), which is equilibrium-limited at higher partial pressures of propane and lower reaction temperatures. As a result, typical reaction temperatures for industrial DDH processes are 550–750 °C. Another key challenge in catalyst design for DDH is the fact that coke is also a favoured product under the conditions required for high propene yield and its formation is assumed to be initiated by deep dehydrogenation. Fig. 1 illustrates the typical reaction pathways observed in DDH. Catalytic and thermal (gas-phase radical) cracking reactions lead to the formation of methane and ethene. Ethene can then hydrogenate to ethane. The hydrogenolysis of propane is also possible, which forms methane and ethane.

As described above, the atom economy for DDH is high (95%) and the only by-product (in theory) is molecular hydrogen, which is a valuable resource with many uses and applications, not least as a carbon-free fuel. In practice however, frequent regeneration steps are required to remove coke, which involves combustion to form carbon dioxide. This means that the environmental impact of this process will depend to some extent on the prevalence of coke formation on the catalyst surface. As a feedstock, C_3H_8 is non-toxic, unlike methanol in the MTO process. The high flammability of C_3H_8 may present a safety risk in a chemical plant, but such a risk is present in all forms of C_3H_6 production.

2.2 ODH-O_2

ODH-O_2 is exothermic ($\Delta H^{\circ}_{298} = -117\,\mathrm{kJ\,mol^{-1}}$) and conversion is not limited by thermodynamic equilibrium. Additionally, the formation of coke is suppressed substantially, with overoxidation constituting the main competing pathway. Fig. 2 shows the typical reaction pathways that occur over ODH-O_2 catalysts. Overoxidation is the main drawback, with CO and particularly CO_2 reported as by-products. Cracking products are also reported, but generally as minor products. In common with ODH-CO_2, water is formed *via* oxidative dehydrogenation. CO_2 can also be formed *via* direct combustion of C_3H_8.[19]

Stuart H. Taylor

Stuart Taylor completed his PhD at the University of Liverpool in 1994, and then took up an academic position at Cardiff University School of Chemistry in 1997. Promoted to Professor in 2013, currently he is the Director of Research for the School and has more than 29 years of experience in heterogeneous catalysis research, publishing over 320 papers and patents. He has wide-ranging expertise in experimental studies of fundamental catalysis, which impacts fuels, sustainability, energy and the environment. His research receives support from a wide range of funding bodies and industry and collaborates extensively with universities and industry alike.

Graham J. Hutchings

Graham Hutchings is Regius Professor of Chemistry at Cardiff University. His early career was in industry with ICI and AECI Ltd where he became interested in gold catalysis. In 1984 he moved to academia and has held chairs at the Universities of Witwatersrand, Liverpool and Cardiff. He has published over 900 papers and patents. He was elected a Fellow of the Royal Society in 2009 and was awarded the Davy Medal in 2013, the ENI Award for Advanced Environmental Solutions in 2017, the RSC Faraday Lectureship and Prize in 2018, a CBE in the Queen's Birthday Honours List in 2018 and the Michel Boudart Award in 2021.

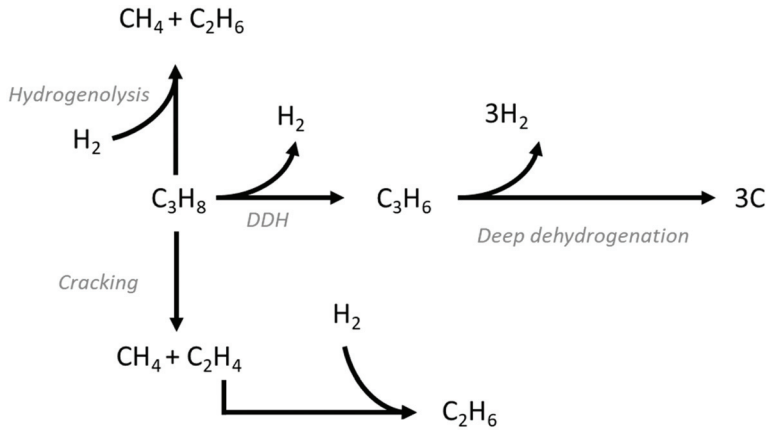

Fig. 1 Reaction pathways commonly observed during the DDH of propane. In addition to DDH, unfavourable deep dehydrogenation to coke, hydrogenolysis and cracking are also observed.

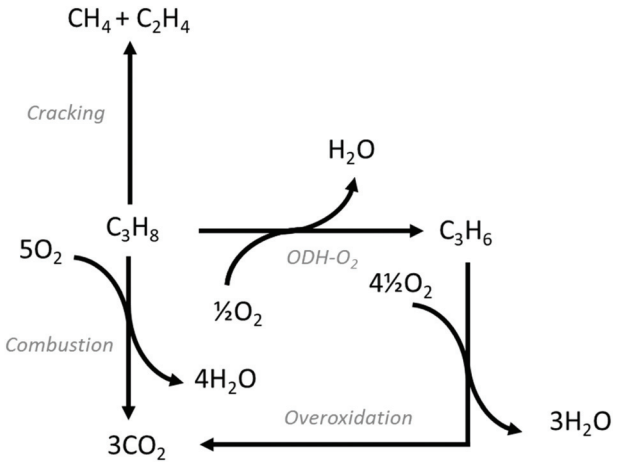

Fig. 2 Reaction pathways commonly observed in ODH-O_2 reactions. In addition to ODH-O_2, overoxidation, combustion and cracking are often observed.

The addition of O_2 enables lower operating temperatures to be utilised (typically 450–550 °C) and is exothermic, meaning the energy costs of sustaining the reaction temperature are less than those in DDH and ODH-CO_2. However, the atom economy of ODH-O_2 is 70% and H_2O is generated as a by-product rather than H_2. While CO_2 may be generated as a by-product, this depends on the catalyst, and the overall CO_2 generated may be comparable to a DDH process. There will be increased energy consumption associated with supplying the oxidant in sufficient purity and volume. If air is used, downstream separation of N_2 will be necessary, which would increase process energy consumption. The reactants and products are non-toxic, but the use of O_2 and C_3H_8 introduce an elevated safety risk. Although an in-depth environmental analysis of an ODH-O_2 process for C_3H_8 has not yet been carried out, it may be concluded that ODH-O_2 is comparable, if not more environmentally-friendly than DDH due to the lower expected costs associated with maintaining the reaction temperature. However, the performance and composition of the catalyst will be a crucial factor in this comparison. The economic aspects of ODH-O_2 have not been analysed for C_3H_6 production. However, the oxidative dehydrogenation of C_2H_6 has been investigated extensively, and such an analysis is available. Gaffney and Mason compared ODH-O_2 of C_2H_6 with thermal cracking and showed that ODH-O_2 has the potential to significantly reduce the plant capital costs and the overall cost of production.[20] Given the similarities in the cracking and dehydrogenation of ethane and propane, it is reasonable to conclude that the economic factors associated with the ODH-O_2 of C_3H_8 are also favourable compared with steam cracking.

2.3 ODH-CO_2

ODH-CO_2 is even more endothermic than DDH ($\Delta H^{\circ}_{298} = 164\ \mathrm{kJ\ mol^{-1}}$), due to the contribution of the mildly endothermic reverse water–gas shift (RWGS) reaction (Fig. 3). While it seems as though the addition of CO_2 would be detrimental on this basis, the removal of hydrogen *via* the RWGS reaction favourably shifts the thermodynamic equilibrium to enable higher propene yields. Hence, ODH-CO_2 can be carried out at lower reaction temperatures than DDH (450–600 °C). Although the reaction can proceed *via* a one-step oxidative dehydrogenation pathway or a two-step DDH + RWGS reaction, the net reaction is the same. A key competing reaction pathway in ODH-CO_2 is dry reforming of propane (DRP) (Fig. 3), which can occur under the same conditions as ODH-CO_2.[21] In addition to DRP, CO_2 can react with coke to generate CO *via* the reverse Boudouard reaction, which is reported to proceed under typical reaction conditions for ODH-CO_2 (500–600 °C). Zangeneh *et al.*[22] carried out a full thermodynamic analysis of the ODH-CO_2 reaction, considering coke-forming and dry reforming side-reactions. The inclusion of these reactions in the thermodynamic model strongly impacted the equilibrium product of propene, increasing the equilibrium conversion of propane at the expense of propene selectivity. Dry reforming of propane was favoured at higher temperatures, while coke-formation was favoured at lower temperatures and at lower

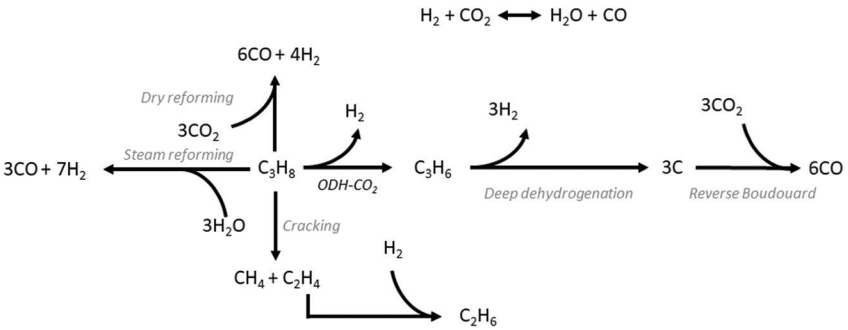

Fig. 3 Reaction pathways commonly observed in ODH-CO_2 reaction. In addition to ODH-CO_2, deep dehydrogenation, cracking and in some catalysts dry reforming are observed. The reverse Boudouard reaction is also frequently reported to occur under typical reaction conditions.

CO_2 : C_3H_8 ratios. It was also pointed out that the reported experimental data showed conversions well below equilibrium values, suggesting rapid catalyst deactivation. This analysis highlighted the need for kinetic control of dry reforming and coke forming reactions in order to maximise propene yield. Instead of hydrogen, water is formed either as the primary oxidative dehydrogenation product or as a result of DDH followed by the RWGS reaction.

From an environmental perspective, ODH-CO_2 has the greatest potential in the context of a circular economy. Although the formation of water is less desirable than hydrogen, ODH-CO_2 has the benefit of consuming CO_2 in the process, and this is often cited as the motivation for investigating this route. Chemical CO_2 utilisation is an attractive prospect in the context of combatting climate change: if CO_2 can be consumed in large scale processes, the overall carbon footprint of certain products/technologies could be significantly reduced. However, it is important to consider how CO, which is formed from ODH-CO_2, could be used in a sustainable way to justify the apparent greenness of ODH-CO_2. If the CO is used in the water–gas shift (WGS) reaction for hydrogen production, then CO_2 is immediately formed as a result, and the process becomes carbon neutral. Equally, if CO is combined with H_2 to be used in various *syn*-gas processes, *e.g.* methanol or Fischer–Tropsch synthesis, then it is likely that the carbon will be burned as a fuel and ultimately returned to CO_2. While this may not be considered to be as desirable as sequestering CO_2 from the atmosphere, the utilisation of CO_2 in this technology would form part of a 'renewable carbon' cycle, and avoids additional CO_2 emissions. This concept of carbon avoidance forms an important part of the short and medium term strategies to curb CO_2 emissions, and carbon capture and storage technologies are a fundamental aspect of this.[23] The source of CO_2 is also an important consideration. CO_2 may be sequestered from the environment at additional process costs, or may be recovered from other CO_2 forming processes. In comparison to other dehydrogenation reactions, ODH-CO_2 has the lowest atom economy (48%), but compared to cracking processes, where C_3H_6 is a minor product, this is respectable. The overall efficiency of the reaction will also depend on the catalyst, and if the above undesirable pathways can be sufficiently minimised.

Overall, each dehydrogenation reaction has unique operating conditions and challenges, which are dictated by their thermodynamics. In the case of DDH, the formation of coke remains the biggest challenge, as it is thermodynamically favoured under conditions that enable high propane conversion. In ODH-CO_2, dry reforming is also a competing pathway under typical reaction conditions and in the case of ODH-O_2, overoxidation is prevalent due to CO_2 being the thermodynamically favoured product. The thermodynamic tendency to form undesirable by-products means that such reactions must be carefully kinetically controlled. Careful catalyst design can inhibit and even switch-off some of these side-reactions, as will be discussed in the subsequent sections.

3. Commercial processes

The commercial dehydrogenation of propane is exclusively carried out in the absence of an oxidant. There are several technologies that currently operate, using various catalysts based on Pt or Cr, as shown in Table 2.

The Oleflex process from UOP employs alkali metal-promoted Pt–Sn/Al_2O_3 catalysts in a reaction system composed of four moving bed reactors. In this process, the catalyst is continuously regenerated in a separate regeneration circuit. The reactors are connected in series with gas flow pre-heaters operating at pressures between 1 and 3 bar in the region of 650 °C. The typical catalyst in the Oleflex process consists of spherical pellets of γ-Al_2O_3 (surface area *ca.* 100 m^2 g^{-1}) containing Pt (<1 wt%) promoted with Sn and alkali metals.

The Dow FCDh technology utilises a fluidised reactor system coupled with a fluidised regeneration reactor, which enables continuous operation/regeneration.[24] The catalyst is comprised of a commercially available Al_2O_3 support that is impregnated with Ga and Pt. The catalyst can be fully recoverable after the regeneration step, which involves high temperature oxidative treatment to remove retained carbon species *i.e.* coke. Compared with the Oleflex process, which requires a complicated regeneration protocol involving Cl_2, O_2 and then H_2, the Dow FCDh technology enables a much simpler regeneration cycle.

Table 2 Commercial propane dehydrogenation technologies for a selection of catalysts.[24,25]

Technology Name	Oleflex	Dow FCdh	Uhde STAR Process	CATOFIN	K-PRO
Licensor/ developer	UOP LLC Honeywell	Dow	Krupp-Uhde	ABB Lummus	KBR, inc.
Reactor type	4 moving-bed reactors + 1 regeneration unit	Fluidised circulating reactor and regenerator	Adiabatic	Fixed bed parallel reactors	Orthoflow FCC continuous + continuous catalyst regeneration
Catalyst	Alkaline promoted Pt–Sn/Al_2O_3	Pt–Ga/Al_2O_3	Pt–$Sn/ZnAl_2O_3$/ $CaAl_2O_3$	(Na/K) promoted CrO_x/Al_2O_3	Proprietary – precious metal and Cr free
Catalyst Life	1–3 years	Unknown	Unknown	2–3 years	Unknown
Temperature/ °C	650	Unknown	550–590	560–650	Unknown
Pressure/bar	2–3	1.3–1.7	5–6	0.5	1.5
Cycle Time	5–10 days	<2 min	7 h (+1 h) regeneration	15 min	<1 min
Conversion/%	30–40	43–53	~40	48–53	45
Selectivity/%	84 (at 40% conversion)	92–96	~89	88	87–90

The Steam Active Reforming (STAR) process from Phillips Petroleum, developed by Uhde employs a Sn promoted Pt catalyst, (0.2 to 0.6 wt%), dispersed on a zinc–aluminate support, with a calcium/magnesium aluminate binder. The operating pressures and temperatures are between 6 and 9 bar and 550 to 590 °C, respectively.[2] Also, due to its non-acidic nature, the support does not promote undesired side reactions, such as cracking, isomerization or coke formation and contains Sn as a promoter to reduce coke formation and increase selectivity. Catalyst development for the STAR process continues: BASF and Thyssenkrupp announced a joint development agreement in 2020, which aims to reduce CO_2 emissions, reduce feedstock consumption and the operating costs of the process. This underlines the opportunities in catalyst design in improving even already-commercialised processes.

Chromium oxide supported on aluminium oxide (CrO_x/Al_2O_3) is commonly employed industrially in the CATOFIN process and is composed of 18–20 wt% chromium oxide supported on 1–2 wt% alkaline metal (Na or K) promoted aluminium oxide.[2,26] The alkali promoter influences both the activity and selectivity of the catalyst by reducing the surface acidity of alumina, thus suppressing undesired side reactions. In the context of the commercialised CATOFIN process, improvements in the catalyst design and process conditions have been made, however challenges still exist relating to their activity, selectivity and stability. To boost the yield of propene and reduce emissions, the addition of a heat-generating material (HGM) has been employed, a notable example of which was developed by Clariant.[27] The exact composition of the HGM is likely to include copper oxide and additional promotors such as MnO_2, supported on α-Al_2O_3.[28] This is loaded with the catalyst in the reactor, and is reduced during the reaction, which generates heat and therefore offsets the heat consumption that occurs during the DDH reaction. Since its rollout in 2015 in Ningbo Haiyue New Material Co., who are based in Ningbo City, China, the same HGM technology has been implemented in additional CATOFIN processes and Ineos recently awarded Clariant a long-term contract to supply the HGM.[29]

K-PRO was developed by KBR and is the latest process to be commercialised; the first contract was awarded in January 2020, around 1 year after the company introduced the technology and since then a licence has been agreed with JS Energy Ltd.[30] The significance of this process is that the catalyst does not contain precious metals or chromium, although the active component(s) remain proprietary information. The reactor is based on KBR's FCC orthoflow reactor, which is an up-flowing vertical reactor riser, conceptually similar to the Dow FCDh process in that the reactor is a fluidised bed, but the regeneration section is different.[25]

The commercial interest in further developing dehydrogenation technologies is evident from a simple examination of the patent literature. Fig. 4a shows the number of patents filed annually since 1980 that disclose inventions of novel catalysts for propane dehydrogenation. There is a marked increase over time, which has accelerated in the last decade. This growing interest and development are driven by the demand for propene itself, but also by the opportunity to further improve dehydrogenation catalysts. It is also evident from the sub-reaction breakdown that the majority (86%) of filed patents are for DDH catalysts, followed by ODH-O_2 (12%) and finally ODH-CO_2 (2.4%). Fig. 4b shows the breakdown of these patents by the 14 most prolific companies. China Petroleum & Chemical Corporation (SINOPEC) have published more patents than the next 13 companies combined, underlining the interest in direct propane dehydrogenation in the East Asia. It is also clear from this data that the interest in propane dehydrogenation is global, with companies from the USA, Europe and Asia all filing multiple patents.

4. Direct dehydrogenation

4.1. Pt-Based DDH catalysts

Platinum is the primary component in many dehydrogenation catalysts due to its ability to activate C–H bonds, coupled with its low activity for the breaking of C–C bonds. As shown above

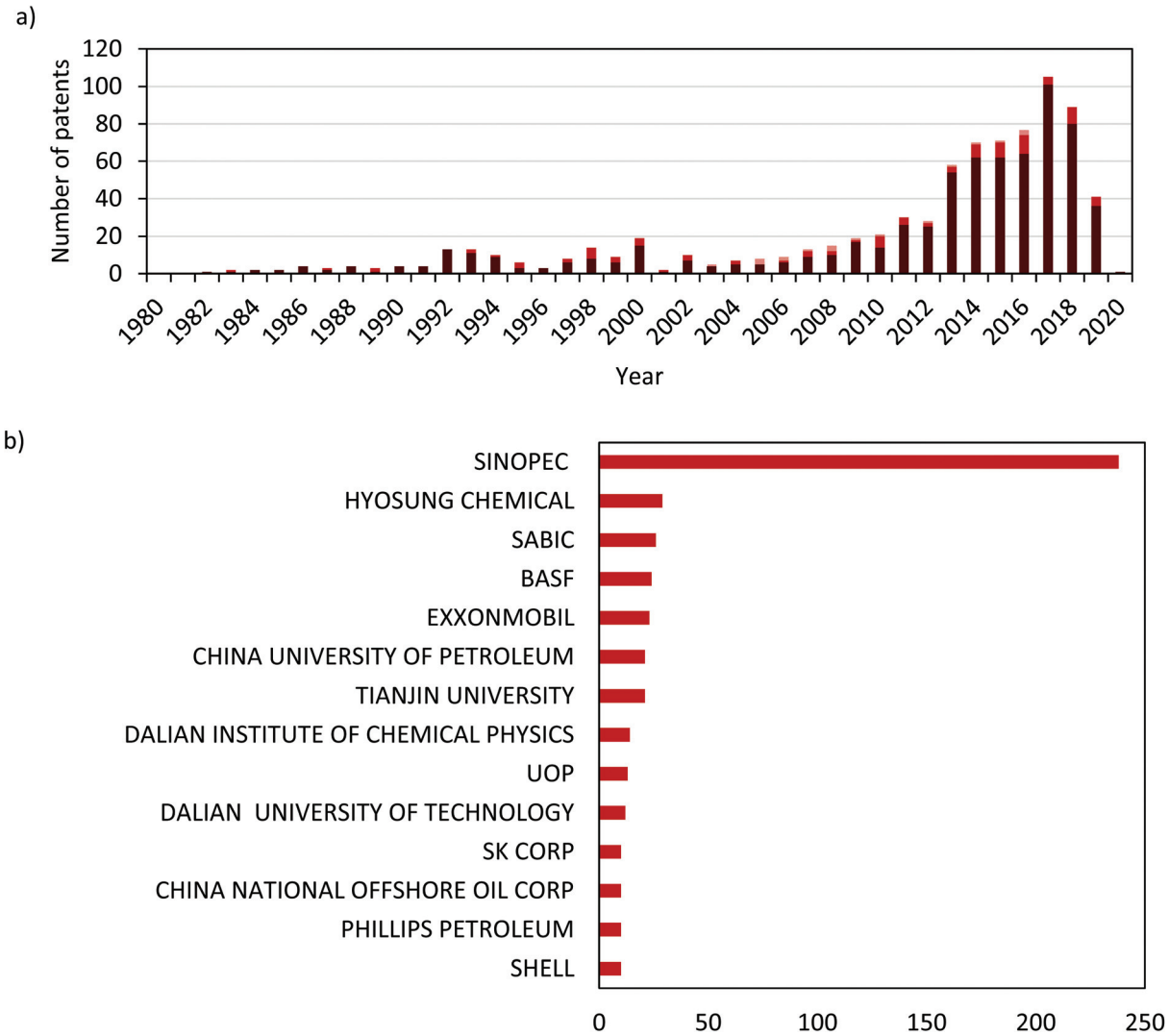

Fig. 4 (a) The number of patents published per year from 1980–2020 including the breakdown based on sub-reaction (DDH, dark red; ODH-O_2, medium red and ODH-CO_2, light red) and (b) the breakdown of patents filed per company for the top 14 companies active in this area.

in Table 1, Pt is present in three commercial processes. In this section, the most significant publications in the field of Pt-catalysed DDH are discussed.

The superiority of Pt as a DDH catalyst over other transition metals was recently illustrated by Araujo-Lopez *et al.* who used DFT calculations to measure the transition state energy for non-oxidative (and oxidative) C–H bond activation.[31] It was shown that Pt has the lowest value out of a range of transition metals, consistent with Pt typically outperforming other such metals experimentally. Interestingly, while Ag and Au did not facilitate non-oxidative C–H bond activation, in the presence of hydroxyl groups the energy barrier was much lower. These calculations help to explain the success of Pt catalysts for DDH and also highlight that other elements should be considered in ODH reactions.

The reaction mechanism for DDH has been the subject of much research. In describing catalytic dehydrogenation reactions, the most commonly quoted mechanism is the Horiuti–Polanyi mechanism, proposed in 1934.[32] The mechanism proceeds as follows:

i. Dissociative adsorption of the alkane (cleaving the first C–H bond).

ii. C–H cleavage of a second hydrogen from C_3H_7.

iii. Formation of a hydrogen molecule.

iv. Desorption of both hydrogen and the corresponding alkene.

The dissociative adsorption of propane and the C–H cleavage steps have been suggested as being rate-limiting,[33] although this depends on the catalyst. Due to the reaction conditions, side reactions frequently compete with the dehydrogenation reaction, reducing catalyst activity and selectivity. At high reaction temperatures, side reactions such as hydrogenolysis, cracking, aromatization and isomerization are thermodynamically and kinetically favoured.[34–36]

DDH is possible over almost all Pt sites, but the intrinsic selectivity and activity depends on Pt particle size: atomic steps and kink sites *i.e.* coordinatively-unsaturated species are responsible for C–H and C–C bond cleavage, which can take place here with near zero activation energy, leading to coke formation and thus catalyst deactivation.[37–39] While turnover frequency (TOF) increases as the Pt particle size decreases, selectivity is high in very small Pt species (<1 nm) and larger Pt nanoparticles (>3 nm).[40] A similar trend was also observed for stability, which is likely related to less selective Pt NPs forming coke more readily and blocking active sites.

One of the most fruitful areas of development in Pt-catalysed DDH is in the use of promotors. Specifically, Sn and Ga have been very successful, and this is reflected in their application in commercial processes, as discussed in section 3. The origin of the promotional effect of Sn has been discussed in detail in previous review articles.[2,41] Practically, the addition of Sn results in higher propene selectivity, lower support acidity, and increased diffusion of coke away from the active Pt site. Both geometric and electronic effects have been cited to explain these observations. Regarding geometric effects, Sn can modify the Pt particle size, which as previously discussed, strongly influences the reactivity of propane.[42] Specifically, Sn (oxide) can partially obscure the surface Pt species, which in turns creates smaller Pt ensembles. Regarding electronic effects, evidence for electron transfer from Sn to Pt has also been reported by DFT[43] and XPS analyses.[44] In an early report of Sn promoting Pt catalysts, Bariås *et al.* demonstrated that the effect is support sensitive, in comparing Pt/Al_2O_3 and Pt/SiO_2.[45] The addition of Sn to Pt/Al_2O_3 was wholly beneficial, improving Pt dispersion and selectivity, while maintaining specific activity. Over Pt/SiO_2, however, the Sn was more readily reduced and although an improvement in Pt dispersion and stability was noted, it came at the expense of specific activity. In fact, the oxidation state of Sn in the active catalyst is still debated and a range of different species may co-exist from Sn^{4+} through to Sn^0 before and during the DDH reaction.[41]

Pt promotion using Ga has also yielded highly active catalysts, and the role of Ga has been compared to that of Sn, *i.e.* due to both geometric and electronic effects. Wang *et al.* prepared a highly active Pt_3–Ga/Al_2O_3 catalyst and showed it could be improved by the addition of CeO_2: Pt_3–Ga/CeO_2–Al_2O_3 yielded an initial STY of 87 $mol_{C_3H_6}\ kg_{cat}^{-1}\ h^{-1}$ (compared to 83 $mol_{C_3H_6}\ kg_{cat}^{-1}\ h^{-1}$ without CeO_2) (Table 3, entries 12 and 15).

Ge was recently shown to also boost the performance of Pt catalysts: Rimaz *et al.* prepared various Ge loadings, followed by reduction at different temperatures.[46] An initial propene yield of 53.8% was achieved on a Pt–Ge/Al_2O_3 catalyst, comprising 0.5 wt% Pt and 1.5 wt% Ge reduced at 600 °C. The improvement of the bimetallic catalyst was ascribed to the electron withdrawing Ge promotor, which aided C–H activation. Isolated single Pt atoms in a Cu matrix (10 wt% Cu and 0.1 wt% Pt) supported on Al_2O_3 simultaneously displayed enhanced catalyst activity, selectivity and stability over a 120 h period.[47] In producing supported single atom materials, undesired side-reactions were suppressed. Thus, isolated Pt atoms dispersed on Cu nanoparticles were identified as active centres with high propene selectivity; dramatically enhancing the desorption of surface bound propene, prohibiting its further dehydrogenation.

Numerous Pt-based catalysts supported on alumina (Al_2O_3) have been reported. The development of new catalysts with simultaneously enhanced activity, selectivity and stability is the ultimate goal. Gamma-alumina (γ-Al_2O_3) is characterized by a high number and density of medium-strong acid sites, which can lead to undesired side reactions. Brønsted and Lewis acid sites on the support surface promote cracking and surface acid sites result in faster dehydrogenation for propene than propane, leading to deep dehydrogenation. Limited support acidity is needed to avoid undesirable side reactions, such as catalytic cracking and coke formation. However, Lewis

Table 3 Comparison of the catalytic performance of selected Pt-based catalysts for DDH

Entry	Catalyst	T/°C	Feed composition	WHSV /h^{-1}	$X_{C_3H_8}$/%	$S_{C_3H_6}$/%	STY /$mol_{C_3H_6}\ kg_{cat}^{-1}\ h^{-1}$	Ref.
1	$Pt/Mg(ln)(Al)O_x$	550	C_3H_8 = 100	1.6	24.2	98.2	7.8	54
2	Pt–Sn/B–ZrO_2	550	$C_3H_8/H_2/N_2$ = 1 : 1 : 8	1.8	36	97	13	69
3	Pt/Silicalite-1	550	C_3H_8/N_2 = 1 : 1	2.8	35	95	20	59
4	Pt_3–Mn/SiO_2	550	C_3H_8/N_2 = 1.25 : 98.75	29.5	6.8	95	41	65
5	Pt–Sn/Mg(3Zn)AlO	550	C_3H_8/N_2 = 1 : 4	3.8	55.2	99.4	47	56
6	Pt–Ga/Hd-Al_2O_3	580	C_3H_8/N_2 = 1 : 9	2.4	65.5	97	32	51
7	Pt/Al_2O_{3-600}	590	C_3H_8/H_2/He = 1 : 1.25 : 4	5.2	48.5	96.9	51	50
8	Pt–Sn/Al_2O_{3sheet}	590	$C_3H_8/H_2/N_2$ = 1 : 1.25 : 4	9.5	48.7	99.1	95	49
9	Pt–Cu/h-BN	600	$C_3H_8/H_2/N_2$ = 1 : 1 : 3.9	4.0	24	97.3	20	70
10	Pt–ln/$LaAlO_3$/γ-Al_2O_3	600	$C_3H_8/H_2/N_2$ = 8 : 7 : 35	2.6	47	96	26	53
11	Pt/TiO_2–Al_2O_3-10	600	$C_3H_8/H_2/N_2$ = 1 : 1 : 1.85	10.2	47.3	78	80	52
12	Pt_3–Ga/Al_2O_3	600	$C_3H_8/H_2/N_2$ = 1 : 1 : 1.85	10.2	39.4	98	83	79
13	Pt–Zn@Silicalite-1	600	C_3H_8/N_2 = 1 : 1.73	6.5	45	99.8	66	63
14	Pt/TiO_2–Al_2O_3-20	600	$C_3H_8/H_2/N_2$ = 1 : 1 : 1.85	10.2	45.5	88	86	52
15	Pt_3–Ga/CeO_2–Al_2O_3	600	$C_3H_8/H_2/N_2$ = 1 : 1 : 1.85	10	41.1	98.5	87	79
16	$Pt/ln/Mg(Al)O_x$	620	C_3H_8/H_2/Ar = 8 : 7 : 35	3.3	69	98	45	55

T = reaction temperature; feed composition = molar ratio of C_3H_8/H_2/carrier in the reaction, $X_{C_3H_8}$ = initial propane conversion, $S_{C_3H_6}$ = initial propene selectivity, STY = space time yield. Hd = Hydrothermally synthesized.

acid sites and amphoteric –OH groups can function as nucleation sites for Pt, enhancing dispersion. This, coupled with the high specific surface areas frequently reported for γ-Al_2O_3 explain its popularity as a catalyst support.[48] Recent advances in the use of numerous supports and catalysis synthesis methods for Pt-based catalysts and the underlying structure–activity correlations are considered below.

The importance of Al speciation in improving catalyst performance and stability was investigated by Shi *et al.* The effect of surface penta-coordinated (Al^V), Al^{3+} sites on a Pt–Sn/γ-Al_2O_3 nanosheet catalyst was investigated and after a 24 h reaction, a 4.1% drop in propane conversion with 45% propene yield was observed, corresponding to a STY of 95 $mol_{C_3H_6}$ kg_{cat}^{-1} h^{-1} (Table 3, entry 8).[49] By comparison, the conventional Pt–Sn/γ-Al_2O_3 catalyst rapidly deactivated, retaining only 65% of its initial activity. The Pt–Sn/γ-Al_2O_3 nanosheet catalyst also exhibited enhanced activity due to the high proportion of Al^V sites and their ability to uniformly disperse and stabilise Pt–Sn clusters.

Jang *et al.* explored calcination process parameters, namely temperatures of 600 °C and 750 °C, to modulate the surface properties of Pt–Sn/γ-Al_2O_3 catalysts.[50] It was shown that calcination at 600 °C resulted in a 41.2% propene yield over a 20 h DDH reaction, equivalent to a STY of 51 $mol_{C_3H_6}$ kg_{cat}^{-1} h^{-1} (Table 3, entry 7). The increased sintering resistance of the metal was ascribed to stabilization from the larger fraction of Al^V, strong Lewis acid sites, which enhanced the metal–support interactions and suppressed coke deposition.

Yu *et al.* investigated the influence of sol–gel (Sg), hydrothermally synthesized (Hd) and commercially (C) obtained Al_2O_3 in tuning the coordination structure of Al^{3+} species in Pt–Ga/Al_2O_3 catalysts.[51] At 580 °C, initial propene yields of 63.5% and 57.5% were observed for Pt–Ga/Hd-Al_2O_3 and Pt–Ga/Sg-Al_2O_3, respectively. Pt–Ga/Hd-Al_2O_3 achieved a STY of 32 $mol_{C_3H_6}$ kg_{cat}^{-1} h^{-1} (Table 2, entry 6). It was shown that Al^V sites facilitate high dispersion of the active Pt and Ga ions, and result in strong metal–support interactions. Additionally, hydrogen spillover was more effective due to the increased dispersion, which aided the desorption of H_2 from the catalyst. This study demonstrated the importance of careful support preparation and the importance of the support surface in determining support metal nanoparticle dispersion and catalytic activity.

The modification of Al_2O_3 with metal oxides, such as TiO_2[52] has been undertaken with some promising results. In the case of TiO_2, it was shown that the addition of 10 and 20 wt% TiO_2 to Al_2O_3 greatly enhanced the activity of the catalyst. The most active catalyst, a Pt/TiO_2–Al_2O_3 catalyst (with a TiO_2 loading of 20 wt%) exhibited an initial STY of 86 $mol_{C_3H_6}$ kg_{cat}^{-1} h^{-1} (Table 3, entry 14). The enhanced performance was ascribed to electron transfer and acid site modulation effects resulting in changes to the adsorption properties of Pt. Similarly, Chen *et al.* reported a Pt–ln/$LaAlO_3$/γ-Al_2O_3 catalyst with an initial STY of 26 $mol_{C_3H_6}$ kg_{cat}^{-1} h^{-1} (Table 3, entry 10).[53]

Alternative supports, such as calcined hydrotalcite, Mg(Al)O_x, have also been extensively investigated. Pt/Mg(Al)O_x modified with ln was prepared using the co-precipitation method by Tolek *et al.* At 550 °C, the catalyst achieved an initial propane conversion of 24.2% and 98.2% selectivity to propene.[54] This corresponded to a STY of 7.8 $mol_{C_3H_6}$ kg_{cat}^{-1} h^{-1} (Table 3, entry 1). The Pt/Mg(ln)(Al)O catalyst performance was attributed to a high fraction of metallic state ln (In^0) coupled with a high Pt dispersion with an average Pt particle size of 0.91 nm. Shen *et al.* prepared Pt/Mg(ln)(Al)O catalysts, where promising results were obtained by altering the calcination temperature and Mg/Al ratio.[55] An optimised Mg/Al ratio of 4 led to an initial STY of 45 $mol_{C_3H_6}$ kg_{cat}^{-1} h^{-1} at 620 °C (Table 3, entry 16). These optimised Pt/Mg(Al)O catalyst materials were characterised by having the lowest fraction of strong acid sites and highest specific surface areas. Wu *et al.* studied zinc-modified Pt–Sn/Mg(Al)O_x, which exhibited an initial STY of 47 $mol_{C_3H_6}$ kg_{cat}^{-1} h^{-1} (Table 3, entry 5).[56] Doping the support with an optimal amount of Zn resulted in smaller, and more uniformly dispersed metal particles distributed on the Mg(Al)O_x support. Overall, there have been several attempts to enhance catalyst activity through introducing a second metal to Al_2O_3 to form a mixed metal oxide support, or by preparing Al containing layered double hydroxides. Generally these have been shown to modestly boost catalyst performance, and the role of the second metal in most cases is to either enhance the dispersion of Pt, or adjust the acid–base properties of the support to inhibit side reactions.

Zeolites have been studied as potential supports for Pt-based catalysts due to their high surface areas, well-defined pore architectures and tuneable acid properties.[57,58] Wannapakdee *et al.* explored silicate-1 and Al_2O_3 based monometallic Pt catalysts.[59] The performance over 10 h on-stream differed between the Pt/silicalite-1 and Pt/Al_2O_3 materials, shown by >99% and 60% propene selectivity, respectively. The modified hierarchical pore structure, high specific surface area and presence of weak acid sites on Pt/silicalite-1 was concluded to be beneficial. Other zeolites which have been listed in patent literature for DDH of propane include Ta incorporated MCM-68, and H-ZSM-5.[60,61] In addition, non-zeolite porous silicates have been successfully applied to Pt nanoparticles.[62]

Pt–Zn nanoclusters encapsulated in silicalite-1 was investigated by Wang *et al.*, An initial STY of 66 $mol_{C_3H_6}$ kg_{cat}^{-1} h^{-1} was measured, along with excellent cyclic stability during four DDH cycles at 600 °C (Table 3, entry 13).[63] Xu *et al.* evaluated a series of Pt–Sn/Si-beta catalysts with different Pt/Sn ratios at 570 °C and reported high initial propane conversions, *ca.* 50%, irrespective of Pt/Sn ratio.[64] The Pt–Sn_2/Si-beta demonstrated an initial propene yield of 47.5%, which decreased by 3.4% over a 48 h reaction period, in contrast to the unmodified Pt/Si-beta catalyst which displayed a 47% reduction in the propene yield under identical reaction conditions. Through extensive characterisation the enhanced performance and stability was attributed to ultra-small, uniformly dispersed particles, ranging in size from 1.0 to 1.4 nm, consistent with previous studies that observed structure-sensitivity. It was found that embedding Sn in the zeolite framework was an effective

geometric diluter for Pt ensembles resulting in smaller, isolated Pt clusters which increase propene selectivity.

Wu *et al.* investigated the importance of sub-surface layers in supported nanoparticles. They reported that a Pt_3–Mn/SiO_2 catalyst was enhanced by the presence of a Pt_3–In subsurface layer (compared with a Pt subsurface layer). The optimised catalyst exhibited an initial STY of 41 $mol_{C_3H_6}\ kg_{cat}^{-1}\ h^{-1}$ (Table 3, entry 4).[65] Computational and experimental results suggested the role of the subsurface was to facilitate the activation of propane on the surface. Continuous testing for a week revealed long-term stability, and particle size distributions in the spent catalysts that were similar to those of the fresh catalysts. While the results in this work reveal a crucial role in the sub-surface composition of the catalyst, this aspect of catalyst design is often overlooked. Another sometimes neglected area of catalyst design is the role of heat treatments in modifying the nanostructure of the supported phase. Deng *et al.* reported highly selective Pt/SiO_2 and $Pt–Sn/SiO_2$ catalysts prepared under oxidative, reductive and inert atmospheres.[66] The $Pt–Sn/SiO_2$ materials prepared in inert and reductive atmospheres displayed initial propene yields of 17.8% and 25.7%, respectively. This was attributed to the reductive treatment and the presence of Sn which induced electronic and surface modifications of Pt nanoparticles following direct reduction in an H_2 atmosphere at temperatures in excess of 500 °C.[67,68]

Pt-Based catalysts supported on a boron-modified ZrO_2 have been reported by Miao *et al.*[69] The most active and stable catalyst, Pt–Sn/B-ZrO_2, achieved a STY of 13 $mol_{C_3H_6}\ kg_{cat}^{-1}\ h^{-1}$, that was attributed to the moderate surface acidity of B-ZrO_2 (Table 3, entry 2). Wang *et al.* explored the use of hexagonal boron nitride (h-BN) nanosheets as a support for Pt–Cu clusters (with 0.01 wt% Pt and 1.0 wt% Cu loadings).[70] This afforded a STY of 20 $mol_{C_3H_6}\ kg_{cat}^{-1}\ h^{-1}$ at 600 °C, respectively (Table 3, entry 10). The role of Cu in the catalyst was to dilute the Pt species and promote desorption of propene, thereby enhancing selectivity. When tested under identical reaction conditions, this catalyst showed enhanced STY and stability compared to analogous catalysts supported on $MgAl_2O_4$, H-ZSM-5, SBA-15, SiC and Al_2O_3. The h-BN nanosheets provided abundant stacking fault edges terminated with B–O defects that are associated with unpaired electrons, which strongly interact with active metal species, helping to strengthen the interaction between the metal and support.[71,72]

Finally, other support materials which have been included in patent literature over the years have tried to improve upon the catalytic activity of those currently used in industrial processes. Support materials such as carbon nanotubes and nanodiamonds tend to impart good dispersion and high stability of Pt nanoparticles,[73–75] whereas a support made entirely of TiO_2 was shown to exhibit high activity while reducing carbon deposition.[76] Au and Sn supported Pt has also been investigated, as well as various metallic sulfide materials, all designed to increase the activity of the catalyst.[77,78]

In summary, supported Pt catalysts constitute a major category of DDH catalysts, and have been studied extensively. Improvements in performance have been realised by tuning the particle size, promotion with other elements and selecting appropriate supports. Structure–activity relationships have been observed with regards to particle size, composition (presence of promotor/metal), as well as metal–support interactions. Control of these variables has been shown to influence the catalytic properties, and the reaction mechanism. Table 3 compares the activity of Pt catalysts over a wide range of conditions and with different supports and promotors. Pt–Sn and Pt–Ga supported on Al_2O_3 (often but not always γ-Al_2O_3) are the most active in this class of DDH catalyst, which is unsurprising given their application in commercial catalysts. Additionally, the incorporation of Ti into an Al_2O_3 support appears to boost activity significantly. Finally, Pt–Zn/silicalite-1 also exhibited a high STY, but Zn has not received the same attention as other promotors. Further studies may reveal that this bimetallic catalyst can compete with the current commercial catalysts.

4.2. Cr-Oxide based DDH catalysts

Chromium oxide-based catalysts have been extensively studied for DDH since the pioneering work by Frey and Huppke in 1933.[80] This proved the importance of Cr_2O_3 as a key catalyst component for the dehydrogenation of light alkanes to their corresponding alkenes at relatively high temperature and low pressure. Since the discovery of Cr-based dehydrogenation catalysts, several industrial companies have developed commercial dehydrogenation processes and catalysts.

Understanding the nature of the active chromium sites is fundamental to optimizing catalyst properties and limiting catalyst deactivation. Considerable research efforts have been undertaken to understand the nature of active sites and factors influencing catalytic performance in CrO_x/Al_2O_3 catalysts.[81,82] Spectroscopic analysis reveals a number of surface species with different oxidation states (Cr^{6+}, Cr^{5+}, Cr^{3+}, Cr^{2+}) and speciation (chromates, polychromates, crystalline and amorphous phases).[83–86] Weckhuysen *et al.* demonstrated that two types of surface chromium oxide species exist with differences in their reducibility: monomeric and polymeric species.[87] The relative concentration of different Cr surface species is strongly influenced by chromium loading and specific surface area of the selected support. Various studies have shown that low Cr loadings contribute to the dispersion of monomeric Cr^{6+} species, with some Cr^{3+} species and coordinative vacancies also being observed.[88–91] Meanwhile, at high Cr loadings, polymeric Cr^{3+} species exist as clusters and/or crystalline Cr_2O_3. This limits the accessibility of the reactants to the Cr sites, thus limiting catalytic activity.

Therefore, different surface Cr species are known to coexist in the Cr-oxide based supported catalysts, causing differences in the catalytic performance for DDH. In particular, it has been reported that the redox cycle between active Cr^{6+} and Cr^{3+} species are responsible for the activity in the dehydrogenation reaction, but the reduction of Cr^{6+} to Cr^{3+} is rapid under reaction conditions.[91–93] Thus, dehydrogenation activity has been mostly attributed to monomeric Cr^{3+} and less so to polymeric

Cr^{3+} and Cr^{2+} sites produced in the initial steps of the DDH reaction. This is in agreement with De Rossi *et al.* who reported a correlation between DDH activity and the concentration of the coordinatively unsaturated Cr^{3+} species over CrO_x/Al_2O_3 and CrO_x/SiO_2 catalysts.[94] Additionally, through IR spectroscopy studies of CO and NO adsorption, the authors concluded that the most active Cr^{3+} species had two coordinative vacancies.

As described above, the Horiuti–Polanyi mechanism is widely accepted as the mechanism for the DDH reaction. However, an alternative dehydrogenation mechanism for Cr-based catalysts has been suggested,[95,96] which proceeds as follows:

i. The formation of Cr^{3+}–C_3H_8 species.

ii. Heterolytic activation of the C–H bond of Cr^{3+}–C_3H_8 results in a Cr^{3+}–C_3H_7 intermediate.

iii. The Cr^{3+}–C_3H_7 intermediate undergoes β-H elimination to form Cr^{3+}–C_3H_6 + H^- species.

iv. Propene desorption and formation of Cr–H species.

v. Desorption of H_2 due to proton transfer, completing the reaction cycle.

During the DDH process, the rate determining steps are the activation of the propane molecule to form the adsorbed Cr^{3+}–C_3H_7 intermediate, and the β-H transfer to form the Cr^{3+}–C_3H_6 hydride surface species which can significantly affect the DDH performance. In this instance, it is proposed that Cr^{3+}–O surface species can activate propane *via* sigma-bond metathesis by generating a Cr–alkyl intermediate that subsequently undergoes β-hydride elimination to form propene.[92,95]

As a catalyst support component, Al_2O_3 has been widely used in alkane dehydrogenation processes due to its appropriate chemical properties, high structural stability and low cost. However, an inherent and major problem of the CrO_x/Al_2O_3 catalyst system is rapid deactivation, which occurs as a consequence of coke formation. Cr nanoparticles dispersed on a series of rod-shaped porous alumina supports, followed by calcination at various temperatures (T), denoted Cr–Al-T, were prepared by Gao *et al.*[97] Catalytic tests, at 600 °C, revealed that Cr–Al-800 afforded an initial propene yield of 30%, from which it was inferred that the reducibility and lower surface acidity of the Cr–Al-800 catalyst were advantageous, leading to a higher proportion of DDH active Cr^{3+} species and better anti-coking ability. Over the course of five dehydrogenation–regeneration cycles, the Cr–Al-800 catalyst demonstrated superior regenerative ability, and the initial STY was 60 $mol_{C_3H_6}$ kg_{cat}^{-1} h^{-1} (Table 4, entry 9), which is comparable to many of the Pt catalysts reported in the literature.

Lang *et al.* compared the Cr loading in a number of CrO_x/Al_2O_3 catalysts.[98] The 7.5 wt% Cr/Al_2O_3 catalyst exhibited superior catalytic performance, exhibiting an initial propene selectivity and yield of 88.5% and 55.3%, respectively. This corresponded to a STY of 27 $mol_{C_3H_6}$ kg_{cat}^{-1} h^{-1} (Table 4, entry 11). The surface Cr^{6+}/Cr^{3+} ratios produce differences in the reducibility of the catalysts and a direct correlation between increasing Cr metal loading and Cr^{6+}/Cr^{3+} ratios exists, leading to increased activity, decreased propene selectivity and excellent regenerative ability.

Węgrzyniak *et al.* investigated the influence of both mesoporous alumina and chromium metal loading in the range of 1–30 wt%.[99] The yield of propene achieved at 550 °C increased from 10.4 to 31.7% with 1 to 20 wt% Cr loading, however, further increase in Cr loading caused a decrease in the propene yield. The highest STY was achieved over the 20wt% CrO_x/Al_2O_3 catalyst, which achieved 9.3 $mol_{C_3H_6}$ kg_{cat}^{-1} h^{-1} (Table 4, entry 8), with a Cr concentration of 6.6 Cr atoms nm^{-2} which corresponded to 18% of Cr redox species. In agreement with catalytic activity, beyond this concentration of Cr the formation rate declines rapidly with the subsequent drop-in activity correlating well with the appearance of α-Cr_2O_3 crystallites located outside of the mesopore system. The catalytic performance after four dehydrogenation–regeneration cycles of the 20 wt% CrO_x/Al_2O_3 catalyst did not show any significant differences, demonstrating good long-term stability. The irreversible initial deactivation in the consecutive DDH cycles was attributed to either: (i) structural changes of active species (such as agglomeration), or (ii) collapse of pore structure.

Numerous efforts have been made to improve the performance of the CrO_x/Al_2O_3 catalyst using different promoting elements. Notably, Zhang *et al.* reported the modification of a commercial CrO_x/Al_2O_3 catalyst with Ce, which decreased the

Table 4 Summary of catalytic performance over various reported Cr-based catalysts for DDH

Entry	Catalyst	T/°C	Feed composition	WHSV /h^{-1}	$X_{C_3H_8}$/%	$S_{C_3H_6}$/%	STY/$mol_{C_3H_6}$ kg_{cat}^{-1} h^{-1}	Ref.
1	$Zn_{0.3}Cr$	480	C_3H_8/Ar = 1 : 19	0.5	21	94	2.1	108
2	$Cr_{2.5}Ni_{5.0}/Al_2O_3$	550	C_3H_8/Ar = 1 : 9	1.2	47	95	11	101
3	$Cr_{10}Zr_{90}/SiO_2$	550	C_3H_8/N_2 = 2 : 3	4.3	15	95	13	103
4	Cr_2Zr_{30}/SiO_2-600	550	C_3H_8/N_2 = 2 : 3	7.4	20	95	29	104
5	K–$CrZr_5O_x$	550	C_3H_8/He = 1 : 14	1.2	54	95	13	107
6	Cs–P/$CrZrO_x$	550	C_3H_8/N_2 = 2 : 3	5.9	30	97.5	38	106
7	CrO_x/H-ZSM-5 (260)	580	C_3H_8/N_2 = 1 : 19	0.6	60.8	78.2	5.9	102
8	CrO_x/Al_2O_3	600	C_3H_8/He = 1 : 14	1.2	41.8	89.8	9.3	99
9	CrO_x/Al_2O_3	600	C_3H_8	9.5	33.2	90.4	60	97
10	$Cr_{7.5}/Al_2O_3$	600	C_3H_8/Ar = 1 : 4	2.4	62.5	88.5	27	98
11	Ce–CrO_x/Al_2O_3	630	C_3H_8/N_2 = 1 : 6.1	1.2	86	78	17	100

T = reaction temperature; feed composition = molar ratio of C_3H_8/H_2/carrier in the reaction, $X_{C_3H_8}$ = initial propane conversion, $S_{C_3H_6}$ = initial propene selectivity, STY = space time yield.

amount of inactive isolated Cr^{6+} sites.[100] This increased the amount of oxygen vacancies on the catalyst, thus promoting the interaction between Ce and Cr species. Consequently the Ce–CrO_x/Al_2O_3 catalyst, when tested at 630 °C, displayed an STY of 17 $mol_{C_3H_6}\ kg_{cat}^{-1}\ h^{-1}$ (Table 4, entry 12) and better regeneration ability over four cycles than that of the corresponding CrO_x/Al_2O_3 catalyst over a single regeneration cycle.

Ni-Modified CrO_x/γ-Al_2O_3 catalysts (5 wt% Ni and Cr loading) exhibited enhanced activity and selectivity to monometallic Ni/γ-Al_2O_3 and CrO_x/γ-Al_2O_3, displaying an initial conversion of 47%, propene selectivity of 95% and yield of 44.7% at 550 °C. This equates to a STY of 11 $mol_{C_3H_6}\ kg_{cat}^{-1}\ h^{-1}$ (Table 4, entry 2).[101] The presence of Ni promoted the formation of oligomeric Cr species and specifically Cr^{3+} active sites.

Other metal oxides have been utilised as supports for Cr-based catalysts in an attempt to improve the catalyst stability, including materials such as ZrO_2, mesoporous SiO_2 and nanocarbons. He *et al.* investigated the effect of Cr loading on mesoporous MCM-41 with the CrO_x/MCM-41 (10 wt% loading) catalyst displaying a propene yield of 47.5% at 630 °C.[93] FT-IR analysis of this material suggested that high Cr loadings depleted surface hydroxyls, which were postulated to be essential for suppressing coke deposition.

The influence of surface acidity on activity has been investigated more in-depth by Hu *et al.* who prepared SiO_2, Al_2O_3 and H-ZSM-5 (SiO_2/Al_2O_3 = 28, 43, 80 and 260) supported Cr (5 wt%) catalysts.[102] Under identical reaction conditions, the CrO_x/H-ZSM-5 (nominal SiO_2/Al_2O_3 ratio = 260) materials displayed better catalytic performance and stability than a commercial CrO_x/Al_2O_3 catalyst, maintaining *ca.* 32.6% conversion and 94.2% propene selectivity after 50 h on stream. The authors attributed this enhanced performance to a high dispersion of Cr species, moderate acidity and strong metal–support interactions in the CrO_x/H-ZSM-5(260) catalyst. Fig. 5 illustrates the effect of surface acidity and Cr loading on the propene formation rate. Additionally, it was found that the CrO_x/H-ZSM-5(260) catalyst possessed strong anti-coking capability over long-term testing.

Moreover, Han *et al.* introduced Zr as a promoting element for Cr-catalysts on a number of supports (Al_2O_3, $AlSiO_x$, $SiTiO_2$

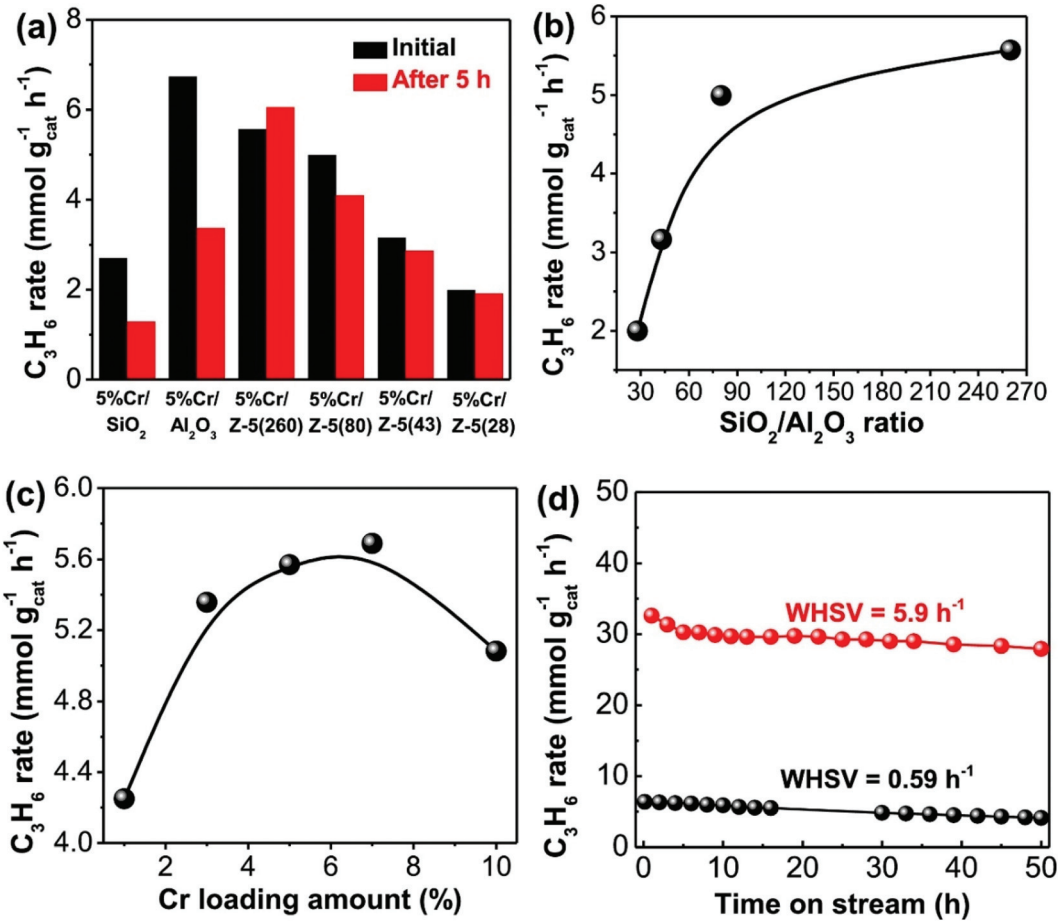

Fig. 5 Catalytic performance of the CrO_x catalysts on different supports. (a) Propene formation rates of the supported CrO_x catalysts before and after 5 h on-stream. (b) Initial propene formation rates of 5% CrO_x/H-ZSM-5 catalysts as a function of SiO_2/Al_2O_3 ratio. (c) Initial propene formation rates of CrO_x/H-ZSM-5(260) catalysts as a function of Cr loading amount. (d) Stability testing (propene formation rates) of 5% CrO_x/H-ZSM-5(260) catalyst at a WHSV of 0.59 and 5.9 h^{-1} for 50 h time-on-stream. The tests in (a–c) were performed at a WHSV of 0.59 h^{-1}. Reproduced from ref. 102 with permission from Elsevier.

and SiO_2).[103] The Zr addition improved the turnover frequency for all Cr loadings when compared to analogous Cr-only catalysts and it was found that the greatest promotional effect was observed over the smallest ZrO_2 crystallites. The order of reactivity was: $CrZr/SiO_2$ > $CrZr/AlSiO_x$ > $CrZr/SiTiO_x$. Likewise, the degree of crystallinity in $CrZr/SiO_2$ catalysts proved to be an important structural property affecting both the rates of propene and coke formation.[104] With increasing calcination temperature (450–600 °C) the catalysts displayed enhanced activity, selectivity and long-term stability (150 h) over consecutive dehydrogenation/regeneration cycles. However, the catalyst calcined at 600 °C exhibited a STY of 13 $mol_{C_3H_6}$ kg_{cat}^{-1} h^{-1} (Table 4, entry 3).

Fujdala and Tilley reported $CrO_x/Si/Al/O_x$ and $CrO_x/Si/Zr/O_x$ catalysts exhibiting propene yields in excess of 33% at 450 °C.[105] Further improvements were observed when basic promoters (Cs and Ca) were added to $CrZr/Al_2O_3$ catalysts which displayed a superior propene formation rate of 38 $mol_{C_3H_6}$ kg_{cat}^{-1} h^{-1} after modification of the support with an acidic P-based modifier (Table 4, entry 6).[106] The positive effect was attributed to the promoters' ability to block the sites responsible for coke formation and negligible contribution to undesirable secondary reactions by the additional acid sites generated by the P-based modifier.

Mixed metal oxide catalysts have also been widely studied in the context of Cr-based catalysts. WÈ©grzyniak *et al.* demonstrated that ordered mesoporous Cr–Zr–O and Cr–Zr–K–O catalysts had improved catalytic performance compared to CrO_x/Al_2O_3 materials and other promising catalysts in the DDH process.[107] It was found that all the catalysts modified with K displayed respectable regeneration ability as well as an improvement in the catalyst's STY, which was measured to be 13 $mol_{C_3H_6}$ kg_{cat}^{-1} h^{-1} (Table 4, entry 5).

Another series of binary Zn–Cr mixed oxides with different Zn/Cr molar ratios (0–0.5) proved advantageous for the DDH reaction.[108] An optimal Zn/Cr ratio of 0.3 produced a highly active catalyst which displayed conversion, propene selectivity and propene yield values of 31.3%, 94% and 29.4%, respectively. The activity of the binary-component oxide catalyst was attributed to the defect-rich spinel structure, which generated a higher concentration of active Cr^{3+} species.

In summary, the dehydrogenation performance of CrO_x-based catalysts is largely influenced by the catalyst preparation method, identity of the support, as well as the promoting elements and active sites present in the resultant catalyst. The aforementioned factors influence activity, selectivity and stability and can be enhanced by optimizing elements of the catalyst design process. The most common deactivation pathway is coking, which can cause sintering in both the support and Cr. Efforts to improve catalyst design include using supports with ordered mesoporosity and moderate surface acidity, both of which aid mass transfer and avoid undesirable secondary reactions. Numerous Cr deposition methods have been explored, with novel surface organometallic chemistry methods emerging as viable preparation methods for ensuring isolated CrO_x species, although these may not be appropriate for large-scale application. Promoting elements have been found to cause beneficial geometric and electronic effects on both the supports and CrO_x species. However, recent advances in unsupported, binary metal oxides have been successful in yielding catalysts with respectable activity, selectivity and resistance to coking. However, significant environmental and safety concerns still exist in the preparation, usage and disposal of CrO_x-based catalysts due to the associated toxicity. In comparison to Pt catalysts, CrO_x catalysts generally exhibit lower STYs, although the most active CrO_x catalysts (typically supported on Al_2O_3) are as active as moderate supported Pt catalysts.

4.3. Ga-Based DDH catalysts

Historically, a bifunctional Ga/H-ZSM-5 material has been applied as a catalyst for the commercial process for propane aromatization, developed jointly by UOP and BP as the Cyclar Process.[109,110] More recently, the Dow FCDh process was developed which uses a Pt–Ga based catalyst. Gallium oxide (GaO_x)-based catalysts have been the subject of intensive research as candidate catalysts and/or supports for the DDH reaction. This is because Ga is another non-noble metallic element known to catalyse the dehydrogenation of propane, usually through oxidic, tetrahedrally coordinated Ga^{3+} species, which are considered to be active sites for C–H activation.[111,112] However, several surface gallium species (*e.g.*, Ga_2O_3, GaO^+ and Ga^{n+}) can exist and are considered active constituents exhibiting different performance for the DDH reaction. Furthermore, the types of surface Ga species present are dependent on the identity of the support, Ga loading, as well as the preparation method.

Numerous studies have shown that Ga_2O_3 dispersed on TiO_2, MgO, Al_2O_3, ZrO_2, H-ZSM-5, ZSM-8 and MWW zeolites display distinctly different catalytic properties for alkane dehydrogenation.[113–116] Sattler *et al.* reported a Pt-promoted $Ga/\gamma\text{-}Al_2O_3$ species ($Pt_3Ga/\gamma\text{-}Al_2O_3$) as a highly promising catalyst for propane dehydrogenation, which showed remarkably high activity, selectivity, and long-term stability.[117] For catalysts containing both Ga and a low amount of Pt (~0.1 wt%), the observed conversion was close to the equilibrium value, 55% at 620 °C with the addition of Pt as a promoter facilitating recombination of hydrogen atoms into H_2. By modulating the support acidity further with a K-dopant, the resultant $Pt_3GaK/\gamma\text{-}Al_2O_3$ catalyst demonstrated enhanced stability, displaying a propane conversion of 31.1% and a selectivity for propene of 92.6% after approximately 150 cycles or 14 days of operation. The authors postulated the main active site for C–H activation was Ga^{3+} embedded within the $\gamma\text{-}Al_2O_3$ framework.

Further investigations by Searles *et al.* showed that a $Ga^{\delta+}Pt^0/SiO_2$ catalyst, featuring a highly dispersed Ga_xPt alloy structure, had a long-term stability evident in unchanged propene selectivity (>99%) over the course of a 20 h DDH reaction.[118] Both the moderate surface acidity of the support and good dispersion of the generated gallium single-sites proved beneficial. Additionally, the monometallic Ga^{3+}/SiO_2 catalyst also displayed minimal deactivation over a 20 h DDH reaction, retaining a high propene selectivity (94%) throughout.

A comparative approach to study the effect of the support acidity was taken by Szeto *et al.* through which marked differences were observed in the reactivity of silica and alumina supported Ga catalysts.[119] An initial conversion and selectivity of 24% and 79%, respectively, were reported for Ga/Al_2O_3. The STY was 5.9 $mol_{C_3H_6}\ kg^{-1}{}_{cat}\ h^{-1}$ (Table 5, entry 4). On the other hand, the Ga/SiO_2 catalyst was reported to have low activity (8% conversion initially) and moderately high selectivity to propene (90%) under identical testing conditions. This highlights the importance of selecting an appropriate support for different active centres.

Cybulskis *et al.* reported that the preparation strategy could greatly influence the structure of Ga/SiO_2 catalysts.[120] Utilizing a pH-controlled incipient-wetness impregnation method the resultant catalyst contained a high proportion of isolated Lewis acidic Ga^{3+} sites dispersed on SiO_2, with the ability to activate hydrocarbon C–H bonds with up to 99% selectivity through a non-redox pathway at 550 °C. A variety of spectroscopic characterisation methods further verified isolated four-coordinate Ga^{3+}–O centres as catalytically relevant sites in these Ga/SiO_2 catalysts. Meanwhile the $Ga^{\delta+}$–H and $Ga^{\delta+}$–O species, which were identified as spectators, remained stable in inert and reductive atmospheres from room temperature to 550 °C, before reversibly decomposing in the presence of C_3H_6 under reaction conditions to regenerate the Lewis acidic Ga^{3+}–O centres.

Other supports (H-ZSM-5, SBA-15, γ-Al_2O_3 and SiO_2) and the effect of Ga loading have also been investigated. Shao *et al.* established an optimal Ga loading of 5 wt%, reporting an initial propene yield on different supports that followed the trend: Ga/H-ZSM-5 (48%) > Ga/γ-Al_2O_3 (43%) > Ga/SBA-15 (28%) > Ga/SiO_2 (9%) (Table 5, entries 7–9).[121] This was attributed to differences in surface acidity between supports, with strong acid sites largely determining the dispersion of Ga species, as well as inducing adverse side reactions. Zeolite supports can in principle hinder the formation of large hydrocarbon molecules due to their unique framework and channel structure, which are beneficial to the catalytic stability. Consequently, it was found that the Ga/H-ZSM-5 catalyst displayed the highest initial activity but lowest stability. Factors such as the highest specific surface area and lowest acidity were associated with the superior catalytic stability of the Ga/SBA-15 catalyst over the 30 h DDH reaction at 620 °C.

Further improvements reported by Kim *et al.* explored the catalytic function of Ga-based catalysts supported on bulk and hierarchical MFI-type zeolites, where Ga was used in place of Al.[122] Catalytic testing at 600 °C revealed substantial activity, selectivity and stability improvements in hierarchical Ga/MFI relative to the corresponding bulk Ga/MFI catalyst. The authors hypothesized that the enhanced activity and selectivity of the hierarchical catalysts arose from their quasi-2D structure and lower surface acidity. Generally, it is accepted that lowering the surface acidity can further enhance the catalytic performance of a DDH catalyst. The addition of 3-mercaptopropyl-trimethoxysilane (MPS) reduces Brønsted and increases Lewis acid sites in the preparation Ga/MFI catalysts, which resulted in improved performance.[123] When compared to a CrO_x/Al_2O_3 catalyst, the Ga/MFI catalyst, although less selective, was more stable and retained the moderate propene selectivity over the 12 h DDH reaction. Acidity characterization techniques confirmed a high concentration of strong Lewis acid sites and a reduction in the concentration of Brønsted acid sites in the Ga-MFI catalyst (Table 5, entries 5 and 6).

Schreiber *et al.* further verified the active sites for MFI supported Ga catalysts with moderate acidity, reporting an optimal Ga/Al ratio of 0.5, which enhanced the dehydrogenation rate.[124] The authors attributed high Ga/Al ratios (>0.5) with the formation of additional Ga_xO_y clusters which negatively affected the dehydrogenation rate and thus catalytic performance. Therefore, for Ga/MFI zeolites a synergy between Ga^+ species and a Brønsted acid site (BAS) (optimised to one Ga^+ per BAS) exists forming a Lewis–Brønsted acid pair during the dehydrogenation of propane. DFT calculations indicated that the generated Lewis–Brønsted acid pair is much more active than an isolated Ga^+, due to the large increase in Lewis acidity upon protonation of Ga^+ by the BAS, which facilitates heterolytic C–H bond activation. The BAS also significantly reduces the activation barrier for H_2 elimination by recombination with a hydride. This was in agreement with findings by Phadke *et al.*[125]

Using a different approach, Raman *et al.* reported the synthesis of Ga–Rh supported catalytically active liquid metal solutions.[126] A correlation between alloy composition and specific activity was observed with Ga_{125}–Rh exhibiting STYs of 5.0 $mol_{C_3H_6}\ kg_{cat}{}^{-1}\ h^{-1}$ (Table 5, entry 1). Bauer *et al.* reported

Table 5 Performance of selected Ga-based catalysts for the DDH reaction

Entry	Catalyst	T/°C	Feed composition	WHSV /$g_{C_3H_8}\ g_{cat}{}^{-1}\ h^{-1}$	$X_{C_3H_8}$/%	$S_{C_3H_6}$/%	STY/$mol_{C_3H_6}\ kg^{-1}{}_{cat}\ h^{-1}$	Ref.
2	Ga_{125}-Rh	450	C_3H_8/He = 1 : 9	0.88	29	95	5.0	126
3	Ga/SiO_2	550	C_3H_8/Ar = 1 : 4	2.4	10	90	4.5	49
4	Ga/Al_2O_3	550	C_3H_8/Ar = 1 : 4	1.5	24	79	5.9	119
5	Ga-MFI	600	C_3H_8/Ar = 1 : 19	0.79	41	75	3.7	123
6	Ga-MFI	600	C_3H_8/Ar = 1 : 19	2.4	12.2	82	4.9	122
7	Ga/SBA-15	620	C_3H_8/Ar = 1 : 19	0.6	29.7	92	3.3	121
8	Ga/Al_2O_3	620	C_3H_8/Ar = 1 : 19	0.6	46	95.2	5.5	121
9	Ga/H-ZSM-5	620	C_3H_8/Ar = 1 : 19	0.6	78.1	60.2	5.9	121

T = reaction temperature; feed composition = molar ratio of C_3H_8/H_2/carrier in the reaction, $X_{C_3H_8}$ = initial propane conversion, $S_{C_3H_6}$ = initial propene selectivity, STY = space time yield.

that an alternative liquid metal solution, Ga_{37}–Pt/Al_2O_3, exhibited propane conversion as low as 350 °C.[127] The Ga–Pt alloy melts at temperatures between 270 °C and 330 °C.[20] At 400 °C and 450 °C, selectivity to propene was *ca.* 95% and 90%, respectively and activity was attributed to isolated Pt atoms in the supported liquid Ga–Pt alloy.

In summary, GaO_x based catalysts are promising propane dehydrogenation candidates. However, these catalysts are limited by deactivation through coke formation and the sintering of GaO_x species which are dependent on the support, Ga loading and preparation method. Studies have also shown the advantages of incorporating promoter elements and/or the formation of intermetallic alloys in enhancing the dehydrogenation performance. Ga catalysts generally exhibit STYs that are one order of magnitude lower than Pt catalysts, and the most active CrO_x catalysts, but have the advantage of being benign and inexpensive.

4.4. V-Based DDH catalysts

Vanadium-based catalysts have garnered increased interest as alternative materials to Pt- and Cr-based catalysts for the DDH reaction, to their comparative low cost and toxicity. Numerous studies have elucidated the effect of the preparation method, vanadium loading, promoter and support characteristics on the surface chemistry and catalyst performance of vanadium species.[128–131] Generally, the oxidation state of vanadium (*i.e.*, V^{3+}, V^{4+}, V^{5+}) determines the catalytic activity.[132] In addition, the distribution of V oxidation states is controlled by the V loading, which in turn influences the degree of polymerization. It has been reported that V^{5+} is the least active, whereas V^{4+} and V^{3+} species (generated from the reduction of V^{5+}) are more active in the DDH reaction.[133–137] Additionally, these studies suggest that a number of VO_x species exist including monovanadate (isolated V), polyvanadate (oligomeric V^{n+}) and V_2O_5 crystallites.

The nature of the support is an essential parameter to consider as several possible VO_x can species exist. It is generally accepted that the metal–support (V–O–support) interactions affect the resultant catalyst performance.[138] It is proposed that V–O–support bonds are active sites, as lattice oxygen in V–O bonds directly catalyses C–H activation forming H_2. The activity is dependent on the bond strength of the V–O–support bond. Therefore, it is expected that catalyst performance is affected when different supports, such as SiO_2, Al_2O_3 and ZrO_2 are utilised.

From a comparison of VO_x/MCM-41, CrO_x/MCM-41 and Pt–Sn/Al_2O_3 catalysts, it was shown that VO_x/MCM-41 exhibited superior propene selectivity (above 90%) and stability during several successive dehydrogenation–regeneration cycles.[90] Subsequent studies expounded on the importance of the support surface acidity on a range of aluminosilicates with varying SiO_2 contents.[139] Sokolov *et al.* investigated the effect of the support on the stability of Al_2O_3, SiO_2 and $AlSiO_x$ supported VO_x catalyst. It was reported that at 1 wt% $V/AlSiO_x$ (with 10 wt% SiO_2 in the support) was only around 25% less active than a Pt–Sn/Al_2O_3 comparison sample. However, the STY of this most active catalyst at 550 °C was 5.1 $mol_{C_3H_6}$ $kg^{-1}{}_{cat}$ h^{-1} (Table 6, entry 1), which is an order of magnitude below the values commonly reported for supported Pt catalysts tested at 600 °C, suggesting that more active Pt–Sn catalysts can be prepared than the one reported in this work. The catalyst deactivated quickly due to carbon deposition, but retained its initial activity over the course of ten successive dehydrogenation–regeneration cycles. The authors observed a positive correlation between the rate of coke formation and the acidity of the support, as well as reporting that coke can actually catalyse the DDH reaction. Additional studies attributed the dependence of coke formation on the degree of polymerization of VO_x species over catalysts supported on a range of aluminosilicates, with differing SiO_2 contents varying from 1 to 100 wt%.[140] It was concluded that coke preferentially formed on larger V_2O_5 crystallites rather than small or isolated VO_x species.

The cation–anion double hydrolysis approach (CADH), used for the synthesis of mesoporous Al_2O_3 with high surface area and a pure γ-Al_2O_3 phase, was undertaken with the crystallisation temperature varied between 25–120 °C.[141] It was found that the crystallisation temperature of the support directly influenced the catalytic performance of the VO_x/Al_2O_3 catalysts, which was a consequence of the increase in Lewis acid

Table 6 Catalytic performance of selected vanadia-based catalysts for the DDH reaction

Entry	Catalyst	T/°C	Feed composition	WHSV/$g_{C_3H_8}$ g_{cat}^{-1} h^{-1}	$X_{C_3H_8}$/%	$S_{C_3H_6}$/%	STY/$mol_{C_3H_6}$ $kg^{-1}{}_{cat}$ h^{-1}	Ref.
1	V/SiO_2	550	C_3H_8/N_2 = 2 : 3	0.95	30	85	5.1	139
2	$VZrO_2$	550	C_3H_8 /H_2/N_2 = 1 : 1 : 5.1	2.06	25	85	9.2	149
3	$VZrO_2$	550	C_3H_8/Ar = 1 : 6.5	4.7	25	98	24	150
4	V-SiO_2	580	C_3H_8/Ar = 1 : 10	0.59	64	90	7.9	145
5	VO_x/SiO_2	580	C_3H_8/Ar = 1 : 10	0.6	55	91	6.2	147
6	$7VO_x$/Si-Beta	600	C_3H_8/N_2 = 1 : 19	0.6	40	90	4.4	148
7	VO_x–Mg/Al_2O_3	600	C_3H_8 /H_2/N_2 = 1 : 1 : 1.6	1.3	31	85	7.8	143
8	V-DMSN	600	C_3H_8/N_2 = 1 : 7.5	6.7	18.1	91	22	146
9	VO_x/γ-Al_2O_3	600	$C_3H_8/H_2/N_2$ = 1 : 1 : 1.6	3.3	15	94	15	132
10	VO_x/Al_2O_3	610	C_3H_8/N_2 = 4 : 1	2.8	30	85	15	141

T = reaction temperature; feed composition = molar ratio of C_3H_8/H_2/carrier in the reaction, $X_{C_3H_8}$ = initial propane conversion, $S_{C_3H_6}$ = initial propene selectivity, STY = space time yield. DMSN = dendritic mesoporous silica nanoparticles.

sites with increasing crystallization temperatures up to 100 °C. This in turn affected the distribution of different surface V species. After an induction time of 1 h, the VO_x/Al_2O_3 catalyst (crystallized at 100 °C) achieved the best performance giving a propene yield of 60%, equivalent to a STY of 15 $mol_{C_3H_6}\ kg^{-1}{}_{cat}\ h^{-1}$ (Table 6, entry 10).

Similar studies investigating V loading (1–20 wt%) and its effect on the surface V species present in VO_x/Al_2O_3 catalysts reported a volcano plot-type trend between V loading and catalytic performance, with maximum activity being observed at 12 wt% V loading.[132] The authors concluded that the relative proportions of V^{3+}, V^{4+} and V^{5+} species present on the catalyst surface were affected by V loading and at the optimal loading of 12 wt%, a high concentration of isolated V^{3+} species was detected. *In situ* DRIFTS analysis elucidated the mechanistic pathway, whereby a vanadium propyl intermediate is formed after propane activation and rapidly transforms to propenyl-vanadium. Propene is formed from propenyl-vanadium or propyl-vanadium and desorbs from the catalyst surface.

Gu *et al.* reported that P modification could greatly influence the structure and activity of VO_x/Al_2O_3 catalysts.[142] More specifically, P modification decreased the degree of VO_x polymerization, which had positive implications on the catalyst stability, as evidenced by the retention of high activity (*ca.* 45% propane conversion) after an 8 h DDH reaction in all P-modified catalysts. This was almost twice the conversion reached with the unmodified catalyst. The combined and synergistic effect of the surface acidity modifications, their influence on the active V^{3+} species, and weakened metal–support interactions facilitated desorption of propene and inhibited the deep dehydrogenation that leads to coke precursors.

Subsequent studies on a VO_x/Al_2O_3 catalysts (with 12 wt% V loading) modified with Mg revealed the anti-coking capability and improved catalytic performance evident through propene yields of 19–27% over a 6 h DDH reaction.[143] It was found that the dispersing action of Mg modification to V_2O_5 crystallites and an increase in active V^{3+} species reduced the amount and polymerization of coke deposits. However, the acidity decreases sharply with excessive Mg addition (above 1 wt%) as the excess MgO covers the surface VO_x species, which leads to the loss of DDH activity. The highest STY achieved was 7.8 $mol_{C_3H_6}\ kg^{-1}{}_{cat}\ h^{-1}$ (Table 6, entry 7).

In addition to alumina, other supports have been investigated. Earlier reports by Ovsitser *et al.* described a silica supported VO_x catalyst which exhibited high propene yield (86%), high stability and minimal deactivation over a 20 h DDH reaction.[144] Hu *et al.* explored vanadium doped porous silica ($V–SiO_2$) with varying V : Si mass ratios of vanadium to silicon of 1 : 24, 1 : 12, 1 : 6, and 1 : 3, respectively.[145] The V/SiO_2 catalyst (with mass ratio of 1 : 12) displayed the optimal catalytic performance, achieving a superior initial propene yield of 59.5% and a stable propene selectivity of ~90% over 6 h at 580 °C. This was equivalent to a STY of 7.9 $mol_{C_3H_6}\ kg^{-1}{}_{cat}\ h^{-1}$ (Table 6, entry 4). Results from successive dehydrogenation–regeneration cycles indicated that the catalyst reached a stable state displaying excellent regeneration stability after two dehydrogenation cycles. In common with VO_x/Al_2O_3 catalysts, moderate V loadings were concomitant with increased activity, which was attributed to more vanadium active sites in the channels of the porous silica with increased doping. The moderate vanadium doping level was conducive to highly dispersed vanadium species in the form of isolated and low-polymerized VO_x species.

As previously discussed for other DDH catalysts, innovative techniques have also been applied in the preparation of V/SiO_2 catalysts. Vanadium-containing dendritic mesoporous silica nanoparticles (V-DMSNs) exhibited an initial propane conversion and propene selectivity of 18.1% and 91% respectively. The STY was calculated to be 22 $mol_{C_3H_6}\ kg^{-1}{}_{cat}\ h^{-1}$ (Table 6, entry 8), which is one of the highest VO_x containing catalysts reported to date.[146] Compared to analogous catalysts synthesized *via* wet impregnation, the direct co-assembly process for the V-DMSNs catalysts contributed to enhancing the interaction between the V^{5+} species and the silica support. Highly dispersed and stable VO_x species, and an absence of V_2O_5 crystallites, were conducive to high catalytic activity and stability. When tested for both ODH-O_2 and DDH reactions, the V-DMSNs catalysts displayed superior performance, signifying the importance of the preparation conditions and synthesis strategy to form well-defined structure of the support and sufficient concentration of highly dispersed and isolated VO_4 active sites.

Hu *et al.* investigated the influence of gelation and calcination temperatures on the properties and catalytic performance.[147] Interestingly, enhancement to catalytic performance in terms of propane conversion, propene selectivity and yield of propene were observed for VO_x/SiO_2 catalysts (gelation temperature: 60 °C, calcination temperature: 580 °C). The VO_x/SiO_2 catalyst exhibited an initial propane conversion of 55% and stable propene selectivity of *ca.* 91% over 4 h, with excellent reusability displayed over eight successive reaction-regeneration cycles. The STY was 6.2 $mol_{C_3H_6}\ kg^{-1}{}_{cat}\ h^{-1}$ (Table 6, entry 5), due to the low GHSV so while the catalyst achieved high selectivity at reasonable propane conversion, it was not as intrinsically active as other supported VO_x catalysts.

Dealuminated beta zeolites (Si-beta) are promising catalyst supports due to their high surface area and thermal stability as mentioned before. Chen *et al.* synthesized numerous VO_x/Si-beta zeolites with various V loadings (in the 0.5–10 wt% range) with the initial propane conversion shown to linearly increase with the amount of acid sites, Fig. 6.[148] This demonstrated the dependency of catalytic activity on total Lewis and Brønsted acid sites generated by VO_x on silica, with Brønsted acid sites disappearing after high temperature treatment due to decomposition of hydrated VO_x. The most active catalyst, V/Si-beta (having 3 wt% V loading) displayed an initial propene yield of 33.4% and retained activity over multiple dehydrogenation–regeneration cycles. Thus, only weak and medium strength sites were generated and ascribed to mono- and polymeric VO_x species, respectively, both of which aided the adsorption and activation of propane. A correlation between

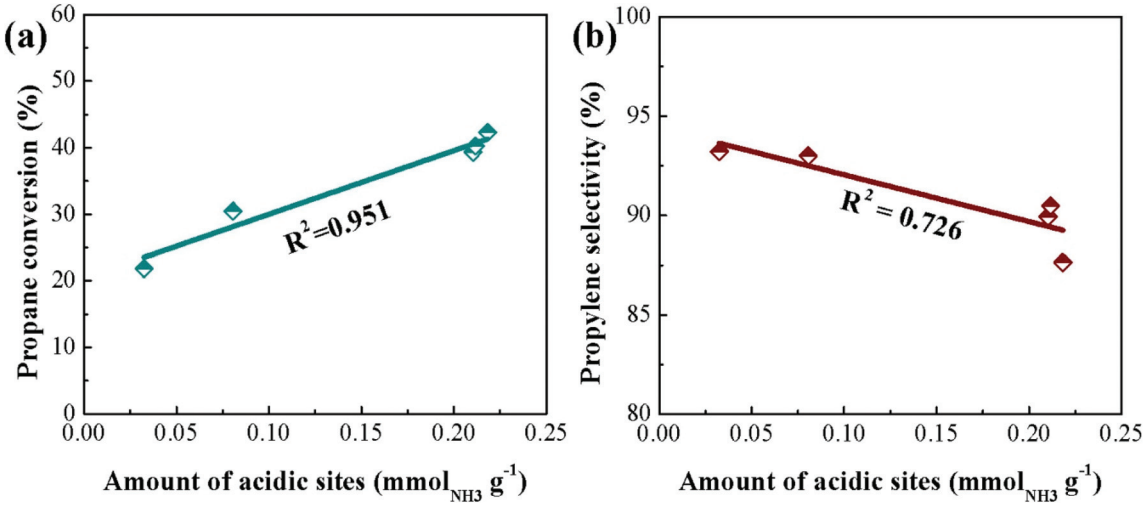

Fig. 6 Correlations between the (A) initial propane conversion and (B) propene selectivity as a function of the total amount of acidic sites, created by the interaction sites between V species and Si-Beta support in V/SiBeta catalysts. Reproduced from ref. 148 with permission from Elsevier.

increasing V loading, increased degree of polymerization and a subsequent increase in strong surface acid sites was reported. At 7 wt% VO_x/Si-beta, the STY was 4.4 $mol_{C_3H_6}$ kg^{-1}_{cat} h^{-1} (Table 6, entry 6), which is 5–6 times less active than the most active VO_x catalysts reported to date, suggesting that Si-beta does not facilitate a high concentration of active V sites.

Alternatively, ZrO_2 can be used as a support for VO_x. It was found that VO_x/ZrO_2 is approximately five times more active than VO_x/Al_2O_3 and pure ZrO_2, exhibiting a STY of 9.2 $mol_{C_3H_6}$ kg^{-1}_{cat} h^{-1} (Table 6, entry 2).[149] The authors proposed that the enhanced performance of VO_x/ZrO_2 results from the facile reduction of V=O, V–O–V and V–O–Zr bonds, thus producing higher proportions of the active V^{3+} species. In view of this, Jeon *et al.* investigated various loadings of V on VO_x/ZrO_2 catalysts.[150] For the most active catalyst, with 8 wt% V loading, the initial yield of propene increased from 24% at 550 °C to 28% at 575 °C with a negligible (<1%) increase at 600 °C. This corresponded to a STY of 24 $mol_{C_3H_6}$ kg^{-1}_{cat} h^{-1} (Table 6, entry 3), which is one of the most active VO_x-based catalysts reported. As discussed later in section 4.5, ZrO_2 is active by itself and therefore this result likely reflects the contribution from an active ZrO_2 support rather than an optimised or improved VO_x catalyst. Indeed, the authors alluded to a correlation between activity and the formation of a higher concentration of coordinatively unsaturated (Zr_{cus}) sites, created by the addition of the V dopant into the Zr lattice, increasing the density of Lewis acid sites. As discussed below, the STY of ZrO_2 without VO_x is actually much higher than in the current work.

To date, many studies have investigated VO_x-based catalysts, which in some cases have been said to exhibit a catalyst performance similar to that of Pt- and CrO_x-based catalysts. However, comparing the typical STY values for VO_x with those of CrO_x or Pt, it is clear that the VO_x catalysts reported in the literature are not as active as supported CrO_x or Pt catalysts. In view of catalyst design, the nature of the support is an essential consideration, due to the importance of metal–support interactions and the influence of acid sites on the formation of different surface VO_x species. Of particular importance is the role of the support in altering stabilization and electronic effects of the active sites. Much like the industrial (Pt- and Cr-based) catalysts, the surface acidity and selectivity of the catalyst is affected by the nature of the support. Although the most active V species has been identified, the relative proportion and stability of this surface V species can be tuned by varying the preparation method. On the other hand, the role of the other V species on the DDH reaction remains unclear so further work to elucidate this could yield more active and stable DDH catalysts. The range in performance of V-based catalysts varies quite significantly, with the most active catalysts exhibiting STYs that are around 3–4 time less active than the most active Pt catalysts.

4.5. Other DDH catalysts

As previously discussed, the industrial application of Pt- and CrO_x-catalysts is well established because they offer superior activity, selectivity and stability for the direct dehydrogenation of propane. However, these catalysts are limited in two main areas: economically, by the high cost of Pt and environmentally, by the toxicity of Cr^{6+} species. Thus, a definite need to develop alternative catalyst formulation exists.

Commonly, coordinatively unsaturated metal cations with neighbouring oxygen vacancies serve as adsorption sites for light alkanes, whereby surface oxygen sites abstract hydrogen from the adsorbed alkane. Armed with this knowledge, researchers continue to focus their efforts on catalyst design with the aim of enhancing dehydrogenation performance, creating both economic and environmental benefits.

Bulk ZrO_2, characterized with coordinatively unsaturated Zr cations (Zr_{cus}^{4+}) as active sites, has emerged as a highly active and selective unsupported catalyst for the direct dehydrogena-

tion of propane. Kondratenko and co-workers first reported that ZrO_2 is active in its own right for DDH and subsequently demonstrated the importance of crystallite size and phase composition in determining activity.[151,152] The rate of propene formation was inversely proportional to the crystallite size, but crucially, amorphous ZrO_2 was very poorly active. Time on-stream conversions dropped significantly over time due to carbon deposition, but regenerative cycles were completed to examine if the activity could be regained. At 550 °C, ZrO_2 was durable after 20 cycles but at 600 °C the ZrO_2 crystallites sintered, causing a loss in activity. The initial performance corresponded to an STY of 64 $mol_{C_3H_6}$ kg^{-1}_{cat} h^{-1} (Table 7, entry 13), which is one of the highest non-Pt values reported.

Jeon *et al.* reported the modification of ZrO_2 with a vanadium dopant that exhibited an initial propene yield of 28%, excellent recyclability over ten cycles with no change in the active sites, and twice the activity observed in bulk undoped ZrO_2.[150] This was attributed to an increase in Lewis acidic (Zr_{cus}^{4+}) active sites, that are a consequence of structural transformation. Additionally, the authors discovered that regardless of the vanadium content, all the catalysts exhibited a propene selectivity in excess of 98%.

Similarly, a positive effect from the modification of ZrO_2 with a Cu dopant was reported by Jeon *et al.*[153] The optimal $CuZrO_x$ catalyst displayed improved activity and selectivity at 600 °C compared to conventional (1 wt%) Pt/Al_2O_3, (0.5 wt% Pt-1.5 wt% Sn) $Pt–Sn/Al_2O_3$ and (5 wt% CrO_x/Al_2O_3). The authors established a correlation between the specific activity of $CuZrO_x$ catalysts and the number of weak acid sites, resulting from the substitution of Cu in the Zr sub-lattice generating oxygen vacancies and Zr_{cus}^{4+} ions. The STY of the $CuZrO_x$ catalyst was 26 $mol_{C_3H_6}$ kg^{-1}_{cat} h^{-1}, compared to 22 $mol_{C_3H_6}$ kg^{-1}_{cat} h^{-1} in the unmodified catalyst (Table 7, entries 9 and 10). While this improvement is promising, the STY was lower than half of an optimised ZrO_2 catalyst previously reported in ref. 151, suggesting that there is still room for improvement in the $CuZrO_x$ preparation, or that it is possible to promote activity through careful catalyst preparation rather than adding metals.

The concentration of dopant atoms, and the temperature of reduction were other contributing factors that affected the catalytic behaviour for ZrO_2-based catalysts.[3] Numerous binary $YZrO_x$ and $LaZrO_x$-based catalysts displayed high activity, selectivity and stability as well as comparable performance to $K–CrO_x/Al_2O_3$ catalysts over the course of 60 DDH cycles at 550 °C, 600 °C and 625 °C under industrially relevant conditions. The experimental parameters had a beneficial effect on the concentration of Zr_{cus}^{4+} ions, and the concentration of surface lattice oxygen, which in tandem play an active role in propane activation.

As discussed in the above sections, Zn has been used as a promotor in Cr and Pt catalysts. Sun *et al.* also investigated it as a promotor for Nb catalysts.[154] However, its use as a catalyst in its own right has recently been reported, notably by Yuan and co-workers. It was shown that ZnO nanoclusters supported in dealuminated zeolite-beta exhibited an initial propane conversion and propene selectivity of 53% and 97%, respectively at 600 °C. The initial STY was 4.2 $mol_{C_3H_6}$ kg^{-1}_{cat} h^{-1}, and the conversion dropped to 40% after 6 h on-stream due to coking. ZnO/H-ZSM-5 was also investigated by the same group and it was shown that high $SiO_2:Al_2O_3$ ratio supports yielded more selective DDH catalysts.[155] The presence of strong acid sites is known to promote coke formation *via* deep dehydrogenation and therefore this trend is expected. The highest STY yield was observed over 10 wt% ZnO/ZSM-5 where the SiO_2:Al_2O_3 molar ratio was 280, which produced 6.3 $mol_{C_3H_6}$ kg^{-1}_{cat} h^{-1} (Table 7, entry 12).

Kondratenko and co-workers reported the activity of ZnO supported on composites of N-doped carbon in silicalite-1.[156] Initial propane conversion and propene selectivity of the catalyst was *ca.* 52% and 89% respectively at. This corresponds to a STY of 6.3 $mol_{C_3H_6}$ kg^{-1}_{cat} h^{-1} (Table 7, entry 11). Although the catalyst was active in the absence of the N-doped carbon composite, *i.e.* ZnO/silicalite-1, the activity was over 3 times lower. The role of the N-doped carbon was to encapsulate the ZnO nanoparticles and maintain high dispersion of the active component.

Table 7 Catalytic performance of other selected catalysts for DDH reaction

Entry	Catalyst	T/°C	Feed composition	WHSV/$g_{C_3H_8}$ g_{cat}^{-1} h^{-1}	$X_{C_3H_8}$/%	$S_{C_3H_6}$/%	STY /$mol_{C_3H_6}$ kg^{-1}_{cat} h^{-1}	Ref.
1	$Pd_3–Fe$	510	$C_3H_8/H_2/Ar$ = 1.5 : 1.5 : 97	8.0	22	87	32	165
2	$Zn/ZrTiO_x$	550	$C_3H_8/H_2/N_2$ = 8 : 1 : 11	4.7	30	95	55	157
3	OMC-2	600	C_3H_8/N_2 = 1 : 19	0.6	66	71	5.7	169
4	$Co–Al_2O_3$	590	$C_3H_8/H_2/N_2$ = 1 : 0.8 : 3.2	3.2	25	97	16	160
5	Sn-HMS	600	C_3H_8/C_3H_6 = 99.87 : 0.13	0.4	40	90	3.0	163
6	PT-MCN	600	C_3H_8/Ar = 1 : 19	0.6	33	85	3.4	171
7	$CMSC_{700}$	600	C_3H_8/Ar = 1 : 19	0.6	41	89	4.5	168
8	$Ni_3–Ga/Al_2O_3$	600	C_3H_8/Ar = 1 : 9	2.4	13	94	6.1	166
9	ZrO_2	600	C_3H_8/Ar = 1 : 7.5	2.8	22	99	22	153
10	$CuZrO_x$	600	C_3H_8/Ar = 1 : 7.5	2.8	26	99	26	153
11	ZnO/CN-silicalite-1	600	$C_3H_8:H_2:N_2$ = 1 : 1 : 5	0.54	52	89	6.3	156
12	ZnO/H-ZSM-5	600	C_3H_8/Ar = 19 : 1	0.54	70	80	6.3	155
13	ZrO_2	600	C_3H_8/Ar = 1 : 1.5	11.7	28	86	64	151

T = reaction temperature; feed composition = molar ratio of C_3H_8/H_2/carrier in the reaction, $X_{C_3H_8}$ = initial propane conversion, $S_{C_3H_6}$ = initial propene selectivity, STY = space time yield.

While the above studies indicated that supported Zn catalysts can be selective DDH catalysts, the STY values were an order of magnitude below typical Pt and CrO_x based catalysts. However, this gap in performance was recently closed by Han *et al.*, who investigated a range of Zr-containing metal oxides as supports for Zn, including ZrO_2, $TiZrO_x$ and $CeZrO_x$ (as well as control catalysts without ZrO_2 such as Al_2O_3 and SiO_2).[157] High catalyst activity was observed when Zr was present in the support, which is expected given that it is active by iteslf.[151] However, the origin of the high activity could also be linked to the speciation of Zn. In the most active catalyst, 4 wt% Zn/$TiZrO_x$, the Zn was present exclusively as isolated tri-coordinated $Zn^{2+}O_x$. This catalyst produced a STY of 55 $mol_{C_3H_6}$ kg^{-1}_{cat} h^{-1} at 550 °C (Table 7, entry 2). Long term stability studies over 250 h and 10 regeneration cycles showed that a small drop in propane conversion and no loss in propene selectivity takes place. The drop in propane conversion was confirmed by ICP analysis to be due to loss of Zn from the catalyst. Temporal analysis of products studies were carried out to probe the rate-determining step of the reaction over supported Zn catalysts. Interestingly, it was shown that the formation of H_2 was rate-limiting in the catalyst, not C–H bond activation. Additionally, the presence of Ti in the catalyst support was shown to promote H_2 formation, which suggests that Ti in general is a good choice for a propane dehydrogenation catalyst. The observation that Zn–Zr catalysed DDH is not limited by C–H bond activation is a significant finding. As observed over similar catalysts, the rate of coke formation was dependent on acid and base sites, in this case present on the support. However, the best predictor of coke formation rate was the number of basic sites on the catalyst, which showed a strong positive correlation.

In section 3, the current commercial processes for propane dehydrogenation were presented and discussed. With the exception of the K-PRO process by KBR, all of the commercial catalysts have been disclosed. It is only known that the catalyst does not consist of Pt or Cr. We note that a patent was filed in the US in 2020 by Mukherjee *et al.* at Exelus, inc. (who developed the catalyst that is licensed to the K-PRO process)[158] for alkane dehydrogenation using a catalyst consisting of Zn, Zr and Ti oxides.[159] The optimal loadings and formulations disclosed in the patent are very similar to those reported by Han *et al.*[157] and therefore we tentatively suggest that the catalyst in the K-PRO process is likely to be based on Zn–Zr–Ti–O_x.

Co-Based catalysts have also been demonstrated as potential alternatives to Pt- and Cr-based catalysts. Dai *et al.* reported a Co/Al_2O_3 catalyst with a high stability and selectivity (>97% propene selectivity), and a corresponding STY of 16 $mol_{C_3H_6}$ kg^{-1}_{cat} h^{-1} (Table 7, entry 4).[160] Through extensive characterization it was observed that the Al_2O_3 sufficiently stabilized isolated Co_2^+, preventing surface reconstruction of Co species under reaction conditions. As a result, the catalyst efficiently facilitated propene desorption, inhibiting the formation of coke and other by-products. The application of a reductive-reoxidation treatment positively affected dehydrogenation performance of Co/Al_2O_3 catalysts.[161] An initial propene yield of 28% and high selectivity to propene (>93%) was obtained over the course of the reaction. The authors attributed this to increased dispersion of Co metal species, a consequence of the mild reoxidation conditions resulting in markedly smaller (6 nm) Co metal nanoparticles, contrary to those observed in the fresh (34 nm) and reduced counterparts (25 nm).

As an efficient promoter of Pt-based catalysts, Sn was previously thought to be an inactive metal for dehydrogenation reactions. Surprisingly, metallic Sn supported on SiO_2 has proven to be an efficient, dehydrogenation catalyst, exhibiting a sustained propene yield of 30% over the course of a 70 h DDH reaction at 600 °C.[162] The incorporation of a hydrogenation component (Pd) can improve the stability of this catalyst, however, loss of Sn metal under reaction conditions, as a consequence of its low melting point, requires further investigation into more suitable supports than SiO_2. Hexagonal mesoporous silicas have emerged as possible candidates due to Sn-HMS exhibiting high propane conversion (*ca.* 40%) and enhanced stability after multiple oxidative regenerations and 170 h on-stream.[163] The improved stabilization is a result of two factors: firstly, Sn incorporation into the lattice of HMS forms strong Sn–O–Si bonds, which inhibit Sn reduction to low melting point Sn^0, and secondly, additional stabilization of the Sn species is induced by the mesoporous structure of the HMS support.

Wang *et al.* revealed the dependency of the nature and distribution of SnO_x species on the Sn loading, and through advanced characterization revealed uniform distribution and stabilization of isolated Sn^{4+} species in fresh samples, whilst being stabilized in the Sn^{2+} state after reduction on SiO_2 due to strong metal–support interactions.[164] Superior long-term stability, as well as recovery of the initial activity upon oxidative regeneration, suggests that these materials could be very promising DDH catalysts.

Pd and Pd_3–Fe supported on SiO_2 exhibited propene yields of 4.5% and 9.4% respectively at 510 °C. The bimetallic catalyst exhibited a much higher propene yield than Pd-only, despite both catalysts having a similar average nanoparticle size (*ca.* 2 nm).[165] The STY of the Pd_3–Fe catalysts was 32 $mol_{C_3H_6}$ kg^{-1}_{cat} h^{-1} (Table 7, entry 1). This was partly due to a geometric effect in the formation of the Pd_3–Fe alloy nanoparticles, breaking the ensemble of Pd, thus enhancing the selectivity and suppressing structure sensitive C–C hydrogenolysis and coking reactions. Electronic effects, often thought to promote high selectivity in Pt dehydrogenation catalysts, were not concluded to strongly influence the selectivity of Pd_3–Fe/SiO_2.

Recent advances in catalyst design have yielded non-noble-based intermetallic compound (IMC) catalysts, which present unique surface and catalytic chemistry that may be promising for propene production. He *et al.* explored highly selective and stable phase-pure Ni_3–Ga IMC nanoparticles with Ga-rich surfaces supported on Al_2O_3. These exhibited high selectivity (~94%), good stability over long term (82 h) testing and regeneration ability at 600 °C, resulting in a STY of 6.1 $mol_{C_3H_6}$

kg^{-1}_{cat} h^{-1} (Table 7, entry 8).[166] In order to compare with industrial-type catalysts, Pt–Sn/Al_2O_3 (Oleflex) and CrO_x/Al_2O_3 (CATOFIN) catalysts were prepared and tested under the same reaction conditions. It was shown that the Ni_3–Ga/Al_2O_3 catalyst exhibited comparable conversion to Pt–Sn/Al_2O_3 and inferior conversion to CrO_x/Al_2O_3, although after 14 h on-stream the CrO_x/Al_2O_3 had deactivated to a similar conversion as Ni_3–Ga/Al_2O_3. Although the authors claim that Ni_3–Ga/Al_2O_3 exhibited comparable performance to the commercial catalysts, there is no indication that the Pt–Sn/Al_2O_3 and CrO_x/Al_2O_3 catalysts prepared in this work would be as active as the actual commercial catalysts. Furthermore, the STY of all of the catalysts was an order of magnitude below the literature values associated with Pt–Sn and CrO_x catalysts (Tables 3 and 4, respectively).

Typically, oxygenic functional groups on the surface of carbonaceous materials, high surface area, stable structure, tuneable nanoscale dimensions and porosity are all important parameters which determine the efficiency of metal free carbon-based dehydrogenation catalysts. The induced activity of the oxygenic functional groups is a consequence of localization of π-electrons from defects, edges and vacancies.[167] Meanwhile, their porous structures are key determinants in achieving efficient mass and diffusion transfer.

Hu *et al.* recently reported the exploitation of biomass-derived porous carbon materials as dehydrogenation catalysts prepared by a simple alkali (KOH) activation method.[168] The carbon catalyst activated with KOH at 700 °C exhibited the best catalytic activity, displaying an initial propene yield of 36.6% and a STY of 4.5 $mol_{C_3H_6}$ kg^{-1}_{cat} h^{-1} (Table 7, entry 7). The activity was attributed to the carbon catalysts possessing high surface area, hierarchical porous structure, and abundant oxygenated functional groups. Interestingly, no carbon deposition was observed with a carbon balance of 100% being maintained over 10 h of reaction time, rendering high stability signified by negligible loss in surface area and pore volume.

Recent interest into mesoporous carbons has yielded numerous dehydrogenation catalysts, with the large and well-ordered porosity proving beneficial for mass transport while long term stability (of up to 100 h) has also been shown, which exhibited an STY of 5.7 $mol_{C_3H_6}$ kg^{-1}_{cat} h^{-1} (Table 7, entry 3).[169] As discussed above, it has been previously mentioned that coke formed in the DDH reaction can catalyse the reaction itself, so it is expected that carbonaceous catalysts would exhibit some activity. Of course the obvious drawback of such catalysts is the inability to burn off the coke, as would be typically done over mixed metal oxide or supported Pt catalysts in order to regenerate them. Mesoporous carbons prepared *via* a soft templating method and carbonized at 600 °C, 700 °C and 800 °C were investigated by Hu *et al.*[170] The increase in carbonization temperature positively influenced the propene selectivity of the aforementioned catalysts to 85.6%, 88.7% and 93.5%, respectively. The authors observed tuneable concentrations of the C=O, O=C–O and –OH functional groups by adjusting the carbonization temperature. As such, low carbonization temperatures (600 °C) enhanced deep cracking due to surface acidic sites (*e.g.* O=C–O), hindering propene desorption. The subsequent increase in carbonization temperature (up to 700–800 °C) caused the decomposition of the acidic sites, thus increasing propene selectivity. Consequently, a linear relationship between the concentration of C=O groups and specific activity was established. The application of resorcinol-formaldehyde and Pluronic F127 also induced different pore ordering, with highly ordered mesoporous carbons displaying improved catalytic performance as a result of more accessible active sites and favourable mass transport properties.

Moreover, Pan *et al.* reported the modification of carbon with phosphorus from various sources, which introduced defects, forming numerous surface functional groups.[171] It was found that P modification of mesoporous carbon with triethyl phosphate had a promoting effect relative to $(NH_4)_2HPO_4$- and H_3PO_4-modified mesoporous carbon displaying initial propene yields of 27.2%, 18.7% and 17.2%, respectively. The most active catalyst exhibited a STY of 3.4 $mol_{C_3H_6}$ kg^{-1}_{cat} h^{-1} (Table 7, entry 6). The improved catalyst performance was attributed to larger specific surface area, pore volumes, and pore sizes, as well as an increased number of carbonyl/quinone groups and a higher degree of graphitization.

There are many non Pt, Cr, Ga and V containing catalysts in the literature that have not been given the same attention as the aforementioned elements. Notable examples include Zn/$ZrTiO_x$ and ZrO_2, which in terms of STY, outperform many Pt and Cr-based catalysts. These catalysts consist of non-toxic, abundant elements and are good candidates for commercialisation. Based on an analysis of the patent literature and commercial press releases, we suggest that the catalyst in the K-PRO process consists of a mixed metal oxide of Zr, Zn and Ti. Despite very impressive catalyst performance, investigations into Zn and Zr catalysts are very few. In contrast to Pt, Cr, Ga and V catalysts, which have been extensively studied and are fairly well-understood, Zn and Zr catalysts should be studied in greater detail to better understand the active species involved and how the performance can be further improved.

In conclusion, the direct dehydrogenation of propane can be catalysed by a broad range of metal oxides. Pt and Cr-based catalysts constitute the most commonly reported catalysts and are amongst the most active, which is not surprising given that both of these have been implemented in commercial processes. However, improvements in this sub-field of catalyst research has been incremental for some time and it is unlikely that a step-change in activity will be realised by further investigation. In contrast, Zr and Zn based catalysts are relatively immature and there are many opportunities to prepare highly active, stable DDH catalysts using these elements. Despite numerous investigations into coke formation over various catalysts, all DDH catalysts are prone to coking to some extent, and this remains the frontier in DDH catalyst design. More often than not, the origin of coke formation is due to strong acid/base sites on the support, or specific structures of the active component. Careful preparations and appropriate promotors can help to neutralise coke formation, but this can come at the expense of propene selectivity or propane conversion.

5. Oxidative dehydrogenation with oxygen

The oxidative dehydrogenation of propane using oxygen (ODH-O_2) is an attractive route to propene due to favourable thermodynamics, theoretically being unlimited and exothermic is highly beneficial for industrial scale-up. Oxygen is cheap and non-toxic, but conditions must be controlled to ensure that the oxygen/propane ratio is not flammable. Regarding safety and industrially relevant processes, if selectivity is improved further for ODH-O_2, then the reaction could be an exciting and useful process. In general, productivities are not currently high enough to be of interest for industrial application due to the low selectivity of many metal oxide catalysts, but more recent developments in the field may change this, with boron-based catalysts forming ethene as a secondary product in contrast to CO_x products over metal oxide catalysts.

ODH-O_2 reaction pathways are much simpler than DDH and ODH-CO_2, with fewer side reactions and products forming over typical catalysts. Overoxidation is the main limitation in ODH-O_2. For metal oxide-based catalysts, gaseous oxygen is utilised *via* a Mars-Van Krevelen mechanism, with lattice oxygen abstracting hydrogen from propane. The following section describes the most significant literature reports on catalysts for ODH-O_2.

5.1. Vanadia based ODH-O_2 catalysts

The first vanadia-based catalysts for oxidative dehydrogenation were V–Mg–O catalysts applied for the ODH-O_2 of butane. In 1988, V–Mg–O catalysts were found to be active and selective to propene when compared to V_2O_5 and MgO.[172] Since this early discovery, there have been many investigations into V-based catalysts for ODH-O_2, which have focussed on catalyst optimisation as well as understanding the nature of the active site.

Sam *et al.*[173] analysed $Mg_2V_2O_7$, which in contrast to other V–Mg–O phases tested, contained vanadium species with a V=O bond. $Mg_2V_2O_7$ exhibited a conversion of 6.9% and propene selectivity of 53.5% at 550 °C, which was much more productive than $Mg_2V_2O_8$ and $Mg_2V_2O_6$. This early work highlighted the importance of the V=O bond in producing effective ODH-O_2 catalysts. Corma *et al.* later examined the influence of supports for supported vanadia catalysts.[174] It was shown that VO^{2+} pairs present in V_2O_5 are active for ODH-O_2 but were also the source of overoxidation to CO_x products. More acidic supports, such as silica, decreased dispersion and therefore more V_2O_5 was detected, compared to more basic supports such as MgO and TiO_2. It was also found that if the V=O bonds were adjacent to V–O sites, then overoxidation occurred. Limiting the formation of V_2O_5 and forming V–O sites with tetrahedral coordination was found to be crucial to forming a selective catalyst.

Subsequent reviews of the literature by Kung and Kung,[175] and Blasco and López Nieto[176] further highlighted that V=O bonds were the active sites for ODH-O_2 in these materials. These reviews have guided modern investigations to focus on preparing isolated V species on metal oxide supports, rather than Mg-containing mixed oxide materials. It was shown that ODH-O_2 rates initially increase with VO_x surface density but decrease when V_2O_5 crystallites form at high V loadings, due to agglomeration of particles. It was also found that the formation of V_2O_5 crystallites significantly reduced the selectivity to propene, as the surface propyl species will react over two V atoms.[177] The formation of V_2O_5 was shown to occur at lower V loadings for more acidic supports, such as SiO_2, whilst using a high surface area silicate, MCM-41, was found to maintain a high STY due to a larger area for dispersion.[178] A general trend can be shown across the literature in which isolated VO_4 species (sometimes denoted as monomolecular or monomeric) are predominant at low vanadium loadings, and as the VO_x surface density increases, the predominant V species become V_2O_7 dimers, forming polymeric vanadia across the surface (also commonly denoted in the literature as polyvanadate, V_2O_5-like, 2-dimensional or more generally, VO_x). With higher V loadings, V_2O_5 crystallites become present (also denoted as 3-dimensional species), as shown in Fig. 7. This has been shown to be the case for many supports including SBA-15,[179] TiO_2[180] and γ-Al_2O_3[181]

The density of isolated V sites can also be influenced by the nature of the support, and some supports can sustain a higher density of isolated V sites compared to others. For example, a higher density of isolated V sites was achieved on SBA-15, when compared to conventional SiO_2 and MCM-41, due to a lower surface acidity.[183] The loading of vanadia required to sustain only monomeric sites is 8–9 V nm^{-2} on most supports, with SiO_2 showing a maximum loading of 3.3 V nm^{-2} for monomer only coverage.[184] SiO_2 tends to have a poor interaction with the vanadia precursor species in general due to similarities in the acidity of both, so dispersion of V atoms is lower. Depending on the preparation method, monomolecular or polymeric species can exist with high dispersion, or 3-dimensional V_2O_5 crystallites can form even below monolayer coverage.

An in-depth review of vanadia based catalysts for ODH-O_2 was undertaken by Carrero *et al.*[4] in 2014. The review highlighted that the activity of supported vanadia catalysts can be explained by one scaling parameter: the energy of oxygen defect formation. This in turns defines the reducibility of the site and therefore the redox potential. In practice, the formulation of the oxide support, the V loading (and subsequently, the dispersion and speciation) all affect the final catalyst structure and give rise to the wide-range of performances reported. The review also highlighted the complexity in the relationship between V species and catalytic activity: not all VO_4 units are equally active; the local geometry and support affect the reducibility and therefore activity. In fact, the authors concluded that despite many reports in advancing the synthesis of supported VO_X catalysts, only a minority of surface species are highly active. Since 2014, several studies have further improved vanadia dispersion and subsequently, the catalyst performance. The most significant advances in this endeavour are discussed below.

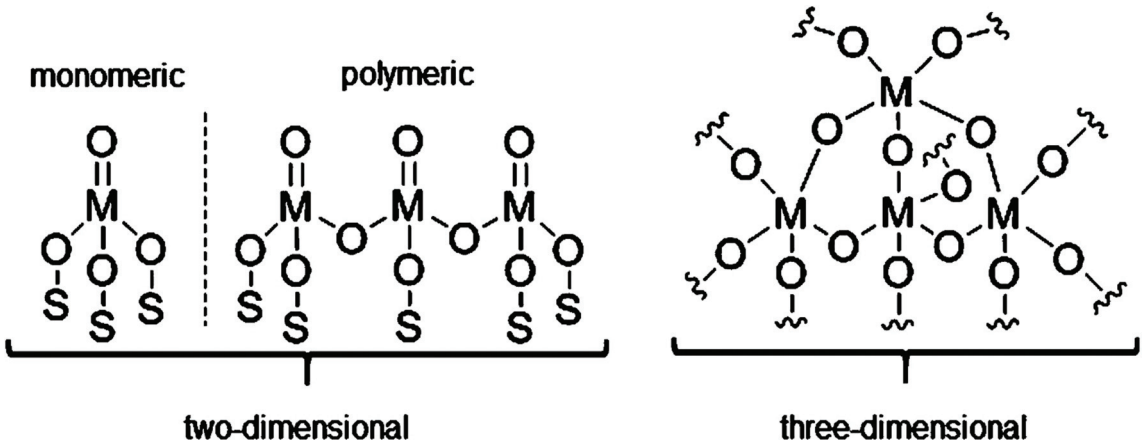

Fig. 7 Two dimensional (monomeric and polymeric) and three-dimensional structures for supported metal catalysts. S = support atom, M = support metal.[182]

The use of acidic supports has been probed, as acidity has been shown to increase the activity of ODH-O_2 catalysts. Supporting VO_x supported on H-ZSM-5 was shown not to enhance performance since, despite the acidity of the support increasing propane conversion for low V loadings. The support influence was detrimental to selectivity and overall lowered the propene yield. The isolated VO_x species present at low V loadings became reduced at a lower temperature compared to polyvanadate species and V_2O_5, suggesting that isolated species can facilitate oxidation of propane more effectively.[185]

In contrast, vanadia has been supported on Al_2O_3 that was doped with varying concentrations of MgO to induce basic site functionality.[186] Increasing the Mg content led to a decrease in strong acid sites, decreasing activity, consistent with the fact that strong acid sites can activate propene. An Mg/V ratio of 0.8 showed the highest yield of propene, as the ratio of Mg/V balanced the effects of strong acid sites for propane conversion, whilst limiting overoxidation through the addition of Mg resulting in a change of surface species and acidity. The strength of the V–O bond was also influenced by Mg doping, with the binding energy of V–O bonds increasing with increasing Mg content. This effect increased selectivity by decreasing overoxidation due to the inhibited lability of lattice oxygen.

Zhang and Liu[187] also investigated V–Mg–O catalysts with the aim of increasing the loading whilst maintaining a high level of dispersion on SBA-15, which has previously been show V_2O_5 crystallite formation even at low loading levels. To limit agglomeration of vanadia, co-impregnation of V and Mg was undertaken which resulted in the suppression of 3D V_2O_5 crystallite formation. In this investigation, it was shown that with increasing V content, the V environments went from isolated VO_4 species to $Mg_3V_2O_8$, and no crystalline V_2O_5 was detected, even with V loading levels of 25 wt% when using co-impregnation of V and Mg. The $Mg_3V_2O_8$ phase was shown to be intrinsically more selective than dispersed VO_4, and at 20% propane conversion, propene selectivity was found to be higher for Mg–V–O catalysts, than V–O catalysts, with some dependence on crystallite size (a 20–30 nm crystallite size gave the highest propene selectivity of ~59%). Small $Mg_3V_2O_8$ crystallites showed preferential kinetics (*i.e.*, a higher rate of propene formation compared to rate of combustion and rate of propene formation) when compared with dispersed VO_4 species, since the latter have an increased preference for propene oxidation compared to $Mg_3V_2O_8$. This is interesting as H_2-TPR showed a lower level of reducibility for $Mg_3V_2O_8$ when compared to VO_4 species, suggesting that former catalyst was sufficiently reducible to achieve oxidation of propane, but not to overoxidise to CO_x products.

Supporting vanadia on SBA-15 *via* wet impregnation has been explored and a loading of 6.6 wt% V achieved a surface density of 1.6 V nm^{-2}, the highest surface density achieved on SBA-15 without V_2O_5 crystallite formation; coverage was increased by rehydrating the support before impregnation, aiding dispersion.[188] The increased dispersion led to an increased selectivity when compared to similar catalysts. Zhu *et al.* investigated pre-treatment of the support, with the simple idea that modifying the support before loading V could control the dispersion.[189] A SiO_2 support was treated at different temperatures before grafting $VOCl_3$ onto the surface. Higher temperature treatments (700 °C to 1000 °C) resulted in the removal of neighbouring silanols and only isolated silanols were detected using IR spectroscopy. Isolated silanols can anchor VO_x species, and isolated silanols would be expected to produce monomeric VO_4. Due to the silanol site concentration decreasing, the loading of vanadia decreased with increasing support pre-treatment temperature. However, the increase in pre-treatment temperature also led to an increase in monomeric vanadia sites compared to dimeric sites. The catalysts with the highest abundance of isolated monomers showed the highest propene selectivity of 90% at 500 °C and 68% at 600 °C (Table 8, entry 4), leading to the conclusion that monomeric sites are more selective than the polymeric structure. This study highlighted the difference in selectivity between different VO_x species. It must be noted that no 3D V_2O_5 crystal-

Table 8 Summary of catalytic performance of selected vanadia based ODH-O_2 catalysts

Entry	Catalyst	T/°C	O_2/C_3H_8	WHSV/h^{-1}	$X_{C_3H_8}$/%	$S_{C_3H_6}$/%	STY/$mol_{C_3H_6}$ kg_{cat}^{-1} h^{-1}	Ref.
1	5V-Zr–O fibres	400	0.5	70.8	4.0	64.6	38	192
2	0.4Na^+–V–SiO_2	490	0.5	19.3	6.5	66	17	182
3	3V/γ-Al_2O_3	500	0.5	4.7	12.5	75.9	9.4	194
4	$VO_x/SiO_{2-(1000)}$	500	1	4.7	30	60	18	189
5	3V-DMSN	500	0.5	6.3	10.4	66.5	9.1	146
6	V/SiO_2 (SOMC)	525	0.5	118	5	66	82	190
7	1.8V-KIT-6	550	1	4.7	46.2	64.5	30	193

T = reaction temperature O_2/C_3H_8 = molar ratio of $CO_2 : C_3H_8$ in the reaction, $X_{C_3H_8}$ = initial propane conversion, $S_{C_3H_6}$ = initial propene selectivity, STY = space time yield. Value next to element/phase represent wt%.

lites were detected when using $VOCl_3$ grafting on heat-treated SiO_2 supports, and therefore selectivity to propene was maintained.

To probe the influence of monomer sites, Barman *et al.*[190] grafted monomeric V species onto SiO_2 using surface organometallic chemistry (SOMC). This approach represents another example of changing the preparation technique to increase dispersion. It was found in this study that monomeric vanadia species are intrinsically more selective. The incipient-wetness impregnation technique formed catalysts which were more selective than SOMC catalysts below 500 °C, but above this temperature, the SOMC catalysts exhibited an equivalent or even higher selectivity. A STY of 82 $mol_{C_3H_6}$ kg_{cat}^{-1} h^{-1} (Table 8, entry 6) was measured over V/SiO_2 prepared *via* SOMC.

In addition to high dispersion and control of oxygen environments of the vanadia, tailored support properties are crucial in optimising ODH-CO_2 performance. A widely debated topic in catalysis is the effect of support porosity on catalytic properties. The preparation route of Al_2O_3 was varied to form flower-like, sphere-like and bulk-like morphologies to investigate the influence of varying porosities. Bulk-like morphology only exhibited intraparticle pores, and the monolithic architecture of γ-Al_2O_3 (formed by a roasting method) achieved the highest productivity for ODH-O_2, despite the surface vanadia species being consistent across all architectures, with the degree of polymerisation being fairly similar for all Al_2O_3 structures as (shown by adsorption edge energy analysis).[191] The bulk-like morphology showed a lower resistance to external mass transfer, and reduced the residence time of propene through the catalyst bed, lowering the tendency for further reactions.

Mesoporosity was also explored when forming fibrous vanadia catalysts *via* electrospinning. A comparison between fibrous catalysts which presented mesoporosity, and particle-like catalysts without apparent mesoporosity, indicated no influence on catalytic performance due to porosity,[192] consistent with the aforementioned morphology analysis. However, it is interesting to note that a change in preparation technique changed performance. A one-step synthesis to form $VZrO_x$ catalysts was found to form the most active catalyst with 5 wt% V loading, when compared to incipient wetness impregnation catalysts. Incipient wetness impregnation with 5 wt% V loading showed the formation of 3D-V_2O_5 crystals, known to be detrimental to selectivity, whilst the one-step process did not show evidence of V_2O_5 formation and improved the dispersion of isolated VO_x sites. It is also noteworthy that the $VZrO_x$ catalysts from the research by Ternero-Hidalgo *et al.* operate at a lower temperature, namely 400 °C, when compared to other catalysts in the field (Table 8, entry 1) and achieved a STY of 38 $mol_{C_3H_6}$ kg_{cat}^{-1} h^{-1}.

Vanadia supported on dendritic mesoporous silica nanoparticles (V-DMSN) was formed *via* a one-step synthesis as DMSN materials were found to have large pore volumes and a larger surface area than conventional mesoporous silica.[146] The one step synthesis, similar to the $VZrO_x$ catalysts discussed previously, led to higher dispersion and a higher stability of vanadia on the DMSN support when compared to incipient wetness impregnation (denoted V/DMSN). A surface V density of 0.55 V nm^{-2} (2 wt% V), gave the highest STY of 9.1 $mol_{C_3H_6}$ kg_{cat}^{-1} h^{-1} (Table 8, entry 5). H_2-TPR analysis revealed that the isolated V species were more reducible, which is a strong predicter of activity in ODH-O_2.

Despite SiO_2 having a large surface area, and that many different types of silica supports having been tested, the low reactivity of silanol groups towards V precursors means that a relatively low loading of isolated V sites are reported. Doping the SiO_2 surface with 0.4 wt% Na^+ enhanced the V dispersion to a level corresponding to monolayer coverage (*i.e.*, 8.6 V nm^{-2} for 6.2 wt% V loading) (Table 8, entry 2), which is equivalent to many other metal oxide supports.[182] It was hypothesised that Na^+ ions provide a source of Si–O–Na^+ surface species, which facilitate increased monomeric vanadia species, boosting the propane conversion. However, it should be noted that the intrinsic activity of the V/SiO_2 catalysts did not increase; the calculated TOFs were similar for V supported on promoted and unpromoted SiO_2. Instead, the presence of Na^+ simply facilitated a greater density of isolated V sites. The activity of the Na^+ promoted V/SiO_2 was sustained for 4.5 days and post-reaction Raman spectroscopy showed no formation of 3D V_2O_5 crystallites. This is an excellent example of doping having a beneficial effect. However, it is sometimes found that doping has deleterious effects on redox properties. For instance, doping with K^+ was found to decrease the selectivity and activity when compared to V-only supported catalysts.[193] When loaded onto KIT-6 supports, the V began to segregate

with the addition of K^+ ions because VO_x and K^+ have a strong interaction, which led to the formation of unselective K^+ and V mixed phases such as potassium vanadate. The interaction between K^+ and VO_x species decreased the reducibility of the catalyst. Interestingly, K^+ incorporation led to an increase in the ethene to propane ratio, but the alkene yield was decreased overall. The incorporation of basic metal oxides should be done cautiously, as the benefit of enhanced propene desorption can be outweighed by the detrimental effects on the redox properties of the catalysts.

In conclusion, vanadia catalysts have been extensively investigated for ODH-O_2, with the main focus being on maximising the number of isolated vanadia species, which is fundamental to increasing propene selectivity. A more precise view of vanadia species in recent studies has shown isolated vanadia sites to be more selective than polymeric species which contain V–O–V bridging bonds. Therefore, high activity is associated with high V dispersion. Acidic supports inherently decrease V dispersion, thus decreasing selectivity and overall productivity despite increasing activity. More frequently, there are reports of dispersion being influenced by the preparation technique, with grafting vanadia onto the support surface showing promise. However, a one-step synthesis of support and vanadia, in contrast to analogous surface impregnation catalysts, has been shown to improve catalyst productivity. The one-step synthesis method was shown to improve productivity for different support materials, morphologies and loadings when compared to analogous catalysts formed with more traditional surface loading techniques. Research into one-step synthesis methods is far from exhausted and shows considerable potential for further development. In contrast, incipient-wetness techniques can still be improved, with hydration of the surface or doping being effective strategies. Doping has been shown to influence the intrinsic reactivity of the active sites, but an increase in activity is usually accompanied by a decrease in selectivity. Increasing selectivity *via* dispersion techniques may be deemed a more promising route to improving catalytic performance. The choice of support material composition and chemical properties is more influential than morphology on overall catalytic performance; many studies comparing mesoporous catalysts with bulk-like morphologies found mesoporosity to have either a detrimental or negligible effect on productivity. Porosity can, however, increase specific surface area and therefore support a higher loading of isolated vanadia sites.

5.2. Boron-based ODH-O_2 catalysts

Boron based catalysts are relatively new to the field of dehydrogenation catalysis. Hexagonal boron nitride (h-BN) has historically been used a catalyst diluent due to its high thermal stability under oxidative conditions. The 2-D structure of h-BN also allows for high thermal conductivity *via* efficient phonon transmission across the sheets of BN.[195] High thermal conductivity is appealing with regards to industrial application, as this limits the formation of hot spots, and selectivity becomes more controllable. The discovery that h-BN catalyses propane dehydrogenation was first reported in 2016[196] and since then there has been significant developments in the understanding of the active centres and reaction mechanisms. In the initial investigation, h-BN (Table 9 entry 8) was observed to catalyse ODH-O_2, with similar activity to V/SiO_2 catalysts. However, boron nitride nanotubes (BNNTs) displayed higher productivity, selectivity and yield than conventional V-SiO_2 catalysts with the BNNT having a STY of 110 mol_{C3H6} kg_{cat}^{-1} h^{-1} (Table 9, entry 1), which is ~7 times greater than the analogous V/SiO_2 materials tested.[196] Fig. 8 illustrates this difference in performance. In contrast to supported VO_x catalysts that produce CO_x, the major by-product is typically ethene, which is of course more valuable than carbon oxides.

Such a different product distribution hints at a distinct reaction mechanism from other metal oxide ODH-O_2 catalysts, and investigations into the reaction mechanism have suggested as much. First order dependence on O_2 partial pressure and second order dependence on propane partial pressure was noted by Grant *et al.*[196] It was also suggested that molecular oxygen forms an "armchair" from B to N at the platelet edges to form a B–O–O–N active site, but subsequent studies found catalysts without any N present were also highly active.

Edge-hydroxylated boron nitride (BN-OH) was subsequently reported to have the highest productivity of any previously reported catalyst for the dehydrogenation of propane.[197] BN-OH catalysts were also shown to be stable over 300 h on-stream (with no significant reduction or change in selectivity

Table 9 Catalytic performance of selected boron-based catalysts for ODH-O_2

Entry	Catalyst	T/°C	O_2/C_3H_8	WHSV/h^{-1}	$X_{C_3H_8}$/%	$S_{C_3H_6}$/%	STY/$mol_{C_3H_6}$ kg_{cat}^{-1} h^{-1}	Ref.
1	BNNT	490	0.5	31.7	6.5	76	110	196
2	BN/DFNS	490	1	1.2	18	59.4	2.4	198
3	Elemental B	490	2	152.7	9.8	83	280	199
4	$10B_2O_3$/SBA-15	500	1.5	9.5	31.5	64	43	207
5	BN-OH	530	1.5	37.6	20.6	80.2	130	197
6	Macroporous BPO_4	535	1.5	93.9	20.8	78.1	320	211
7	SiB_6	545	1.5	9.5	31.1	72.1	48	201
8	h-BN	560	0.5	4.0	14	79	11	196

T = reaction temperature; O_2/C_3H_8 = molar ratio of $O_2 : C_3H_8$ in the reaction, $X_{C_3H_8}$ = initial propane conversion, $S_{C_3H_6}$ = initial propene selectivity, STY = space time yield. Values next to element/phase represent wt%.

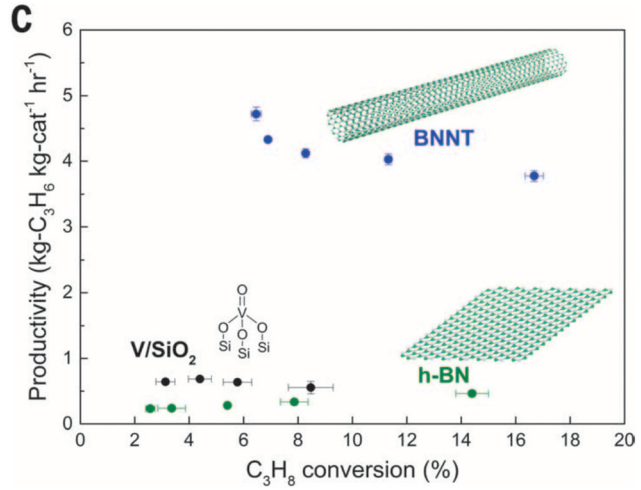

Fig. 8 Comparisons of propene productivity plotted as a function of C_3H_8 conversion between V/SiO_2, h-BN, and BNNT. V/SiO_2: 5 to 15 kg-cat s mol $C_3H_8^{-1}$; h-BN: 15 to 40; BNNT: 2 to 5; T = 490 °C, P_{O2} = 0.15 atm, P_{C3H8} = 0.3 atm. Reproduced from ref. 196 with permission from The American Association for the Advancement of Science.

at 530 °C). The BN-OH materials were catalytically active after O_2 activation, with DFT calculations suggesting that neighbouring B-OH sites formed B–O–B linkages once both B-OH groups are dehydrated. The sites could be reduced back to BN-OH using steam. Clear discrepancies were seen between previously proposed reaction mechanisms and explanations on how structure influences catalytic activity, showing that *in situ* edge functionalisation is key to catalytic activity. When comparing supported BN and supported B_2O_3 on dendritic fibrous nanosilica (termed BN/DFNS and B_2O_3/DFNS respectively), BN/DFNS showed improved productivity relative to B_2O_3/DFNS, although both were active.[198] This finding is noteworthy, as it shows that BN on the surface can be oxidised to B_2O_3 during the reaction. The as-prepared BN catalysts however already contained a large proportion of hydroxyl groups, underlining the importance of hydroxylated B in catalysing ODH-O_2. This observation is consistent with the activity trends noted for edge-hydroxylated BN (Table 9, entry 2).

Subsequently, the Hermans group probed the influence of heteroatoms on activity and selectivity of boron-based catalysts using a range of metal borides, including B_4C, TiB_2, elemental B (Table 9, entry 3) and WB amongst others. Elemental boron showed a remarkably high STY of 280 $mol_{C_3H_6}$ kg_{cat}^{-1} h^{-1},[199] which represented an improved productivity over BN-OH catalysts that had been previously described in the literature. In a subsequent review, it was noted that the propene selectivity was the same at isoconversion for every boron material that was tested,[200] suggesting that the boron heteroatom is the source of the active site. Metal borides with a high oxygen and boron surface content showed the highest productivities and the presence of BO_x species have been identified as essential for catalytic activity. The catalytic activity of various B compounds depended on the concentration of B at the surface. Under ODH-O_2 conditions, the B is oxidised to BO_x, which is the active site. It was also shown that the activation of O_2 is the rate-limiting step for boron-based catalysts in ODH-O_2. These new insights disproved the previously suggested mechanism that required N.

Yan *et al.* reported that silicon boride was active for the oxidative dehydrogenation of propane, ethane and isobutane.[201] At 545 °C, SiB_6 exhibited a STY of 48 $mol_{C_3H_6}$ kg_{cat}^{-1} h^{-1} (Table 9, entry 7) and subsequent stability tests at 545 °C showed that a propane conversion of 20% and propene selectivity of 80% could be maintained over the 100 h experiment.

An extended literature review by Shi *et al.*[5] in 2018 outlined recent advances in testing and further understanding of structure–performance relationships. Key comparisons were drawn between traditional V catalysts and the highly promising B catalysts. In particular, CO_x selectivity for edge hydroxylated boron catalysts was shown to be 0.5%, in comparison to 10–50% for V-based catalysts, whilst productivities for boron catalysts can be maintained for 300 h. Mechanistic studies showed oxygen to have a reaction order of 0.5, suggesting that dissociative adsorption of oxygen is of importance to facilitate the reaction, whilst in the absence of oxygen catalysts had no activity. *In situ* infrared analysis has demonstrated that the presence of OH groups led to the interaction of molecular oxygen with the surface. Interestingly, alkane partial pressure was shown to have a reaction order of 2,[197] with two propane molecules needed during the reduction phase of the redox cycle, to form the two adjacent BN-OH sites in the original catalyst (Fig. 9).

As described above, there are differences in the reaction mechanism between boron-based catalysts when compared to supported metal oxide catalysts. For example, h-BN and other boron-based catalysts do not function for non-oxidative propane dehydrogenation,[199] whilst metal oxides do function initially and do not require an induction period. This shows that boron-based catalysts form the necessary active sites under reaction conditions, and that the initial catalysts can be perceived as precursors to the active phase. Propane partial pressures exhibit a second order rate dependence for h-BN, whereas in metal oxides it is first order. Metal oxide catalysts such as VO_x and MoO_x used for ODH-O_2 operate using *via* a Mars-Van Krevelen mechanism, whilst h-BN cannot do this due to the absence of lattice oxygen.[200] Therefore, in order to optimise boron-based catalysts, a more complete understanding of the reaction mechanism must be developed to tailor the nanostructure to the process.

DFT studies of optimised structures of h-BN have been undertaken to probe the ODH-O_2 reaction mechanism. The dissociative O_2 adsorption was shown to be favoured on B terminated edges, rather than N terminated edges, leading to B atom terminated platelet edges being more active. DFT calculations also showed that the dehydrogenation reaction at B atom terminated edges is favoured over C–C bond breaking due to kinetic and thermodynamicfactors.[203] Other DFT studies have built upon the understanding that boron is the active centre for ODH-O_2 and suggest that C–H abstraction is

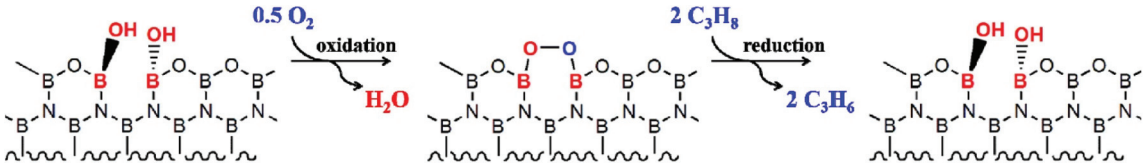

Fig. 9 Proposed reaction mechanism for ODH-O_2 over boron nitride catalysts for the oxidative dehydrogenation of propane. Reproduced from ref. 202 with permission from Elsevier.

undertaken by heterolytic cleavage over a B–O pair in a BO_3 active structure. It has been suggested that O_2 abstracts the hydrogen from the newly formed O–H group, reducing O_2 to HO_2, and subsequently forms B-OOH and B-C_3H_7 on neighbouring BO_3 sites. The HO_2 group then abstracts hydrogen from the propyl surface intermediate to form propene, whilst H_2O_2 breaks down to form H_2O and the BO_3 active site is regenerated.[204]

Experimental studies comparing h-BN and VO_x/Al_2O_3 once more highlighted the different reaction mechanisms at work. It has been shown h-BN exhibited a C_2/C_1 product ratio of 2, whilst the VO_x catalyst shows almost no C_2 products, and complete oxidation to CO_x dominated.[205] This implies that different reaction pathways dominate, with only the first C–C bond cleavage being favourable for h-BN catalysts, leaving the methyl group to have many different reaction pathways. Interestingly, an increase in C_2H_4 selectivity was recorded with increasing temperature. Methyl radicals generated from C–C bond cleavage over h-BN catalysts can undergo four secondary reactions which include oxidative coupling of the methyl groups to produce C_2 products. The oxidative coupling leads to a better yield of C_2 products, whilst other processes such as hydrogenation of methyl to form methane and selective oxidation to CH_xO_y serve to lower the CO_x selectivity. Although the study did not undertake extensive surface characterisation techniques, the origin of selectivity is explained and may lead to improving conditions and structural properties by mapping the various reaction pathways. For example, isoconversion studies would extend understanding of the reaction mechanism and form a better comparison between h-BN and VO_x/Al_2O_3.

Advanced characterisation of gas-phase radicals was undertaken by Zhang *et al.*[204] to develop an understanding of reaction pathways of methyl radicals which are formed during C–C bond cleavage. Using synchrotron radiation vacuum ultraviolet photoionization mass spectroscopy (SVUV-PIMS), methyl radicals were detected under reaction conditions (600 °C, ODH-O_2 conditions with BN treated *via* gas exfoliation to increase surface area to 72.7 $m^2\ g^{-1}$). The detection of gas phase methyl radicals linked with the kinetic data showed that methyl radicals contribute to C_1 and C_2 products. The selective route to propene was expected to be a surface-controlled pathway as no propyl radicals were detected by SVUV-PIMS, despite the group being able to demonstrate a high sensitivity for propyl radicals. Therefore, control of conditions to maximise surface-controlled processes may increase the selectivity to propene and limit C_1 and C_2 products. Both high surface BN and supported oxidised boron catalysts were tested, with both showing formation of gas-phase radicals.

Venegas *et al.*[206] also highlighted the importance of gas-phase reactions in the reaction mechanism over B-based catalysts and suggested that the propyl radicals are not bound to the surface and react with HOO˙ radicals in the gas-phase. The hypothesis is that if propane reaction pathways were surface-mediated, then similar selectivity-conversion trends to metal oxides would be seen. This is a direct contradiction of the analysis of radicals undertaken using SVUV-PIMS shown previously, which did not detect propyl radicals despite previously showing the capability, and so further elucidation may be needed.

Lu *et al.* investigated various B_2O_3/SBA-15 catalysts. 10 wt% of B_2O_3 yielded the highest conversions at 500 °C, while conversion drops above this loading.[207] The supported boron oxide catalysts showed activity at 405 °C, much lower than previous examples of boron-based catalysts. Analysis by ^{11}B NMR detected four different B environments in fresh and spent catalysts: namely $B_3O_{9/2}$ (boroxol ring), $BO_{3/2}$ (non-ring), tri-coordinated planar B species and tetra-coordinated B species. The latter species were fused into the silica matrix. The presence of boroxol ring and non-ring sites was proposed as the reason for activity at lower temperature, but the data presented does not differentiate between the two. Comparison of fresh and spent catalysts showed an increase in the boroxol ring environment and a decrease in $BO_{3/2}$. This suggests a structural change due to oxidative conditions, rather than temperature, as the materials were prepared at 700 °C.[199]

Amorphous $B(OH)_xO_{3-x}$ was identified using ^{11}B solid state NMR, SEM and XAS after h-BN and BNNTs were exposed to ODH-O_2 conditions. Boron species with different levels of hydroxylation were detected using ^1H–^{11}B double resonance experiments[208] to show a wide range of oxidation states associated with boron. A range of oxide bridges, hydroxyl and oxide species were present, which result from oxidation and hydrolysis of BN catalysts. The study clearly demonstrates the complexity of these catalysts under ODH-O_2 conditions, and that *in situ* characterisation of the working catalyst is crucial to understanding the reactivity.

Boron oxide was supported on SiO_2 to probe how structural control of the surface influences the catalytic performance of boron-containing catalysts. The preparation method employed (calcination of tri-isopropyl borate on an amorphous silica support at 550 °C) formed BO_3 chains, which cannot be

replenished, unlike h-BN and BNNT. The BO_x/SiO_2 material showed a ~10% lower selectivity for a similar conversion when compared to h-BN, but the loading of B was comparatively low, and the bare SiO_2 may lower the selectivity.[209] Dual or single boron sites were present with varying levels of oxidation and hydroxylation after exposure to ODH-O_2 conditions, and the active centre of the catalyst may be one or more of these species. The difficulty in fully understanding the active site in this system is due to the co-existing boron species detected after exposure; BO_3 and B-OH have both been implicated but conclusive evidence has not been found. The appearance of metaborate and BO_3OH species in the spent catalysts was detected, but there is no data suggesting that these are desirable. It is clear that restructuring of the surface occurs, with a dynamic active site that undertakes ODH-O_2. It is also reasonable to expect that a hierarchy of activity exists, where some B species are more active than others, but a multitude of oxidised or hydroxylated boron surface sites can catalyse the reaction. The preparation of single-site boron catalysts would be instructive to understand the active phase.

A h-BN/cordierite monolithic catalyst exhibited a productivity increase of 55% when compared to elemental B. This is among the most active B catalysts reported to date. It was shown that optimising conditions for a high WHSV can lower CO_2 selectivity to 0%, which impressive even by the standards of h-BN catalysts.[210] It was hypothesised that the high WHSV did not allow for deep oxidation and therefore limited the formation of CO_x products. The monolith surface was characterised using FT-IR to confirm the presence of BN, but the B speciation was not determined. Wang *et al.* speculated that the linear channel structure of cordierite allowed for gas-phase radical chemistry to be enhanced and therefore showed improvement over h-BN powders. The h-BN/cordierite material was prepared by the chemical vapour deposition process. The geometry of the support was essential in this case, as well as the support forming strong oxygen bridge bonds with the catalytic phase.

When comparing macroporous BPO_4 to bulk BPO_4, it was found that the macroporous structure increased the performance significantly. The STY of macroporous BPO_4 was 320 $mol_{C_3H_6}$ kg_{cat}^{-1} h^{-1} (Table 9, entry 6).[211] When using the same WHSV, macroporous BPO_4 exhibited three-times the conversion of bulk BPO_4 despite being tested at a 30 °C lower temperature, whilst achieving roughly the same product distribution. The surface area normalised results revealed that both catalysts were equally active, suggesting that the same tri-coordinated B–O species is the active, but an increased number of active sites were formed in the macroporous structure. The interconnected macroporous structure was found to achieve outstanding productivity when exposed to a large WHSV by facilitating efficient mass transfer through the catalyst. As macroporous BPO_4 and h-BN/cordierite both exhibited a very high STY, it is implied that optimisation of mass transfer *via* engineering porosity has significant impact on the resulting catalyst. These data suggest that the reaction proceeds in the gas-phase, and as long as it can be rapidly initiated by a large surface area, then a large WHSV will limit surface intermediate contact time, and increase selectivity and turnover frequency.

Overall, it is clear that an important and rapidly developing area of ODH-O_2 catalysis is the application of boron-based materials. Many reports corroborate that B–O and B-OH species, or a mix between the two (*i.e.*, $B(OH_x)O_{3-x}$) are the active sites for h-BN based catalysts. While many reports examine catalyst design, the specific active site and phase is not well understood. This is to be expected with such a new generation of catalysts, but many papers suggesting different active sites and phases of boron exist, resulting in confusion of how to progress with catalyst improvement. Attempts to understand the mechanism have not yet been validated, and a different range of structures have been concluded to be the active sites. Supported catalysts have been formed and show high productivities and potential advancement in the field, but the fundamental understanding of *in situ* phases and mechanistic processes is still somewhat lacking. It may be beneficial to explore applications of boron-based catalysts in other oxidation reactions and start to build up structure–activity relationships. For example, focussing on bulk and layered materials as well as high surface area materials, may be advantageous in developing an understanding of the intrinsic properties which are desirable when using boron-based catalysts for ODH-O_2. Controlling the structure by a consistent synthesis method seems viable, as shown by the formation of nanoporous hexagonal boron nitride nanosheets (h-BNNS) from amorphous h-BN precursors. The h-BNNS catalysts prepared by Chen *et al.*[212] exhibited a surface area of 347 m^2 g^{-1}, as well as high purity, high crystallinity and increased thermal stability when compared to the amorphous h-BN materials. The dehydrogenation activity was measured using dodecahydro-*N*-ethylcarbazole as the substrate. The h-BNNS catalyst achieved a 34% increase in yield when compared to amorphous h-BN. To build on this, nanoporous h-BNNS could be applied to propane oxidative dehydrogenation, and if this is successful, begin to build structure–activity relationships using these highly crystalline materials.

5.3. Other ODH-O_2 catalysts

While the majority of ODH-O_2 catalysts are based on BO_x or VO_x, a multitude of other elements have been demonstrated to be active for ODH-O_2. In this section the most significant reports are critically reviewed and compared to the state-of-the-art VO_x- and BO_x-based ODH-O_2 catalysts. Cavani *et al.* compiled an extensive literature review in 2007, where MoO_x-based catalysts were shown to have a lower catalyst performance when compared to analogous vanadia based catalysts for the for ODH-O_2 reaction.[213] A direct comparison of kinetic parameters for V_2O_5/Al_2O_3 and MoO_3/Al_2O_3 in the ODH-O_2 reaction showed that vanadia-based catalysts had higher selectivity at isoconversion, and were more reducible than the analogous MoO_x-based catalysts.[214] The V and Mo catalysed ODH-O_2 reaction proceed *via* similar mechanisms. When comparing V-based catalysts to Mo-based catalysts, both supported on

ZrO_2, it was found that Mo was less active as the catalyst showed a higher activation energy.[215]

Mo=O bonds were found to be active for C–H abstraction, with the strength of the Mo=O bond influencing the activity: the stronger the bond, the lower the activity. Furthermore the strength of the Mo=O bond was shown to be influenced by MoO_x loading. The bridging oxygen bond between Mo and the support was found to be active in the complete combustion of propane.[216] The reactivity of Mo–O–M anchoring bonds is influenced by the cation electronegativity in the support material; a low support cation electronegativity leads to increased basicity of the bridging oxygen, and therefore has a higher activity for redox processes.[217] Analysing speciation of MoO_x on ZrO_2 supports found that two dimensional polymolybdate species dominated the surface up to loadings of 5 Mo atoms nm^{-2} and that further increasing Mo concentration led to a lower activity per Mo atom, ascribed to either limiting access to active sites or strengthening of the Mo=O bond.[216]

The selectivity of MoO_x/ZrO_2 can be increased by the addition of alkali metal dopants to reduce Lewis acidity of the Mo^{6+} centres allowing propene to desorb more effectively, thus decreasing the rate of consecutive oxidation reactions.[218] However, the overall performance of the catalyst was lower due to decreased reducibility, which inhibited the Mo^{6+} centre from undertaking C–H abstraction. A typical conversion selectivity trend was seen, where selectivity decreases with an increase in conversion. When MoO_x was supported on Al_2O_3, MoO_3 crystallites formed above 4.5 Mo atoms nm^{-2}. Below a surface density of 4.5 Mo atoms nm^{-2}, the polymolybdate regions were abundant and ODH-O_2 rates were high. Above monolayer surface coverage (4.5 Mo atoms nm^{-2}), the formation of MoO_x crystallites occurred which limited the number of exposed Mo–O sites. Unlike VO_x catalysts where V_2O_5 crystallites reduce selectivity, the presence of MoO_3 crystallites were not detrimental to selectivity, just the intrinsic activity. Bridging oxygen bonds between the support and Mo for both Al_2O_3 and ZrO_2 were found to be active for propane combustion to CO_x, in a similar manner to VO_x/Al_2O_3 catalysts.

The above studies of Mo-based catalysts have shown that they are limited when compared to analogous V-based catalysts. A selectivity increase is found for increasing molybdenum loadings up to 10 wt%, indeed suggesting that polymeric MoO_x up to monolayer coverage gives the best selectivity. However, selectivity was slightly lower at the same conversion when compared to 2 wt% V catalysts.[219] Reports involving Mo containing catalysts often concern mixed metal oxide catalysts containing both V and Mo. When comparing Mo-only to mixed Mo and V oxide catalysts formed *via* flame spray pyrolysis, a Mo-only loading of 10 wt% on Al_2O_3 ($10Mo/Al_2O_3$) gave a yield of 9.4%, compared to a mixed catalyst containing 4 wt% Mo and 2 wt% V ($4Mo2V/Al_2O_3$) reaching a yield of 10% (Table 10, entries 8 and 10). The relative rate of oxidation of propene to CO_x products, when compared to oxidative dehydrogenation of propane, was found to be lower for 4Mo2 V/Al_2O_3 than $10Mo/Al_2O_3$ between 350–500 °C. A Mo/V ratio of 2 gave the highest yield for the mixed Mo/V catalysts, and the synergistic nature of the two metals leads to the suppression of overoxidation. This research was limited in that it did not contain any *in situ* characterisation to probe the synergistic nature of the metal species. Interestingly, V catalysts formed *via* co-impregnation with Mo exhibited a V–O binding energy increase which limited overoxidation as the oxygen became less labile.[220] Mo also increased the concentrations of V^{4+} and V^{3+}species, which are more selective than V^{5+} entities. The strength of the V–O bond can therefore be carefully controlled by level of Mo doping, which may be the origin of synergistic properties which were observed for $4Mo2\ V/Al_2O_3$ catalysts.

The cycling of Mo-only catalysts has also been explored.[221] Interestingly, propene selectivity increased by 15% for the second ODH-O_2 phase, at a similar propene conversion, leading to an overall propene yield increase of 5%. *In situ* XANES showed that the oxidation state of Mo in the second ODH-O_2 phase was between +6 and +4 (corresponding tetrahedral and octahedral coordination respectively), with the change from the initial +6 environment happening under the DDH conditions. The distorted structure between +6 and +4

Table 10 Catalytic performance in ODH-O_2 for catalysts which are not vanadia or boron-based

Entry	Catalyst	T/°C	O_2/C_3H_8	WHSV/h^{-1}	$X_{C_3H_8}$/%	$S_{C_3H_6}$/%	STY/$mol_{C_3H_6}\ kg_{cat}^{-1}\ h^{-1}$	Ref.
1	Co_3O_4/ZIF-8	250	1	11.8	7.1	40.8	7.2	232
2	$NiCeO_x$	375	1	3.0	30.3	39.4	7.4	230
3	NiO-polyoxometalate	450	4	0.47	44	45	2.0	227
4	$5CrO_x$–MgO	450	0.5	5.9	10.8	84.1	11	234
5	NiO-SPP	450	1	11.8	21	50	26	228
6	B-$NiMoO_4$	475	1.25	3.2	18.2	63.8	8.4	243
7	Mesoporous $NiMoO_4$	500	2	2.4	11.8	60.1	3.5	225
8	$10Mo/Al_2O_3$	500	5	3.9	32.0	29.4	7.8	219
9	NiO–CeO_2	500	1	10.0	52	72	79	229
10	$4Mo_2V/Al_2O_3$	500	5	15.6	34.0	29.4	33	219
11	g-C_3N_4	515	0.25	1.4	23.9	58.5	4.0	238
12	0.5Pt–5Sn/Si-beta	550	0.5	4.7	48	79	40	241
13	$NiMoO_4$ with Ni/Mo ratio 0.4	600	1	2.4	32.5	48	7.7	223

T = reaction temperature; O_2/C_3H_8 = molar ratio of $O_2 : C_3H_8$ in the reaction, $X_{C_3H_8}$ = initial propane conversion, $S_{C_3H_6}$ = initial propene selectivity, STY = space time yield. The value next to element/phase represents wt% loading.

oxidation state of Mo is seemingly more selective than the tetrahedral Mo moieties in the original catalyst. *In situ* characterisation has thus highlighted a key structure–property relationship which will be useful in guiding future ODH-O_2 catalysts based on Mo.

Mo supported on titanate nanotubes (Mo-TNT) is a rare example of a supported Mo catalyst being developed in recent years. Mo-TNT was explored due to MoO_x/TiO_2 showing high dispersion,[217] an effect that was limited by anatase titania having a low surface area. Doping with K, according to a Mo/K ratio of 10, led to increased dispersion of MoO_x across the TNT surface, achieving a conversion of 21.2% and selectivity of 53.3%.[222] The increased dispersion caused by doping the titanate with K led to an increase in propene yield by 20% when compared to undoped Mo-TNT catalysts, despite a lower conversion.

Transition metal binary molybdates have also been investigated for ODH-O_2 activity. For instance, nickel molybdate catalysts have been shown to be active for ODH-O_2.[223] Increased selectivity was found to be directly correlated with an increase in Mo/Ni ratio. Further investigation of phases present found that NiO, whilst showing complete conversion, favoured overoxidation, whereas α-$NiMoO_4$ was more active for propane conversion, and β-$NiMoO_4$ was more selective. A Mo/Ni ratio of 0.4 gave the highest propane yield of 15.6% (Table 10, entry 13), which was ascribed to the high ratio of β-$NiMoO_4$/α-$NiMoO_4$, the mesoporous structure and redox properties. Although the activity was identified as being sensitive to the phases present, the underlying properties of each phase were not individually explored.

Chen *et al.* reported that nickel molybdates were active for ODH-O_2 and in particular the α-$NiMoO_4$ phase exhibited an enhanced yield compared to NiO and β-$NiMoO_4$.[224] Physical grinding of Mo and Ni precursors also led to the absence of NiO in α-$NiMoO_4$ when compared to the analogous co-precipitation technique. It was shown that $NiMoO_4$ had enhanced ODH-O_2 performance when comparing mesoporous to bulk catalysts, but only due to the enhanced number of active sites related to the increased surface area, and not the improved mass transfer properties that usually accompany mesoporosity.[225] The mesoporous catalysts had a lower specific productivity due to the loss of MoO_3 from the surface of the catalysts during synthesis. This confirmed that MoO_3 exhibits favourable activity to $NiMoO_4$ for the ODH-O_2 reaction (Table 10, entry 7).

NiO has been found to be detrimental to ODH-O_2 selectivity, favouring overoxidation products. Nb was found to be a superior dopant for NiO based catalysts, due to a reduction in the surface concentration of electrophilic O species and increased surface acidity. However, propene was still not the major product over NiO at around 10% conversion,[226] suggesting that NiO-based catalysts are limited in their application for ODH-O_2. In comparison to Nb-NiO catalysts, α-$NiMoO_4$ showed a selectivity of ~75% at roughly 10% conversion, with propene being the major product at similar conversions to Nb-NiO. The NiO-polyoxometalates have been shown to stabilise the adsorbed oxygen at the surface, which would limit overoxidation,[227] leading to the conclusion that NiO oxygen is too labile to achieve a high selectivity. When undertaking surface polymeric phosphate modification of NiO nanoparticles (NiO-SPP), an increase in selectivity of 2–3 times for NiO-SPP's at isoconversion was shown (Table 10, entry 5).[228] This is due to the polymeric phosphates weaker interaction with propene when compared to NiO nanoparticles, leading to a higher desorption rate and therefore higher selectivity.

CeO_2 was found to be a selective catalyst when HCl was added to the gas feed with O_2.[229] O_2 was hypothesised to have filled the oxygen vacancies at the surface, forming O_2^{2-} species, which mediated the oxidation of Cl^- to Cl radicals and resulted in high conversion and selectivity to propene. Once again, radical driven routes showed a high selectivity of 72% and conversion of 52% when the CeO_2 was combined with 8 wt% NiO as NiO was shown to enhance the Cl surface coverage which in turn enhanced the route to selective conversion of propane (Table 10, entry 9). Ni was confirmed to increase oxygen vacancies when incorporated into the CeO_2 lattice, leading to an increase in active sites.[230] XPS studies showed O vacancies doubled in concentration over 250 min, causing the selectivity to drop to 25.2%. Whilst oxygen vacancies are necessary to activate oxygen, they decreased selectivity in the absence of HCl,[231] which is why CeO_2 was shown to have a much lower selectivity without the presence of HCl; a change of active species from oxygen vacancies to Cl radical like species, has been shown to increase selectivity without a large detrimental effect on conversion. However, the space time yields observed are significantly lower than the most active ODH-O_2 catalysts.

Co-Based catalysts have been investigated for ODH-O_2, but their performance is also limited and vastly inferior to V- or B-based catalysts. However, Wang *et al.* developed a Co_3O_4/ZIF-8 catalyst that could operate at 250 °C, which is about 200 °C lower than the operating temperature for many ODH-O_2 catalysts.[232] Such low temperature activity warrants further investigation, but the reported space time yield of 7.2 $mol_{C_3H_6}$ kg_{cat}^{-1} h^{-1} (Table 10, entry 1) is relatively low for an ODH-O_2 catalyst. Tanasoi *et al.* investigated various mixed metal oxides derived from layered double hydroxide precursors. $CoMgAlO_x$ exhibited the highest propene yield, but the propene selectivity was limited due to an increase in cracking, which then led to overoxidation.[233] There was no correlation between reducibility and catalyst performance, suggesting that redox properties are not rate-determining in these ODH-O_2 catalysts. Unfortunately, the balance of acid and base sites was not measured, so a possible correlation in this respect was not identified.

Although CrO_x-based catalysts have been widely investigated for DDH and ODH-CO_2, there is limited research available for CrO_x-catalysts for ODH-O_2. Some CrO_x-type catalysts have been shown to form propene, with the selective phase being Cr_5O_{12} when supported on nano-crystalline MgO.[234] The space time yield was calculated to be 11.3 $mol_{C_3H_6}$ kg_{cat}^{-1} h^{-1} (Table 10, entry 4), which is significantly less than Cr catalysts

for DDH and about equivalent to the performance of CrO_x catalysts for ODH-CO_2. When supported on carbon nanotubes, the presence of Cr_2O_3 increased the C=O active sites on the carbon nanotubes, whilst also increasing propene desorption,[235] suggesting that Cr promotes the functionality of the carbon active centre.

Nanocarbons are an emerging field of catalysts for alkane dehydrogenation. Frank *et al.* showed that propane can be activated by surface oxygen groups on oxidised carbon nanotubes, noting that sp^2 hybridised carbon species are selective and stable for ODH-O_2, and that carbon nanotubes provide a balance between reactivity (sp^3) and stability (sp^2).[236] Nanocarbons also show high selectivity to alkenes when compared to metal oxides, but the intrinsic activity is lower. And additional feature of nanocarbons is that they are tuneable; N or B doping within the lattice leads to a change in electronic structure which can influence intrinsic catalytic activity, whilst changing surface functionality can influence selectivity. For example, adding B_2O_3 to the surface inhibits the activity of electrophilic oxygen species which promote overoxidation. Interestingly, this is one of the first examples of using B_2O_3 for ODH-O_2, where it acts to inhibit the activity through functionalisation of the surface, leading to an increased selectivity. More recently, Qi *et al.* confirmed the ketonic carbonyl groups to be the active site for general ODH reactions, whilst also confirming the effects of B_2O_3.[237] The unique chemical structure of nanocarbons means that the reaction mechanism does not operate under a Mars-van Krevelen or Langmuir–Hinshelwood route. *In situ* characterisation and measurements proved vital to finding the reaction mechanism for nanocarbons; *in situ* experiments for the oxidative dehydrogenation of ethylbenzene using nanocarbons showed the redox cycle of carbonyl-hydroxyl groups being the basis for the reaction mechanism.

Recently, Cao *et al.* discovered that graphitic carbon nitride (g-C_3N_4) are highly selective to propene (75%) at a moderate conversion of 12.8%. Additionally, selectivity to ethene was 15%, meaning total olefin selectivity was around 90%. The highest STY was measured at 515 °C to be 4.0 $mol_{C_3H_6}\ kg_{cat}^{-1}\ h^{-1}$ (Table 10, entry 11). g-C_3N_4 is analogous to graphite in structure, as is h-BN. The rate dependence of propane was first order, which is different to h-BN, but it was found to be the same as h-BN regarding the rate dependence of oxygen. DFT calculations suggested this first-order rate dependence of propane was due to simultaneous H abstraction by carbonyl species, which are similarly distant from one another when compared with the distance between the C–H bonds in propane. The simultaneous H abstraction would therefore lead to a lower concentration of the C_3H_7* reaction intermediate, as well as an increased O_2/O* ratio and therefore a lower likelihood of overoxidation.[238] This new route to propene shows promise and enhances our understanding of selectivity patterns. The materials were shown to be activated in a similar way to h-BN, forming the proposed active site, *i.e.*, carbonyl bonds, on the surface under oxidative conditions. Under these oxidative conditions, the surface area increased from 8.9 $m^2\ g^{-1}$ to 78.1 $m^2\ g^{-1}$, due to the formation of mesopores at the surface. The large increase in surface area when compared to the starting material, was a large factor in obtaining the high activity.

While supported precious metal clusters are amongst the most researched class of catalyst for DDH (and are used in some industrial processes) their application in ODH-O_2 has been relatively limited. Preliminary research into supported Pt metal clusters for ODH-O_2 was reported in the early 90s, with studies comparing particle-support interactions and the influence of supports on the reaction. Notably, Hubbard *et al.* reported Pt/ZrO_2 showed at least one order of magnitude higher activity than Pt/γ-Al_2O_3.[239] This is due to γ-alumina seemingly deactivating the Pt, which was confirmed due to the small Pt particles on γ-alumina having a higher reduction temperature when compared to bulk Pt.

To achieve high activity in supported metal catalysts, the dispersion of the supported metal must be optimised in order to maximise the number active centres and allow efficient use of the precious metal itself, which is often the most expensive component of the catalyst. Additionally, particle size and activity may not scale linearly. Vajda *et al.* reported that supported under-coordinated Pt_{8-10} clusters were highly active for ODH-O_2.[240] The activity of the catalyst in this study was shown to be much larger than the more commonly used vanadia-based catalysts, whilst showing a higher selectivity. The key to an increased activity was due to the under-coordinated Pt cluster strongly adsorbing the propane when compared to an extended Pt surface, confirmed by catalytic data which was in agreement with DFT. DFT showed a significant weakening of the C–H bond when propane interacts with under-coordinated Pt clusters in comparison to Pt(111) surface.

Combining Pt clusters with Sn showed increased productivity due to the electron transfer between the Pt and Sn which were in close proximity. 0.5Pt–5Sn/Si-beta exhibited a STY of 40 $mol_{C_3H_6}\ kg_{cat}^{-1}\ h^{-1}$ (Table 10, entry 12).[241] Pt–Sn catalysts were characterised *via* C_3H_8-TPD and C_3H_6-TPD. In comparison to 0.5Pt/Si-Beta and 5Sn/Si-beta, 0.5Pt–5Sn/Si-beta showed that the combination of the Pt and Sn led to a stronger adsorption of propane to allow for increased activity and propene desorbed more readily, leading to the understanding that propene would not be further oxidised to CO_x products due to a higher rate of desorption. It was also found that Pt–Sn/SAPO-34 catalysts showed an increased conversion when oxygen was introduced into the gas feed (compared to DDH conditions).[242] This was due to the oxygen reacting with hydrogen to form water and driving the equilibrium towards propene formation. Conversion largely depended on the $C_3H_8:O_2$ ratio: an increase in propane conversion was found with an increase in O_2 concentration relative to propane concentration, but too high an oxygen concentration caused overoxidation to CO_x. The activity and selectivity were much higher for Pt–Sn/SAPO-34 – a yield of 72.4% as compared to a ~10–15% yield for most V based catalysts. Introducing oxygen into the feed also reduced the formation of coke, which is a feature of instability in DDH. Water formed *via* ODH-O_2 was found to reduce stability, by increasing sintering of Pt due to a weaker metal–support interaction.[242] Pt–Sn catalysts are of

course widely studied for DDH and are found in industrial catalysts, as described above.

In summary, a variety of different catalysts have been shown to be active and selective for ODH-O_2. While vanadia- and boron-based catalysts comprise a large proportion of the reports to date, Ni-based catalysts have shown promise, particularly NiO-CeO_2. Mo-Based catalysts also prominently feature but are currently limited in comparison to analogous metal oxide catalysts, with low propene selectivity at moderate propane conversion. Graphitic carbon nitride, g-C_3N_4, although much less active than NiO_x per kg, exhibited high selectivity to olefins at moderate propane conversion and may warrant further investigation to maximise performance. High surface area, porous C_3N_4 may be a strong candidate to produce an active and selective catalyst.

ODH-O_2 offers many inherent advantages as the reaction is exothermic, thermodynamically unlimited and avoids formation of coke. Overall, extensive research into VO_x-based catalysts has been undertaken, with the clear limitation being overoxidation to CO_x products, but recent developments with one-step preparations and grafting techniques have improved catalyst performance to be comparable with the most active DDH Pt- and CrO_x catalysts. Deep oxidation remains a challenge for VO_x and other supported metal oxides. However, it is clear than B-based catalysts, although recently developed and less understood in both structure and mechanism, have clear potential for commercialisation due to the high selectivity at high propane conversion. Additionally, ethene is formed as a secondary product. Many B-based catalysts have similar, if not higher, STYs compared to DDH catalysts. Furthering the understanding of the reaction mechanism is essential to developing more efficient catalysts, and this appears to be the focus of recent research in the literature.

6. Oxidative dehydrogenation with carbon dioxide

The so-called 'soft-oxidation' of propane using CO_2 was proposed as an alternative process to using O_2 in order to decrease overoxidation to products such as CO and CO_2. In the context of the global effort to reduce anthropogenic CO_2 emissions, the ODH-CO_2 reaction has gained a renewed interest. CO_2 utilisation technologies are of general interest to develop a circular economy, but it is important to acknowledge that the current demand for propene (*ca.* 130 million tonnes per annum[1]) is a small fraction of the annual CO_2 emissions from fossil fuels (35 Gt).[244] Therefore the ODH-CO_2 process is unlikely to make a significant impact on global emissions. Additionally, there is an increased cost associated with obtaining concentrated CO_2 compared to using air, as could be envisaged in an ODH-O_2 process. It could be argued that commercial ODH-CO_2 processes would significantly reduce the carbon footprint of an individual chemical or industrial plant that would otherwise release CO_2 into the atmosphere, but this would depend on how CO is used as a by-product in the reaction. CO_2 was initially utilised in the dehydrogenation of ethylbenzene,[245] but since then has been reported for other alkane substrates, including ethane and butane.[246] The addition of CO_2 in the dehydrogenation reaction has multiple effects: As discussed in Section 2, it facilitates the RWGS reaction which removes H_2 from the system and shifts the thermodynamic equilibrium limit to favour propene production. Additionally, CO_2 can dissociate on the surface of a catalyst and provide O species to dehydrogenate propane directly. Finally, it can react with coke *via* the reverse-Boudouard reaction to produce CO, which can potentially extend the lifetime of the catalyst.

As an acidic molecule, carbon dioxide will preferentially adsorb on basic sites, which is in contrast to propane which will adsorb on acidic sites. Therefore, the correct balance of acidic and basic sites is a key consideration in catalyst design. Equally, the ratio of carbon dioxide to propane is important to take in account, as it has kinetic and thermodynamic implications. Thermodynamically, higher $CO_2 : C_3H_8$ ratios limit coke forming side-reactions.[22] Interestingly, the addition of carbon dioxide has been found in some cases to be detrimental to the catalyst performance;[247] this underlines the dependency of catalytic reactivity on the structure of the catalyst.

Generally, there are two proposed reaction pathways that describe the soft oxidation of propane to propene. These are described as the direct and indirect pathways:

$$\text{Direct pathway}: \ C_3H_8 + CO_2 \rightleftharpoons C_3H_6 + H_2O + CO$$

$$\text{Indirect pathway}: \ C_3H_8 \rightleftharpoons C_3H_6 + H_2$$

$$H_2 + CO_2 \rightleftharpoons H_2O + CO$$

In the direct pathway, oxygen from CO_2 abstracts the H from propane, forming H_2O as a primary product. Conversely, in the indirect pathway the dehydrogenation occurs in the absence of an oxidant, and the role of CO_2 is to remove H_2 *via* the RWGS reaction. It should be noted that regardless of the pathway, the RWGS reaction must mediate the balance of H_2O, CO, CO_2 and H_2, although the contribution of RWGS to the final product distribution is often overlooked. In the following sub-sections, the literature reports concerning catalysts for ODH-CO_2 are reviewed and discussed.

6.1. Chromium-based ODH-CO_2 catalysts

Chromium oxide is one of the most widely investigated catalysts for the DDH reaction and as described above, is a key component of the industrial CATOFIN process. It is also one of the earliest reported transition metal oxide catalysts for the soft oxidation of propane to propene. Generally, the studies of Cr_2O_3-catalysed ODH-CO_2 reactions are carried out under similar conditions to the DDH process, but with the addition of CO_2 to the gas-feed, typically supplied as a 1 : 1 ratio or in excess of the partial pressure of propane. The performance and reaction conditions of some reported catalysts are shown below in Table 11.

The first study of Cr_2O_3-based catalysts for ODH-CO_2 was reported by Takahara *et al.* in 1996 using Cr_2O_3 supported on SiO_2, activated carbon (AC) or Al_2O_3. The catalyst tests were

Table 11 Comparison of the catalytic performance of selected Cr-based catalysts for ODH-CO_2

Entry	Catalyst	T/°C	CO_2/C_3H_8	WHSV/$g_{C_3H_8}$ g_{cat}^{-1} h^{-1}	$X_{C_3H_8}$/%	$S_{C_3H_6}$/%	STY/$mol_{C_3H_6}$ kg^{-1}_{cat} h^{-1}	Ref.
1	$RuCrO_x/SiO_2$	496	1	7.9	9	85	13	266
2	$5\%Cr_2O_3/ZrO_2$	500	2	—	15	83	—	267
3	Cr_2O_3-(15 wt%)Al_2O_3	550	1	—	4.7	91.3	—	248
4	$10\%Cr_2O_3$-ZrO_2	550	2	0.30	51.1	81.7	2.6	251
5	CrO_x/Na-ZSM-5	550	2	0.30	48	86	2.5	261
6	CrO_x-mesoporous ZrO_2	550	2	0.30	68	60	2.5	252
7	CrO_x/SBA-15	550	2	0.30	24.2	83.9	1.9	250
8	CrO_x/ZrO_2	550	2.6	0.3	40	88	2.2	253
9	$5\%CrO_x$/AC	550	5	3.0	39.8	86.7	21	260
10	CrO_x/MCM-41	550	5	1.2	40	90	8.9	88
11	Cr_2O_3/beta-zeolite	550	5	1.2	33	81.6	6.6	263
12	7% CrO_x/SBA-1	550	5	1.2	37.7	85.8	7.9	85
13	3.4% Cr_2O_3/SBA-1	550	5	1.2	33.2	87.9	7.2	84
14	0.5Ni-CrO_x/SBA-15	600	1	1.8	25	90	8.3	264
15	CrO_x/B-MFI	600	1	1.1	22.1	91	4.7	262
16	CrO_x/SiO_2	600	4	1.2	70	79	14	258
17	CrO_x/SiO_2	600	5	1.2	41	65	6.6	256
18	CrO_x/SiO_2	600	7	0.89	36.3	92	6.2	254
19	CrO_x/SiO_2	600	1	1.8	40	90	13	259
20	CrO_x/SBA-1	600	5	1.2	39.4	86.6	8.4	257

T = reaction temperature; CO_2/C_3H_8 = molar ratio of CO_2 : C_3H_8 in the reaction, $X_{C_3H_8}$ = initial propane conversion, $S_{C_3H_6}$ = initial propene selectivity, STY = space time yield. AC = activated carbon.

performed at 600 °C with a feed of propane and argon or carbon dioxide.[248] It was found that over 5 wt% Cr_2O_3/SiO_2, the propene yield increased from 6.5% to 9.1% when CO_2 was co-fed instead of Ar. In contrast, the alumina supported catalyst was inhibited by the addition of CO_2, as shown by the drop in propene yield from 12.7% to 3.3%. The 5 wt% Cr_2O_3/AC material was unaffected by CO_2 addition. The Cr_2O_3/SiO_2 catalyst deactivated rapidly, retaining just 66% of its original activity after 4 h on-stream. The stability was noted to the same with or without CO_2 in the reactant feed. Not only did this study establish Cr_2O_3 as an active ODH-CO_2 catalyst, it also captured one of the recurring themes in catalyst design for ODH-CO_2: some catalysts are inhibited by the addition of CO_2 while others perform much better.

Relative to many other metal oxides, Cr_2O_3 is considered to be one of the most promising catalysts for ODH-CO_2. Takehira *et al.* compared the catalytic performance of several d block and p block oxides (namely Cr, Ga, Ni, V, Fe, Mn and Co) supported on MCM-41, at 550 °C with a CO_2 : C_3H_8 molar ratio of 5.6.[91] After 30 min on-stream, the propene yield of the Cr-based catalyst was 15% whereas for the Ga-based counterpart it was 5%. The remaining catalysts all exhibited lower propene yields (in the 1–4% range). However, as the catalysts were not characterised, it is unclear if the dispersion of these catalysts was comparable, and therefore if the results reflect the true intrinsic activity of each metal. It was also noted that the order of reactivity resembled the trends observed by Nakagawa *et al.* for diamond-supported metal catalysts in the DDH reaction.[249] This suggests that there are commonalities in catalyst design between DDH and ODH-CO_2 which most likely relate to the interaction of the alkane with the catalyst.

Contrary to this, Zhang *et al.* compared ZrO_2, SBA-15 and γ-Al_2O_3 as supports for Cr_2O_3 in the DDH, ODH-CO_2 and ODH-O_2 reactions.[250] They found that the highest propene yield was observed with different catalyst systems under different dehydrogenation reactions, *i.e.*, the activity trends in DDH did not translate to ODH-CO_2 catalysts. Specifically, Cr_2O_3/ZrO_2 catalyst was the most active for the DDH reaction, while the highest yield of propene for the ODH-CO_2 and ODH-O_2 reactions was observed over Cr_2O_3/SBA-15 (Table 11, entry 7). Across all the catalysts however, the highest propene yields were generally observed in the DDH reaction, ascribed to the production of carbon oxides in the ODH-O_2 and ODH-CO_2 reactions. However, it was reported that Cr_2O_3/ZrO_2 was more stable on-stream in ODH-CO_2 than in the DDH reaction. Wu *et al.* also observed increased stability of Cr_2O_3/ZrO_2 in the presence of CO_2 (Table 11, entry 4).[251] They reported that the CO formation rate was higher than the CO_2 consumption rate and the excess CO was suggested to originate from the Boudouard reaction ($CO_2 + C \rightarrow 2CO$); this could explain the increased stability of this catalyst. It is possible that some dry reforming of propane also took place, which would produce H_2 and CO. Zhao *et al.* recently reported the facile preparation of Cr supported in mesoporous ZrO_2 using an evaporation-induced self-assembly method (Table 11, entry 6).[252] The authors suggested that propene could react with carbon dioxide to form carbon monoxide, methane and water. Other studies have reported a stronger inhibition effect for Cr_2O_3/ZrO_2 catalysts in the presence of CO_2. For instance, Ferreira *et al.* studied the adsorption properties of CO_2 and concluded that it binds strongly to active Cr_2O_3 sites, lowering the activity and stability of the catalyst,[253] whereas Xie *et al.* suggested that coke formation could originate from CO_2 hydrogenation over Cr^{2+} species. These conflicting reports may relate to the structural polymorph of ZrO_2 present in the catalyst support; this factor is often overlooked, but recent studies

from Kondratenko *et al.* revealed that nanocrystalline ZrO_2 is an active DDH catalyst in its own right[151,152] under similar reaction conditions. The ZrO_2 crystal phase and crystallite size were strongly correlated to the catalyst activity: smaller crystallites were more active but amorphous ZrO_2 had very low intrinsic activity. Moreover, monoclinic ZrO_2 was more active than tetragonal ZrO_2.

Cr_2O_3-catalysed ODH-CO_2 has been examined over different polymorphs of SiO_2,[254–256] including various structured porous oxides, including SBA-1,[84] SBA-15,[250,257] MCM-41,[91] amorphous silica[84] and mesoporous silica spheres.[258] Notably, Michorczyk *et al.* reported a detailed comparison of different silica supports, coupled with an in-depth characterisation study.[84] It was shown that in each case, the same active Cr species was formed, namely Cr^{6+}, but higher surface area silicas (*e.g.*, SBA-1 and SBA-15) were able to facilitate a higher number of such sites. A clear correlation was found between the rate of propene formation and the wt% of Cr^{6+}, as determined using X-ray photoelectron spectroscopy (XPS). In DDH, while Cr^{6+} is considered active, under reaction conditions Cr^{3+} is rapidly formed and considered the principle active species.[93,94] The selectivity to propene was similar across the different silica supports (88–93%), with the observed differences being attributable to differences in propane conversion rather than catalytic properties. These Cr_2O_3/SiO_2 catalysts were highly active at 550 °C and the most active catalyst (Cr_2O_3/SBA-1) achieved a STY of 7.9 $mol_{C_3H_6}\ kg_{cat}^{-1}\ h^{-1}$, as shown in Table 11, entry 12. It should be noted that the experiments were carried out with a $CO_2:C_3H_8$ ratio of 5, which as discussed above, has been shown to enable a higher equilibrium yield of propene. Therefore, in studies where high conversions are generally targeted and carbon dioxide is in excess of propane, higher propene yields are reported.

Takehira *et al.* carried out X-ray absorption spectroscopy (XAS) on CrO_x/MCM-41, confirming that the reduction of Cr^{6+} occurs during the reaction.[91] Specifically, they identified $Cr^{6+}O_4$ tetrahedra as the active species. These $Cr^{3+}O_6$ octahedra were formed after reduction, which were considered to be less active. It was shown that CO_2 could re-oxidise the Cr, which suggests that the redox cycle between Cr^{6+} and Cr^{3+} is an important process during the reaction. Yi *et al.* discriminated between isolated Cr^{6+} and polymeric Cr^{6+}, finding that after reduction, isolated Cr^{3+} was more active than polymeric Cr^{3+}. This underlines the importance of Cr dispersion in these catalysts.[259]

In a more detailed examination of Cr_2O_3/SBA-1, the relationship between the physicochemical properties of the catalyst and the observed activity were explored.[85] Michorczyk *et al.* found a strong positive correlation between the initial propene yield and the reducibility of the catalyst, specifically the H_2 consumption. *In situ* UV-vis measurements revealed that Cr^{6+} is rapidly reduced to Cr^{3+} or Cr^{2+} in the presence of C_3H_8 under reaction conditions. The reaction proceeds through a Mars-Van Krevelen mechanism, *via* the $Cr^{2+/3+}$ redox couple. Rapid deactivation, typical of Cr_2O_3 catalysts, was observed, although the majority of the initial activity could be recovered after regeneration in air. The remainder was ascribed to pore collapse and/or the formation of inactive Cr sites, although the loss of surface Cr sites through agglomeration was not considered.

Despite early reports that activated carbon (AC) was not a suitable support for Cr_2O_3, subsequent studies have shown that above 550 °C, the activity of Cr_2O_3/AC in the presence of CO_2 was higher than in the DDH reaction.[260] The enhancement in propane conversion due to the presence of CO_2 increased at higher temperatures (*i.e.*, above 600 °C), although this was chiefly due to propane dry reforming proceeding, generating CO and H_2 rather than propene. While this Cr_2O_3/AC exhibited the highest STY of propene out of all CrO_x-based catalysts (21 $mol_{C_3H_6}\ kg_{cat}^{-1}\ h^{-1}$, Table 11, entry 9), it rapidly deactivated on-stream and due to the support being carbonaceous, cannot be regenerated using air. This severely limits the utility of this catalyst.

Zeolites have also been considered as catalyst supports for Cr_2O_3. Zhang *et al.* prepared CrO_x/Na-ZSM-5 *via* incipient wetness.[261] Although the initial conversion and selectivity was high (48% and 86%, respectively) (Table 11, entry 5), the catalysts deactivated rapidly and the reaction conditions were such that the STY was only 2.5 $mol_{C_3H_6}\ kg_{cat}^{-1}\ h^{-1}$ at 550 °C with a CO_2:C_3H_8 ratio of 2. Zhu *et al.* investigated a range of MFI supports, including silicalite-1 and H[B]MFI.[262] CrO_x/H[B]MFI was found to be the most active catalyst, giving a STY of 4.7 $mol_{C_3H_6}\ kg_{cat}^{-1}\ h^{-1}$ at 600 °C with a $CO_2:C_3H_8$ of 1 (Table 11, entry 15). Although the as-prepared catalyst exhibited typically poor stability for Cr catalysts, steam treating the catalyst resulted in a marked improvement. After 60 h on-stream, the as-prepared catalyst retained only 25% of its initial conversion, while the steam treated catalyst retained *ca.* 74%. The authors ascribed the effect to stabilised Cr^{3+} formed in the steam treatment. Presumably the reduction of Cr^{6+} during the reaction results in an inactive or less active Cr^{3+} species. It should also be noted that the as-prepared catalyst was initially almost twice as active as the steam treated catalyst, which leaves the possibility that at higher conversions, increased coke formation may have occurred which would exaggerate the deactivation compared to the steam treated catalyst. Ideally such stability comparisons would be made at isoconversion, however this discovery is one of only a few that shows improved stability on-stream. Recently, Michorczyk *et al.* prepared a Cr-β-zeolite and investigated the effect of dealumination, which clearly elucidated the effect of acidity on the catalytic performance.[263] It was reported that the dealuminated catalyst, Cr-SiBeta, exhibited significantly higher propene yields (up to 27%), compared to the Al-containing catalyst, Cr-AlBeta (2%). The presence of acid sites in the Cr-AlBeta catalyst resulted in cracking pathways that led to increased production of methane and ethene. Moreover, the Cr–Albeta catalyst performed less well in the presence of CO_2 than in the DDH reaction. This was explained by the strong adsorption of CO_2 on the catalyst, similar to the inhibition observed over Cr_2O_3/Al_2O_3 catalysts. The stability of the dealuminated catalyst was also improved compared with Cr–Albeta, but significant loss

in activity was observed over the 4 h reaction. In considering the redox properties of the catalysts in this work, and their previous investigations, the authors also identified a strong correlation between the H_2 consumption from H_2-TPR studies and the reported propene yield, as shown in Fig. 10.

While the majority of investigations on ODH-CO_2 Cr_2O_3 catalysts have focused on support modifications, the addition of a promotor has also been shown to be beneficial. Yun *et al.* demonstrated that the addition of 0.5 wt% Ni to a 10 wt% CrO_x/SBA-15 catalyst increased the propane and CO_2 conversion, as well as the on-stream stability.[264] After 1 h on-stream, the Ni-promoted catalyst was 50% more active and the conversion and selectivity was almost maintained over 12 h on-stream. In contrast, the less active unpromoted catalyst retained only half of the initial activity over the same time period. Using three-stage H_2-TPR experiments (where the catalyst is reduced twice under H_2 and then re-oxidised in CO_2 before the final H_2-TPR program), the authors showed that the addition of Ni facilitated the re-oxidation of Cr during the reaction. This is consistent with previously reported mechanisms of deactivation over Cr-based catalysts, although coking is also often reported to cause deactivation. Interestingly, the promoted catalyst was marginally more prone to coking. This strongly suggests that overreduction of active Cr sites is the key deactivation mechanism over these catalysts. There is a lot of potential to develop promoted Cr catalysts that could enhance the redox activity of the catalyst; precious metals including Pd and Pt are often supported on reducible supports for this purpose.[265] Crucially, it was found that above 0.5 wt% Ni, propane reforming was prevalent, which underlines the importance of appropriate loadings of promotors.

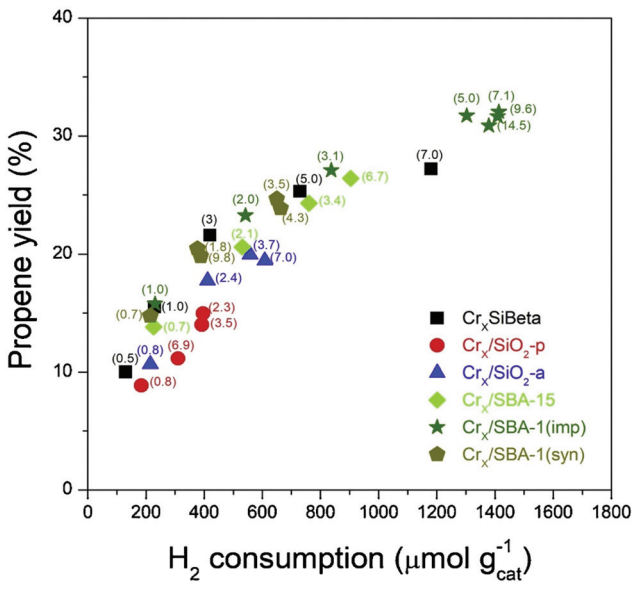

Fig. 10 The relationship between the reducibility of various supported Cr catalysts, and the reported propene yield. Reproduced from ref. 263 with permission from Elsevier.

O'Brien *et al.* investigated the effect of a Ru promoter to a 10 wt% CrO_x/SiO_2 catalyst. Consistent with Yun *et al.* it was shown that the propene formation rate was increased. A 1 wt% Ru loading was optimal and doubled the activity. Interestingly, this is approximately the same molar ratio reported as the optimum by Yun *et al.* for Ni-promoted CrO_x/SBA-15 (Table 11, entry 14).[264] Another similarity was the propensity of reforming to dominate at high loadings (>1 wt%). The enhanced stability seen in Ni-promoted Cr catalysts was not observed in this work and the activity could not be fully recovered after regeneration. Consequently, aggregation of Cr species was suggested as an additional deactivation mechanism in addition to coke formation and overreduction of Cr. Rather than aid Cr re-oxidation in a one-step oxidative dehydrogenation, the authors concluded that the Ru promotes the RWGS reaction, which removes H_2 and increases the equilibrium conversion of propane. However, the results of three-stage H_2-TPR reactions indicated that Cr can be more easily oxidised in the presence of Ru, which suggests that Ru can participate in a similar role as Ni-promoted Cr catalysts.

Overall supported chromium oxide catalysts represent one of the most active classes of ODH-CO_2 catalysts, with STY values in the range of 2–22 $mol_{C_3H_6}$ kg_{cat}^{-1} h^{-1}. The role of the support is simply to maximise the active Cr^{6+} surface area, rather than add any chemical functionality, hence this is the reason why chemically-unreactive supports such as SiO_2 and activated carbon yield the most active CrO_x catalysts. The most significant barrier to commercial application is the poor on-stream stability exhibited by all chromium-based catalysts. While incremental improvements in the activity of Cr catalysts have been reported since their initial discovery, significant advances in catalyst stability have been relatively few.

6.2. Gallium-based ODH-CO_2 catalysts

Gallium oxide is the second most widely studied element for ODH-CO_2 catalysis, owing to its successful application for DDH, as discussed above. It was first identified as an efficient DDH catalyst in 1988 in the context of dehydrocyclodimerisation,[268] but since the turn of the century it has been the subject of more intensive research.

The first application of gallium catalysts in ODH-CO_2 was carried out using ethane as a substrate.[269] Although ODH-CO_2 using ethane is beyond the scope of the current review, it is instructive to consider the catalytic activity of Ga_2O_3 in the early reports from Nakagawa *et al.* TiO_2, Al_2O_3 and SiO_2 were selected as catalyst supports for Ga_2O_3 and it was found that Ga_2O_3/TiO_2 was the most active catalyst.[270] Additionally, it was found that co-feeding steam was beneficial to maintain high activity, although rapid deactivation was still apparent. Consistent with the literature on supported CrO_x catalysts, the addition of CO_2 to Ga_2O_3/Al_2O_3 was shown to be detrimental to ethene yield. This strongly suggests that Al_2O_3 is the origin of the inhibition observed in CrO_x/Al_2O_3 catalysts.[248] It is known that the balance of acid and base sites is important to mediate the activation of the alkane and the desorption of the alkene. The addition of CO_2 is likely to result in competitive

Table 12 Catalytic performance of selected gallium-based catalysts for ODH-CO_2

Entry	Catalyst	T/°C	CO_2/C_3H_8	WHSV/$g_{C_3H_8}$ g_{cat}^{-1} h^{-1}	$X_{C_3H_8}$/%	$S_{C_3H_6}$/%	STY/$mol_{C_3H_6}$ kg^{-1}_{cat} h^{-1}	Ref.
1	Ga_2O_3–Al_2O_3	500	2	0.15	49.7	91.7	1.4	274
2	β-Ga_2O_3	500	2	0.15	23	94	0.7	271
3	Ga_2O_3–Al_2O_3	550	5	1.2	19	91.6	4.3	273
4	CrO_x/β-Ga_2O_3	550	7	0.89	33.7	84.7	5.3	272
5	Ga_2O_3/Al_2O_3	600	2	0.30	26	94	1.5	114
6	GaN/SiO_2	600	2	1.8	31	93	11	276
7	Ga_2O_3–Al_2O_3	600	2	0.15	49.7	91.7	1.6	275
8	Ga_2O_3/ZSM-48	600	2	0.30	52.6	42.2	1.5	113

T = reaction temperature; CO_2/C_3H_8 = molar ratio of CO_2 : C_3H_8 in the reaction, $X_{C_3H_8}$ = initial propane conversion, $S_{C_3H_6}$ = initial propene selectivity, STY = space time yield.

adsorption on basic sites, and this may result in longer surface lifetimes of alkyl intermediates, resulting in undesirable side-reactions.

Zheng *et al.* investigated ODH-CO_2 of propane over different polymorphs of gallium oxide and found that β-Ga_2O_3 (Table 12, entry 2) was the most active, even outperforming Cr_2O_3 at 500 °C.[271] Interestingly, this was not the case for the DDH reaction, where Cr_2O_3 was the most active catalyst. However, the activity of all the Ga_2O_3 polymorphs was lower in the presence of CO_2. Subsequently, Michorczyk *et al.* investigated CrO_x/Ga_2O_3 for ODH-CO_2 and showed that at elevated temperatures (>570 °C), the addition of CO_2 is beneficial (compared to DDH).[272] At 550 °C, the STY was 5.3 $mol_{C_3H_6}$ kg_{cat}^{-1} h^{-1}. A non-oxidative reaction pathway was suggested to proceed *via* an initial heterolytic dissociation of propane, form a gallium alkoxide and a gallium hydride species. Then proton abstraction occurs, leaving H^+ and H^- on the surface of the gallium oxide and propene. The abstraction of the second H atom is slow and considered rate-limiting. The authors suggested that this can be enhanced by a secondary equilibrium involving the surface migration of a surface proton. This equilibrium is as follows:

$$H^- + C_3H_7{}^+ + H^+\text{-support} \rightleftharpoons H^- + H^+ + C_3H_7{}^+\text{-support}$$

This results in the formation of propene *via*:

$$C_3H_7{}^+\text{-support} \rightleftharpoons C_3H_6 + H^+\text{-support}$$

These reactions are facilitated by Lewis acid sites, specifically tetrahedral Ga ions. The role of CO_2 in ODH-CO_2 is to assist the above equilibrium by removing H_2 *via* the RWGS reaction.

The effect of the support was closely examined for propane ODH-CO_2 by Xu *et al.*[114] It was found that Ga_2O_3 supported on TiO_2, Al_2O_3, and ZrO_2 exhibited high activity, while SiO_2 and MgO resulted in poorer performing catalysts. However, consistent with previous reports it was found that the addition of CO_2 to the reaction feed was detrimental when Al_2O_3 and ZrO_2 were used as supports and higher propane conversion was observed when using lower CO_2:C_3H_8 ratios. Despite this, the propene yield was highest over Ga_2O_3/Al_2O_3 in ODH-CO_2, the equivalent of 1.5 $mol_{C_3H_6}$ kg_{cat}^{-1} h^{-1} (Table 12, entry 5). The low activity of Ga_2O_3/MgO and Ga_2O_3/SiO_2 was ascribed to the absence of medium and strong acid sites. In addition to the acid–base properties of the support, the authors considered the interaction between the Ga and the support to be of importance. In the Ga_2O_3/TiO_2 catalyst, a significant proportion of the Ga (45%) was reduced. This catalyst exhibited the highest propane conversion, but with a propene selectivity of 73% it did not result in the highest propene yield.

Although the addition of Al_2O_3 to ODH-CO_2 catalysts is typically not beneficial,[114,273] Chen *et al.* investigated spinel-type Ga_2O_3–Al_2O_3 mixed oxides and showed that they can function as stable catalysts.[274,275] At 600 °C, although the initial propane conversion was similar for DDH and ODH-CO_2, after 8 h on-stream the stability of the catalyst was markedly improved in the presence of CO_2, where $Ga_8Al_2O_{15}$ retained 66% of its initial activity, compared to just 44% in the absence of CO_2. The origin of stability was linked to the low rate of coking associated with the spinel catalyst. Using NH_3-TPD analysis, the authors concluded that weak Lewis acid sites were conducive to high activity. These acid–base properties most likely contribute to the enhanced stability as well; it is known that stronger acid sites promote oligomerisation pathways that produce coke. While many previous studies on ODH-CO_2 have shown Al_2O_3 to be detrimental to catalyst performance (compared with DDH activity), this investigation highlights the sensitivity of the catalyst performance to the structure of the surface, and the acid–base properties therein.

Ren *et al.* studied the effect of acidity and pore geometry in Ga_2O_3 supported on ZSM-48 and ZSM-5.[113] At 600 °C, the most active catalyst, Ga_2O_3/ZSM-48 with a Si : Al ratio of 130, demonstrated a 22.2% propene yield, although the selectivity to propene was only 42% (Table 12, entry 8). Aromatics (including retained carbonaceous products) accounted for 40% of the converted carbon. An increase in the Si : Al ratio resulted in an increase in propene selectivity on both H-ZSM-5 and ZSM-48 supports. Compared with DDH, in ODH-CO_2 the propane conversion was slightly higher, but the propene selectivity was lower, resulting in a marginally decreased propene yield. The increased performance of Ga_2O_3/ZSM-48 was attributed to the abundance of weak and medium strength acid sites.

Recently, it has been shown that gallium nitride can function as a highly active catalyst for ODH-CO_2 when supported on porous SiO_2.[276] At 600 °C with a $CO_2:C_3H_8$ ratio of 2, the catalyst exhibited a propane conversion of 31% and a propene selectivity of 93%, equivalent to a STY of 11 $mol_{C_3H_6}\ kg_{cat}^{-1}\ h^{-1}$ (Table 12, entry 6), the highest value reported for any Ga-based catalyst. Although some deactivation was observed (*ca.* 83% of initial steady state activity retained after 8 h on-stream), the catalysts can be considered to be amongst the most stable reported to date. While the authors did not investigate the reaction mechanism of the supported GaN, it is instructive to consider the observed induction period in each catalyst whereby the propane conversion increases over the first 1–2 h; for the most active catalyst it increases from 20% to 30% in this timeframe. A similar induction period has been observed over BN catalysts for the ODH-O_2 of propane by Hermans *et al.*, amongst others,[196,202,204] which was ascribed to the oxidation of BN to form active B-OH groups. It is reasonable to suggest that a similar oxidation/hydroxylation of the GaN surface occurs here, although it is unclear how, or even if, CO_2 could facilitate this *in situ*. XPS of the as-prepared samples showed a large O 1s signal, but this was ascribed to adsorbed H_2O.

Overall, Ga_2O_3 can be considered to be moderately active for ODH-CO_2, with reasonable propene yields, but generally poor stability. In most cases, the inclusion of CO_2 is not beneficial for the reaction. Compared with CrO_X, Ga typically results in lower propene yield and comparable stability. The recent breakthrough regarding GaN, however, is very noteworthy. With a similar STY to the most active CrO_X catalysts and relatively good on-stream stability at high conversion (*ca.* 30%), this new class of Ga catalysts has real potential. Future research into GaN catalysts should seek to understand the reaction mechanism in order to identify the active sites and improve catalyst performance further.

6.3. Metal oxide based ODH-CO_2 catalysts

In addition to chromium and gallium, a selection of other oxide catalysts, mostly of transition metals, have been explored for their ODH-CO_2 activity. This section details the most significant advances made to date with respect to these other metal oxides.

Bulk and supported iron oxides have been investigated by Michorczyk *et al.*[277] Unsupported Fe_2O_3 exhibited reasonable activity at 600 °C when using a $CO_2:C_3H_8$ ratio of 5, with a propene yield of 7.5%. The activity was four times higher than in the absence of CO_2, and the propene selectivity increased from 84 to 92.5%. The dispersion of Fe_2O_3 on activated carbon significantly improved the conversion of propane from 8.2 to 29.7%, which corresponds to a STY of 16.1 $mol_{C_3H_6}\ kg_{cat}^{-1}\ h^{-1}$ (Table 13 entry 7). In contrast, using Al_2O_3 as a support for the Fe_2O_3 inhibited the performance of the catalyst. The reaction mechanism was concluded to proceed *via* a redox pathway, whereby the lattice oxygen associated with the iron oxide directly participates in the reaction.

A 5 wt% ZnO/H-ZSM-5 catalyst was investigated by Ren *et al.* using a broad range of SiO_2/Al_2O_3 ratios (60, 120, 160, 201 and 242) at 600 °C.[278] While all of the prepared catalysts exhibited some activity (with conversion ranging from 40–86%), the highest propene yield was observed over ZnO/H-ZSM-5 (160), which was 46.8% (Table 13, entry 3). In each catalyst, the main competing pathway was to aromatics, which is consistent with the use of ZSM-5 in aromatisation catalysis.[247] It was recognised that CO_2 both promotes the RWGS reaction over the supported ZnO catalysts, but also blocks active sites. The stability was improved in the presence of CO_2 (compared to DDH); *ca.* 74% of the original activity was retained after 10 h on-stream, which is relatively good compared to Ga- and Cr-based catalysts.

Indium oxide and various mixed-metal oxides containing In have been considered as ODH-CO_2 catalysts in recent years. Chen *et al.* initially demonstrated that In_2O_3 was active, but also showed that the performance is improved as a binary oxide of In_2O_3–Al_2O_3.[279] Specifically, $In_{20}Al_{80}O_X$ exhibited the highest propene yield under the reaction conditions used (600 °C, $CO_2:C_3H_8 = 4:1$), which was *ca.* 27% (Table 13, entry 5). Interestingly, each of the mixed metal catalysts exhibited an induction period over the first 3 h, followed by moderate deactivation. In contrast, Al_2O_3 and In_2O_3 alone deactivated much more rapidly on-stream and without an induction period. The origin of this induction period was found to be reduction of In_2O_3 to In^0 nanoclusters, which suggests the active structure is more of a supported nanoparticle type catalyst than a mixed-metal oxide. Chen *et al.* also considered a wide range of secondary metal oxides for this reaction, using sol–gel or co-precipitation to prepare In_2O_3–MO_x, where x = Al, Zn, Zr, Ti, Fe, Mg, Si and Ce.[280] It was shown that the In_2O_3–

Table 13 The catalytic performance of selected metal oxide-based catalysts for ODH-CO_2

Entry	Catalyst	T/°C	CO_2/C_3H_8	WHSV/$g_{C_3H_8}\ g_{cat}^{-1}\ h^{-1}$	$X_{C_3H_8}$/%	$S_{C_3H_6}$/%	STY/$mol_{C_3H_6}\ kg^{-1}{}_{cat}\ h^{-1}$	Ref.
1	10 mol%Fe_2O_3–CeO_2	550	1	0.59	18	46	1.0	287
2	8 wt% In_2O_3/H-ZSM-5	580	4	1.2	13	81	2.5	282
3	5 wt% ZnO/H-ZSM-5	600	2	0.30	68	47	2.0	278
4	V-MCM-41	600	4	1.0	58	90	11	286
5	In_2O_3–Al_2O_3	600	4	0.15	35	75	0.81	279
6	In_2O_3/Al_2O_3	600	4	0.15	14	80	0.36	281
7	Fe_2O_3/AC	600	4.9	2.77	3	83	16	277

T = reaction temperature; CO_2/C_3H_8 = molar ratio of $CO_2:C_3H_8$ in the reaction, $X_{C_3H_8}$ = initial propane conversion, $S_{C_3H_6}$ = initial propene selectivity, STY = space time yield. AC = activated carbon.

Al_2O_3 combination was the most active, due in part to the high dispersion of In in this particular catalyst. Further investigation into the composition of the support revealed that compared with ZrO_2 and SiO_2, Al_2O_3 was the most effective support for In_2O_3, although ZrO_2 was also active.[281] The basicity of the In/ZrO_2 system was suggested to promote the RWGS reaction, which in turn boosted the ODH-CO_2 activity. This conclusion was supported by the substantial increase in the activity observed in ODH-CO_2 compared with DDH. Tian *et al.* recently investigated In/H-ZSM-5.[282] At 580 °C and a $CO_2:C_3H_8$ ratio of 4 : 1, the highest propene yield was 10%. Although the propane conversion was similar without In present, the selectivity was significantly increased from 28% for H-ZSM-5 to 81% for 4 wt% In/H-ZSM-5 (Table 13, entry 2).

Supported vanadia catalysts have also been considered in ODH-CO_2 having been widely applied in various reactions, including propane ODH-O_2,[4] toluene oxidation[283] and formaldehyde oxidation.[284] Vanadia catalysts for ODH-CO_2 were first reported by Nakagawa *et al.* and in this early study, supported vanadia was found to outperform Ga_2O_3.[249] Despite this, few studies have been reported since.[285] Notably, Ascoop *et al.* investigated the role of CO_2 in the reaction over composite WO_X–VO_X/SiO_2 catalysts. Using D_2 as a co-feed, it was shown that 45% of the resultant water contained D_2O. This confirmed a Mars-Van Krevelen mechanism as well as a two-step DDH + RWGS mechanism proceeds over this catalyst. It was found that CO_2 could partially re-oxidise the catalyst and that coke formation was significantly suppressed in the presence of CO_2. Han *et al.* examined a range of VO_X loadings using an MCM-41 as a support.[286] The most active catalyst, 6.8 wt% VO_x/MCM-41, exhibited an initial propene yield of 51% at 600 °C with a $CO_2:C_3H_8$ ratio of 4 : 1. However, the catalyst retained only 65% of its initial activity after 2 h on-stream. The initial STY of this catalyst was 10.7 $mol_{C_3H_6}$ kg_{cat}^{-1} h^{-1} (Table 13, entry 4), which is amongst the most active reported to date, but requires significant improvements to its on-stream stability.

Tsilomelekis and Wang recently investigated mixed metal oxides comprising Fe and Ce for the ODH-CO_2 reaction. It was found that 10 mol% Fe in CeO_2 exhibited the highest propene yield. The propene selectivity of this catalyst was *ca.* 45% at 550 °C with a propane conversion of *ca.* 18%. The major side-reactions observed were dry reforming and cracking. They showed that reforming pathways were more prevalent at higher $CO_2:C_3H_8$ ratios, such as 2.5 : 1 and 5 : 1. However, the catalysts were relatively stable on-stream over 20 h, retaining 80% of their initial activity. Despite the low selectivity, the Fe–CeO_2 catalysts exhibited a comparable STY to supported In_2O_3 (Table 13) and some Ga_2O_3 catalysts (Table 12).

6.4. Supported nanoparticle based ODH-CO_2 catalysts

Despite forming an active component in various industrial DDH processes and being extensively reported in the academic literature for DDH, the number of studies carried out over Pt-based catalysts for ODH-CO_2 is comparatively low. This is also true of other noble metals such as Pd, Au and Ru, where only a handful of studies are available. In this section, the available literature on supported nanoparticle (NP) catalysts, including noble metals, is discussed.

The earliest report of utilising a supported metal NP in ODH-CO_2 was by Guo *et al.* in 2005 who compared Ga and Re supported on H-ZSM-5 (Table 14, entry 4).[247] It was shown that at 550 °C, the addition of CO_2 inhibited the propane conversion significantly and did not greatly affect the selectivity to propene (5.7%). As described above, aromatisation tends to be the dominant pathway when H-ZSM-5 is used.

Supported gold catalysts, which are widely used as catalysts for oxidation reactions[288] including the epoxidation of propene,[289] were studied by Tóth *et al.* When Au NPs supported on MgO, ZnO or Al_2O_3 were investigated over a broad temperature range (500–750 °C), only Au/ZnO exhibited reasonable catalytic activity. The propene selectivity was 56% at 50% conversion at 600 °C. The Au/ZnO material was shown to be very unreactive towards propene and evidence for propane activation at 25 °C was found. Despite this promising initial data, Au NP catalysts have not been investigated further.

Gomez *et al.* investigated various mono- and bi-metallic NP catalysts using CeO_2 as a support at a reaction temperature of 650 °C and a $CO_2:C_3H_8$ ratio of 1 : 1 (Table 14, entries 2 and 3).[21,290] Among the wide range of catalysts tested were Ni_1, Fe_1 and Fe_3-Ni_1 (where the subscript number indicates the molar ratio). While Ni_1 was active mostly for dry reforming to CO + H_2, Fe_1 was inactive. However, Fe_3-Ni_1 exhibited much higher selectivity towards propene. *In situ* XAS measurements revealed that under reaction conditions Fe was oxidised and Ni was metallic. While the overall performance of Fe_3-Ni_1 was moderate (58% selectivity to propene at 2.7% propane conversion, equivalent to a STY of 3.9 $mol_{C_3H_6}$ kg_{cat}^{-1} h^{-1}), the findings demonstrate the sensitivity of reaction pathways to the nanostructure of the catalyst and suggest further optimisation is possible. Subsequent studies on Fe–Co and Fe–Pd catalysts

Table 14 Comparison of selected literature supported NP and metal carbide catalysts for ODH-CO_2

Entry	Catalyst	T/°C	CO_2/C_3H_8	WHSV /$g_{C_3H_8}$ g_{cat}^{-1} h^{-1}	$X_{C_3H_8}$/%	$S_{C_3H_6}$/%	STY/$mol_{C_3H_6}$ kg^{-1}_{cat} h^{-1}	Ref.
1	$Pd/CeZrAlO_x$	500	1	3.3	9.5	93	4.9	291
2	Fe_3–Ni_1/CeO_2	550	1	11.8	2.7	58.2	3.9	21
3	Co_3–Pd_1/CeO_2	550	1	11.8	2.8	25.8	1.8	290
4	Re/H-ZSM-5	550	2.3	0.70	57.6	5.65	0.48	247
5	Mo_2C	550	0.2	0.96	0.5	99	0.11	295

T = reaction temperature; CO_2/C_3H_8 = molar ratio of $CO_2:C_3H_8$ in the reaction, $X_{C_3H_8}$ = initial propane conversion, $S_{C_3H_6}$ = initial propene selectivity, STY = space time yield.

revealed similar trends, whereby the addition of Fe to Co or Pd boosted the selectivity to propene compared with the corresponding monometallic catalyst. However, in all cases the dry reforming reaction competed with the dehydrogenation pathway, significantly limiting the propene selectivity.[290]

Nowicka *et al.* carried out a detailed investigation into Pd/$CeZrAlO_X$ catalysts.[291] It was shown that CO_2 dissociation on the catalyst support was facilitated by the presence of Pd. At 500 °C the catalyst achieved 9.5% conversion and 93% selectivity to propene. Although the STY was 4.9 $mol_{C_3H_6}\ kg_{cat}^{-1}\ h^{-1}$, (Table 14, entry 1) the reaction temperature was 500 °C, which is low for ODH-CO_2 catalysts. Above this temperature, the selectivity to propene rapidly drops and methane and carbon monoxide production increase. It should also be noted that propene selectivity was calculated based on observed products, rather than propane consumption and therefore the contribution of dry reforming was not measured.

Metal carbides have been intensively investigated in recent years for a broad range of reactions and are often described as having properties analogous to precious metals.[292–294] To date, there have been two reports of metal carbides catalysing ODH-CO_2, both of which focus on Mo_2C.[295,296] It was found that in addition to dehydrogenation, hydrogenolysis and reforming played important roles in the reaction network. Overall, the performance of the carbide catalysts was poor compared to typical metal oxide or supported nanoparticle catalysts (Table 14, entry 5).

The number of studies on supported nanoparticle catalysts for ODH-CO_2 are relatively few and those available indicate that this field of research has great potential. The major challenge is in understanding and inhibiting side-reactions such as reforming, which are known to proceed over this class of catalyst, unlike in Cr- and Ga-based catalysts. Careful consideration of the nanostructure and composition has shown that the selectivity can be readily tuned to favour different pathways, and further investigation in this area may well be able to harness the high activity of supported nanoparticles as well as favour dehydrogenation pathways.

Despite the fact that ODH-CO_2 of light alkanes has been known for over twenty years, catalyst design has largely been limited to a handful of metal oxide catalysts, namely chromia and gallia. The most promising of these catalysts are supported metal oxides, which typically result in high initial propene yields. However, all catalysts suffer from rapid deactivation on-stream, which is typically attributed to coke formation blocking active sites. However, few investigations have studied the long-term stability of the catalyst beyond 12 h on-stream. In many cases, the catalyst can be regenerated periodically, by burning off the coke using O_2. As discussed above, catalyst regeneration is commonplace in commercial DDH processes and therefore isn't necessarily a barrier to commercialisation. However, the best STYs reported are, with few exceptions, in the range of 5–10 $mol_{C_3H_6}\ kg_{cat}^{-1}\ h^{-1}$, whereas for the DDH reaction, values over 100 $mol_{C_3H_6}\ kg_{cat}^{-1}\ h^{-1}$ are possible. As a result, further advances in the activation of propane over ODH-CO_2 catalysts are required. Despite dozens of reports over several decades on Cr- and Ga- based catalysts, the improvements in catalyst performance have been incremental. The knowledge gained from these studies on the importance of reducibility and the balance of acid and base sites should be applied to supported NP catalysts, which are a promising and somewhat neglected category of ODH-CO_2 catalyst.

7. Oxidative dehydrogenation with nitrous oxide

O_2 and CO_2 are currently the most commonly reported oxidants in the oxidative dehydrogenation of propane. However, other oxidants have also been shown to be feasible. Sulfur dioxide and halogen-based compounds have largely been ignored in recent decades due to their corrosive properties, while H_2O_2 has had its commercialisation deferred due to difficulties in its synthesis.[297] Another relevant oxidant, however, is N_2O. It should be noted that N_2O is a greenhouse gas which has a global warming potential approximately 310 times higher than that of CO_2.[298,299] Therefore, processes that remove N_2O gas from the atmosphere are highly desirable. The industrial sector produces N_2O as a by-product from various processes, including nitric and adipic acid production as well as fossil fuel combustion sources which make up a total of 15% of anthropogenic sources.[298] Many production plants will have N_2O abatement in place already, so the possibility for flowing propane through this process exists. Despite this, research into the ODH-N_2O reaction of propane is rather limited, mostly due to the cost of N_2O and product dilution in N_2. Furthermore the research that does exist is reserved for elucidating structure–activity relationships, which can be used to better understand the ODH reaction in general.[300]

7.1. Fe-Zeolite based ODH-N_2O catalysts

In 1998 Panov *et al.*[301] reported a new type of O species observed in Fe-ZSM-5 when it was exposed to N_2O. The species was referred to as α-oxygen and is able to perform highly selective dehydrogenation and oxidation reactions of hydrocarbons such as the oxidation of benzene to phenol, which occurred with nearly 100% selectivity at conversions of 97–98%. In addition, dehydrogenation of ethane and methane oxidation reactions are also possible using N_2O. Panov further detailed the characteristics of α-oxygen. It is typically associated with isolated Fe ions or small complexes found within the zeolite's micropores, as opposed to the tetrahedral Fe ions within the crystal lattice, or the finely dispersed metal oxide phase of the zeolite surface. It has been suggested that this oxygen species could be useful in the oxidative dehydrogenation of propane.

Other examples of ZSM-5 modified catalysts on top of Fe include doping with metals such as Mn and Co.[302] The authors examined the selectivity, conversion and yield of propene of these three materials. While all three showed similar selectivity (between 70–80%), Fe-ZSM-5 was reported to exhibit the highest conversion and therefore best yield towards propene. The α-oxygen species is formed *via* the interaction

between N_2O and framework stabilised Fe^{2+} ions, resulting in the dissociation of N_2O and the formation of mono- and binuclear Fe^{3+}–O^- species, (α-oxygen). These α-oxygen species react with propane by providing atomic oxygen, producing propanol, which is subsequently dehydrated to propene.[303,304] It is from this mechanism that the selectivity originates, because once the hydrocarbon's interaction with α-oxygen is complete, the molecule would need to vacate the zeolite channel in order for a new N_2O molecule to enter and generate an new α-oxygen site, therefore not allowing for immediate further oxidation.[301] It is also evident from this mechanism that coordination of oxygen to an Fe^{2+} species is required, and therefore does not occur on tetrahedral framework Fe species due to a lack of vacant sites in the Fe complex.[303]

By considering simply the activation of N_2O, Groen *et al.*[305] enhanced the activation by performing an alkaline treatment on Fe-ZSM-5, which increased the number of Fe^{2+} sites, decreased the amount of oligonuclear clusters and increased the porosity of the zeolite. The calcined catalysts were treated in 0.2 M NaOH for 2 h, before undergoing an ion-exchange in NH_4NO_3 solution. Where the calcined Fe-ZSM-5 catalyst reached complete conversion of N_2O at 552 °C, the catalysts which had undergone alkaline treatment and subsequent ion-exchange reached total conversion at slightly under 527 °C. This increase in porosity and highly active Fe sites shows potential for the dehydrogenation reaction of propane, however little research effort has extended into this area.[305,306]

Further to this, Pérez-Ramírez *et al.*[303,307] reported highly active catalysts after the steam treatment of Fe-ZSM-5 zeolites, which produced an initial STY of 180 $mol_{C_3H_6}$ kg_{cat}^{-1} h^{-1} (Table 15, entry 2) when carried out at 525 °C. This high productivity is ascribed to the generation of extra-framework Fe sites during the steam treatment.[303,307,308] However, this high productivity is hindered by a rapid deactivation, with the authors observing a minimum decrease in propene yield of *ca.* 3% over 3 h at 452 °C, and a maximum decrease in propene yield of *ca.* 12% over the same timescale at 525 °C. This rapid deactivation, which will be discussed further, is the most significant issue facing the use of N_2O as an oxidant to date.

The main deactivation pathway of this catalyst is ascribed to the build-up of carbonaceous deposits at the Brønsted acid sites in the zeolite pores, therefore blocking the pores and active Fe sites. It has been reported that blocking or removing the Brønsted acid sites lessens the impact of deactivation.[303,309] Despite being the major deactivation pathway, compared to other zeolite examples, ZSM-5 shows significant resistance to deactivation, despite the finding that they produce more coke than other examples. This behaviour is attributed to the location of the coke formation, which occurs at Al-protonic sites, away from the extra-framework Fe-active sites.[303] However, the use of N_2O as an oxidant invariably leads to rapid deactivation despite the positive effect of the zeolite, when compared to other oxidants, such as O_2. Using a mixture of oxidant gases, O_2 and N_2O, was reported to decrease the deactivation of Fe-ZSM-5 further *via* oxidising the carbon deposits.[309] The limitation of this being the inclusion of too much O_2, leads to overoxidation of the desired products and therefore lower selectivity towards propene. Bulánek *et al.* reported that a mixture of N_2O and O_2 over a steam-treated Fe-ZSM-5 catalyst and found that with the inclusion of oxygen the conversion consistently increased; however, the selectivity consistently decreased (Table 15, entry 1).[309] The problem remains, that when comparing oxidant properties for the ODH reaction of propane, N_2O has a significant tendency for rapid deactivation.

In 2010, Kowalska-Kuś *et al.*[310] investigated the role of Brønsted acid sites in Fe-ZSM-5 and their effect on the ODH-N_2O activity. It was found that in the presence of a high number of protonic sites, cracking and ODH reactions of propane occurred simultaneously, and would often lead to high selectivity towards total oxidation products. Conversely, removal of protonic sites *via* doping with sodium reduced the oxidative activity of the zeolite and modified the reaction to favour the ODH pathway. Subsequently, the propene would undergo further cracking reactions. Therefore, shorter contact times result in higher propene selectivity. This method led to propene selectivities higher than previously reported for this reaction, (over 80%), but the limitation of this approach is the significantly lowered conversion due to the lower oxidative activity of the zeolite.

It is clear that adjusting the acidity of the zeolite greatly influences the conversion and selectivity of the ODH-N_2O reaction. As mentioned earlier, steam treatment has been found to increase the number of Fe^{2+} active sites. This, as well as dealuminating the zeolites, leads to a higher presence of weak and medium acid sites, which enhance selectivity towards propene.[304,311] Steam treatment was also found to increase stability towards coking in the zeolites.[311] With these methodologies implemented, Ates *et al.*[311] were able to produce a catalyst with a STY of 10 $mol_{C_3H_6}$ kg_{cat}^{-1} h^{-1} (Table 15, entry 4).

Table 15 Comparison of catalytic performance of selected catalysts for the ODH-N_2O reaction

Entry	Catalyst	T/°C	N_2O/C_3H_8	WHSV /$g_{C_3H_8}$ g_{cat}^{-1} h^{-1}	$X_{C_3H_8}$/%	$S_{C_3H_6}$/%	STY/$mol_{C_3H_6}$ kg_{cat}^{-1} h^{-1}	Ref.
1	FeH-MFI-1200-HT	450	1	3.0	64	29	12	309
2	Steam-activated Fe-ZSM-5	450	1	39.4	48	45	180	303
3	VO_x/MCM-41	475	1	—	—	—	29	313
4	Steam-activated Fe-ZSM-5	500	1	2.4	29.2	68.8	10	311
5	In_2O_3–Al_2O_3 mixed oxide	600	4	0.15	43.6	63.1	6.8	316

T = reaction temperature; N_2O/C_3H_8 = molar ratio of N_2O : C_3H_8 in the reaction, $X_{C_3H_8}$ = initial propane conversion, $S_{C_3H_6}$ = initial propene selectivity, STY = space time yield. Values next to element/phase is the loading in wt%.

In summary, while the ODH-N_2O reaction is hindered significantly by its tendency to deactivate rapidly without the presence of O_2, Fe-ZSM-5 as a catalyst is very resistant to deactivation and its use for the ODH-N_2O reaction is contingent on several factors. The oxidation of extra-framework Fe^{2+} sites to Fe^{3+}–O^- sites is a crucial step in the mechanism, and therefore producing a material with a large number of these sites would increase the yield of propene. The Brønsted acidity of the Fe-ZSM-5 zeolite both decreases the selectivity to propene, due to a high number of protonic sites leading to selectivity towards total oxidation, and increases the rate of deactivation, allowing for the generation of carbonaceous deposits which block the zeolite pores. The most promising materials currently are steamed Fe-ZSM-5, as the steam treatment has been found to produce more Fe^{2+} sites and dealuminate the framework, causing an increase in weak and medium acid sites. With fewer strong protonic sites, the reaction mechanism shifts towards favouring the dehydrogenation of propane, therefore resulting in a consecutive propane dehydrogenation-propene cracking pathway which allows for a higher selectivity to propene with shorter contact times. Despite these advancements, recent research on Fe-ZSM-5 for ODH-N_2O has been minimal due to their rapid deactivation, the high cost of N_2O and the presence of N_2 in the product stream.

7.2. Other ODH-N_2O catalysts

Other catalysts reported to be active for the ODH-N_2O reaction of propane include supported vanadium oxides. In 2001 Kondratenko *et al.*[312] reported that VO_x/γ-Al_2O_3 was active for ODH of propane with O_2 and N_2O and investigated the effect of vanadia loading. It was found that, similar to Fe-ZSM-5 catalysts, on replacing O_2 with N_2O the overall activity of the catalyst decreased, but the selectivity increased. This trend was ascribed to the lower oxidising potential of N_2O.

Further to this, DFT studies were carried out to elucidate the role of the oxidant in the ODH reaction.[300] These calculations first revealed that propene is formed *via* successive removal of two hydrogen atoms *via* a redox mechanism over VO_x active sites. The active sites are reduced from V^{5+} to V^{3+} and V^{4+} during hydrogen removal from the propane molecule, which then require re-oxidation before removal of a second hydrogen. The N_2O was found to only oxidise V^{3+}, whereas O_2 was able to oxidise both V^{3+} and V^{4+}. Upon re-oxidation of the VO_x active sites with O_2, peroxovanadates were formed; however these species were not formed with N_2O as the oxidant. Peroxovanadates are highly active for the total oxidation of propane. The formation of these peroxovanadates is a key explanation for the more selective nature of N_2O compared to O_2. In the most active catalyst, the STY of VO_x/MCM-41 was 29 $mol_{C_3H_6}\ kg_{cat}^{-1}\ h^{-1}$ (Table 15, entry 3), which is less than the most active steam-activated Fe-ZSM-5 catalysts, but more active than some reports over Fe-MFI catalysts.

In addition, V/γ-Al_2O_3, V/MCM-41, and V/amorphous SiO_2 catalysts have also been prepared and characterised in order to elucidate the structure activity relationships between the catalyst and the ODH-N_2O reaction of propane.[313–315] It was found that the selectivity for propene was lower over V/γ-Al_2O_3; a result which was ascribed to the acidic nature of the alumina support, over which dehydrogenated propene adsorbed to the support surface where it further oxidised to CO_x species. This effect is less prominent on less acidic support surfaces such as SiO_2 and MCM-41.

The vanadia loading on the support materials was also found to influence the selectivity.[312–314] On the materials V/MCM-41, and V/SiO_2 materials, the nature and distribution of the V remained consistent up to a loading of *ca.* 5 wt%, above which three-dimensional V_2O_5 clusters began to form, and these have unreactive bulk V sites. At lower loadings however, the support surface is more exposed, allowing for adsorption of propene and total oxidation. Therefore, a loading of *ca.* 5 wt% is optimal to get a high surface coverage, without forming three-dimensional clusters. Kondratenko *et al.* were able to achieve selectivities of over 90% at conversions limited to 2 and 10% with such materials.[315]

Finally, in 2010, Chen *et al.* reported the use of In_2O_3-Al_2O_3 as a novel catalyst for the ODH-CO_2.[279] In 2011 the same group reported the same catalyst's potential for the ODH-N_2O reaction.[316] The activity of the In_2O_3–Al_2O_3 catalyst shows a significant dependence on the concentration of In^0 in the material. The catalyst exhibited a low STY of 6.8 $mol_{C_3H_6}\ kg_{cat}^{-1}\ h^{-1}$ (Table 15, entry 5). Despite this, the In_2O_3–Al_2O_3 catalyst shows potential to surpass the more commonly researched Fe-zeolites in terms of stability. Whereas previous examples of Fe-zeolites have displayed significant deactivation over 3 h time-on-stream, this In-based catalyst was observed to lose 6% propene yield over a total of 12 h on stream. Considering that deactivation is the most significant issue plaguing the use of N_2O as an oxidant in the ODH-N_2O reaction of propane, the In_2O_3-Al_2O_3 has good potential to be an active and stable catalyst.

In summary, although Fe-ZSM-5 has the most potential for the ODH-N_2O reaction for propane, several other catalysts have been tested. Vanadia based catalysts have been shown to be highly active for the reaction, which were found to be more selective when supported on less acidic, silica-based support materials, and at loading levels of lower than 5 wt%. Indium based catalysts have also been suggested for the ODH-N_2O reaction, with the potential for a highly stable catalyst compared to Fe-ZSM-5, which displays significant deactivation and is likely to be the underlying reason behind the relatively low research effort put into the N_2O route compared to the other potential oxidants described in this review article.

8. Summary of propane dehydrogenation and over-arching themes in catalyst design

In the above sections, the literature on the catalytic dehydrogenation of propane has been critically reviewed. Each sub-reaction of propane dehydrogenation has specific kinetic and

thermodynamic requirements, and this is reflected in the diverse variety of catalysts that have been developed in recent decades. Throughout this review we have attempted to compare the productivity of catalysts for DDH and the various ODH reactions by measuring space time yield of the catalyst (*i.e.*, the moles of propene produced per kg of catalyst per hour). This is an imperfect metric with which to compare catalysts, but the wide range of reaction conditions and catalyst types explored means that calculating turnover frequencies for each catalyst is not possible. One assumption when comparing productivity is that catalysts are tested under conditions to maximise their performance. This is of course not the case for all studies, especially those where kinetic measurements were of interest, or where there were other constraints present. However, by comparing the range of values associated with a single class of catalyst, it is possible to identify the highest performing catalysts in each class and broadly assess the potential of each. Fig. 11 below compares a selection of literature catalysts (presented in Tables 2–14) for each reaction, colour-coded to highlight the performance of different elements in different reactions. The horizontal dashed line is marked at the equivalent of 5 $kg_{C_3H_6}$ kg_{cat} h^{-1}, which has been considered to be space time yield that may warrant consideration of commercial application.[196,213] Such a value is difficult to pinpoint, but given that this is where the more active Pt and CrO_X catalysts for DDH are found, it is reasonable.

It is clear that for the DDH reaction, Pt- and Cr-based catalysts dominate the highest space time yield measurements. This is expected given their widespread use in industrial processes. Beyond this, ZrO_2 and ZnO/ZrO_2 catalysts perform strongly, and their low cost and low toxicity make them well-suited for commercial application. These materials have only recently been reported in the literature and with further development they may match or outperform Pt- and Cr-based catalysts. It is also possible that they are already present in the K-PRO process.

In ODH-O_2, B-based catalysts are the best performing, with STY values in excess of 70 $mol_{C_3H_6}$ kg_{cat}^{-1} h^{-1} reported. Some boron catalysts exceeded 200 $mol_{C_3H_6}$ kg_{cat}^{-1} h^{-1}, well above the 5 $kg_{C_3H_6}$ kg_{cat} h^{-1} threshold and underscores their potential for commercial application. Although ODH-O_2 produces H_2O as a side-product (rather than H_2), ethene is typically the major by-product in B-catalysed reactions rather than coke formation. As an exothermic reaction, large-scale implementation may be preferable to the endothermic DDH reaction, which requires specific heat-generating technology to be efficient. Therefore the commercialisation of a ODH-O_2 process using B catalysts may be realistic.

ODH-CO_2 catalysts do not yield more than *ca.* 20 $mol_{C_3H_6}$ kg_{cat}^{-1} h^{-1}, which suggests that CO_2 activation remains a key challenge. While CrO_x based catalysts yield the highest STY, only incremental advances have been made in recent years and it will take a step-change in catalyst development before ODH-CO_2 can be meaningfully compared to DDH and ODH-O_2 reactions, as a mean to produce propene. Interestingly, some of the highest STY values reported are CrO_X/activated carbon and FeO_X/activated carbon. The obvious drawback of activated carbon as a support is that oxidative regenerations will combust the support, but clearly its chemical properties are desirable as a catalyst support.

In ODH-N_2O, Fe-ZSM-5 are the most active catalysts known, and in one example a STY of 178 $mol_{C_3H_6}$ kg_{cat}^{-1} h^{-1} was reported. ODH-N_2O is the least studied sub-reaction and it is thought that the relatively high cost and low availability of N_2O may be the most limiting aspect. N_2O is a by-product in various chemical processes including adipic acid and nitric

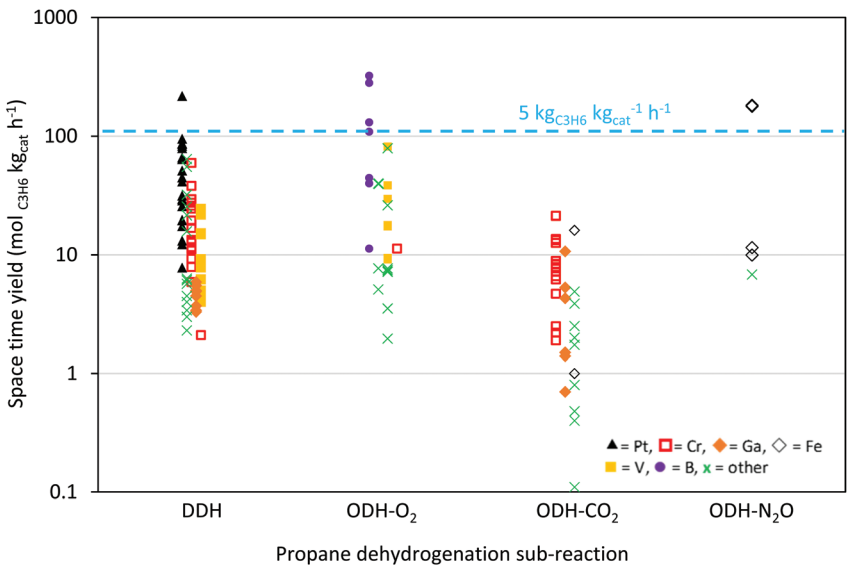

Fig. 11 Space time yield plot of a selection of DDH, ODH-CO_2 and ODH-O_2 catalysts, showing the relative performance of catalysts in each sub-reaction.

Table 16 Summary of reaction conditions and catalyst properties in each dehydrogenation sub-reaction

Reaction	Reaction temperature range /°C	Significant side reactions	Role of redox sites	Role of acid sites	Role of basic sites	Typical deactivation mechanisms
DDH	550–630	Coking, cracking	Not directly involved	Alkane activation, strong acid sites promote coking	Alkene desorption	Coking
ODH-CO_2	400–600	Dry reforming, coking, cracking	CO_2 activation	Alkane activation, strong acid sites promote coking	Alkene desorption, CO_2 activation	Coking, overreduction of catalyst
ODH-O_2	400–600	Overoxidation, cracking	O_2 activation	Alkane activation	Alkene desorption	Sintering
ODH-N_2O	400–600	Overoxidation, coking, cracking,	N_2O activation	Alkane activation, strong acid sites promote coking	Alkene desorption	Coking

acid production, but there may be few other opportunities for large-scale sequestration and utilisation of N_2O on an industrial scale. It is also apparent that the selectivity to propene is often below 70% and the catalysts rapidly deactivate on-stream.

Table 16 below shows a summary of the typical chemical and catalytic properties associated with each reaction. While the temperature range of each reaction overlaps, generally ODH-O_2 and ODH-N_2O are carried out at lower temperature than DDH, while ODH-CO_2 typically lies in between or nearer to DDH reaction temperatures. In terms of side-reactions, cracking is the only common source of by-products in each sub-reaction. Coking remains a major challenge in DDH, ODH-CO_2 and ODH-N_2O, while overoxidation is generally observed in the ODH-O_2 and ODH-N_2O processes. Redox sites play an active role in each of the oxidative dehydrogenation reactions, while in DDH they are not required. The importance of acid and base sites have been frequently examined across each sub-reaction, and interestingly remain the only catalytic properties that are applicable to each sub-reaction. Acid sites are widely known to activate alkanes, but if the acid sites are too strong, the alkane will be retained on the surface and lead to coking, or overoxidation in the case of ODH-N_2O and ODH-O_2 reactions. Basic sites on the other hand, are known to facilitate alkene desorption and in the case of ODH-CO_2, to activate CO_2. Therefore, a balance of these sites is necessary to promote sufficient propane activation and propene desorption. Prevalent deactivation mechanisms also vary between sub-reactions, with coking frequently cited as a cause for loss of on-stream activity in DDH, ODH-CO_2 and ODH-N_2O. The ODH-O_2 catalysts on the other hand are generally much more stable on-stream. It is noteworthy however, that despite relatively fast deactivation of DDH catalysts, the activity can be regenerated after an oxidative treatment, significantly extending the catalyst lifetime.

Regarding catalyst design for each reaction, there are catalysts that can efficiently operate for DDH, ODH-CO_2 and ODH-O_2, while there are some that are reaction-specific. This is exemplified by supported chromium oxides, which have been reported for DDH, ODH-CO_2 and ODH-O_2. On the other hand, Fe-ZSM-5, which is highly active for ODH-N_2O has a unique dimeric Fe^{2+} site that can activate N_2O but not O_2. Therefore, it would not be applicable to ODH-O_2 or DDH. The ability of Cr to catalyse multiple sub-reactions is likely to be related to its stability (and activity) in multiple valence states. In DDH, Cr^{3+} sites are considered the active species, while in ODH-CO_2 and ODH-O_2, the redox cycle of Cr to Cr^{4+} and Cr^{3+} all facilitate the activation of the oxidant. Supported vanadia catalysts can also exhibit multiple valence states, and are also active in DDH, ODH-CO_2 and ODH-O_2.

Aside from the active element, catalyst supports also comprise a vital component of any propane dehydrogenation catalyst. The primary role of the support is to enhance and maintain high dispersion of the active phase. This has been demonstrated multiple times over metal oxides such as those of Ga, Cr, V and Fe, where SiO_2, Al_2O_3, and ZrO_2 have been widely implemented as supports. The acid and base sites of the support also affect the performance of the catalyst and can be adjusted with promotors. This strategy has been widely applied in DDH catalysts. The support may also play a more active role in catalysis, by activating propane, CO_2 or O_2.

A multitude of chemical elements including precious metals, rare earth metals, base metals and non-metals have all been discovered to play a role in catalysing propane dehydrogenation in various contexts. Any sustainable process should aim to use abundant and renewable raw materials, and this applies to the catalyst as well as the starting reactants. It is clear that across the more active propane dehydrogenation catalysts known, there is a range in the abundance and production of the chemical elements required. Table 17 summarises the availability of a range of chemical elements commonly applied in propane dehydrogenation catalysts.

In the DDH reaction, the most active elements are typically Pt and Cr, which are already implemented in commercial processes, and more recently Zr and Zn-based alternatives have been used. While chromium is relatively abundant as a chemical element, Pt is very scarce and production limited to a few countries, namely South Africa. The global reserves of individual platinum group metals (PGMs) is not possible to accurately quantify, but it is estimated that the total global reserve of PGMs is over 100 000 tonnes meaning that Pt and Pd are easily

Table 17 Global production and abundance of chemical elements typically employed in propane dehydrogenation catalysts

Chemical element	Common mineral form	Annual production in 2019/10^3 tonnes	Estimated world reserves/10^3 tonnes
Boron	B_2O_3, other borates	>3500	>1 200 000
Chromium	chromite	44 000	570 000
Gallium	Trace element in other minerals (<50 ppm)	0.44[a]	560[a]
Palladium	Metallic	0.21	Unknown
Platinum	Metallic	0.18	Unknown
Vanadium	Oxidic form	73	>63 000
Zinc	Spharelite	13 000	1 900 000
Zirconium	$ZrSiO_4$	1400	64 000

[a] From ref. 317 which uses data for 2014. Unless otherwise stated, the values were reproduced from ref. 318.

the most scarce chemical elements commonly used for propane dehydrogenation. While supported nanoparticle catalysts use a fraction of the quantity of metal that would be required in a metal oxide catalyst, it would be desirable for any DDH process to use an abundant, non-toxic element as the main component of the catalyst. This makes the recent discovery of Zr/TiZnO_x all the more promising.[157] The ODH-O_2 reaction has recently been dominated by the discovery of boron-based catalysts, which are highly abundant compared to most other ODH-O_2 catalysts such as V. Accordingly it should be considered a good candidate for commercialisation from the point of view of sustainability. ODH-CO_2 catalysts are typically Cr or Ga based. As described above, Cr is highly abundant but also toxic. Gallium is present in the Earth's crust at around 17 ppm (ref. 319) and is typically found as an impurity in minerals such as bauxite, sphalerite and germanite. Although present as a trace element in these minerals, the abundance of bauxite is vast and it is estimated that the amount of gallium contained in bauxite alone is 560 000 tonnes, which places it well above platinum in abundance. The field of research into DDH and ODH-O_2 is very diverse, and in recent years a number of novel discoveries has expanded the range of catalytically active elements known for this reaction. This means that the reliance on scarce elements like Pt, or toxic ones like Cr is limited. Future sustainable DDH and ODH-O_2 processes should capitalise on this knowledge and implement abundant elements such as B, Zn, V or Zr. With regards to ODH-CO_2, the performance of the most active catalysts is still well below what would be considered for commercialisation, but the research community should look to the successes of the above-mentioned abundant elements for inspiration in designing novel ODH-CO_2 catalysts.

9. Outlook

While the current focus of government policy is based on net zero carbon, it is clear that society will still need a wide range of products based on carbon-containing molecules. It is now essential that the chemical industry focusses on accessing such carbon from sustainable sources. It is likely that for the near- and mid-range future the current key platform molecules such as propene will still be required. Against this background, the dehydrogenation of propane will remain a major industrial process and its future importance is guaranteed due to the scale and breadth of propene applications in modern society. Currently, the majority of propane is sourced from non-renewable feedstocks, but the industry has recognised the need to change and steps have been taken to develop processes for renewable propane to be generated. It may be many years before so-called bio-propane can compete with non-renewable propane sources in terms of supply, but the catalytic processes described in this review will be required to enable this technology to be used. Therefore, the development of catalysts for the direct dehydrogenation of propane in the presence or absence of an oxidant will continue to attract attention from academia and industry alike, as significant advances have been made in recent years. An analysis of the sustainability of current C_3H_6 production methods, namely steam cracking and methanol-to-olefins, reveals that direct dehydrogenation has several advantages in efficiency when a selective catalyst is applied. Life cycle analyses of oxidative dehydrogenation reactions using O_2 and CO_2 have not been carried out, due to the fact that these reactions have not been commercialised yet. However, in principle the processes have the potential to offer lower temperature routes to forming C_3H_6 without lengthy catalyst regeneration steps.

DDH is to date the only reaction that has been operated commercially. The most active catalysts reported in the literature are based on chromium oxide or platinum promoted with tin oxide, but even these require frequent regeneration due to coking. Therefore, the future of DDH catalyst design should focus on reducing deep dehydrogenation reactions that lead to coking. Irrespective of catalyst, common themes have been established in efforts to improve C–H bond activation, reducing propane and hydrogen adsorption on surface sites. Of these, supports with weak and moderate surface acidity coupled promoting elements (B, Ga, Cu and Ni to name a few) result in lower Pt utilisation, which is desirable for potentially industrially applicable catalysts. Additionally, a number of noble, non-noble based intermetallic alloys and numerous mixed metal oxides are emerging as viable alternatives to chromium oxide or platinum-based catalysts; and this presents an economic and environmental benefit. In doing so, the frequency of regeneration will be reduced, meaning that fewer CO_2 forming regeneration cycles will be required, thus reducing the carbon footprint of propane production.

ODH-O_2 offers a pathway that avoids the formation of coke entirely, but until recently, the STY typically reported in ODH-O_2 catalysts such as supported vanadia were, with few exceptions, an order of magnitude below that of DDH catalysts. The advent of boron-based catalysts for this reaction has led to a significant increase in the prospects for commercial application. As a relatively stable, non-hazardous and abundant element, boron catalysts may well play a major role in future propene production processes. Furthermore, they appear to be stable on-stream in laboratory tests, although industrially relevant stability tests have not yet been reported.

ODH-CO_2 has attracted interest, mostly in academia,[320] due to the prospect of utilising CO_2 and developing carbon neutral or carbon-negative processes. This is determined by the downstream use of CO, the primary product of CO_2 dissociation. Although ODH-CO_2 catalysts are not known to overoxidise propane, the drawbacks associated with DDH, *i.e.*, coking, often remain and the inertness of CO_2 means that low STYs are frequently reported. The majority of investigations thus far have focussed on Ga- or Cr-based catalysts and improvement in these catalysts has been incremental. Supported nanoparticles on the other hand, have received little attention despite showing some promising results. In this class of catalysts, minimising competing reactions such as reforming, is essential. Future catalyst design should aim to move away from Cr- and Ga-based catalysts to focus on low-temperature CO_2 activation and have controlled redox and acid–base properties. For this reaction to become significant beyond academic interest, a step-change in catalyst performance is needed.

ODH-N_2O is the least studied reaction and progress has not been substantial in recent years. This may be due to the unfavourable economic costs associated with using N_2O as an oxidant, although in an integrated facility where N_2O is produced as a by-product this could be a useful approach. In terms of catalyst performance, the most active catalyst, Fe-ZSM-5, can achieve a similar STY to the more active DDH and ODH-O_2 catalysts. However, the intrinsic selectivity to propene is often below 70% and is undoubtedly the main disadvantage. If propene selectivity can be improved to 90%+, the catalyst would out-perform some of the most active DDH and ODH-O_2 catalysts reported in the literature.

Conflicts of interest

There are no conflicts to declare.

Acknowledgements

This work was carried out as part of the Consortium on Metal Nanocatalysis funded by TotalEnergies. The authors would like to acknowledge the contributions of Moritz Schreiber, Luis Robles and Didier Borremans from Total who were involved in the early conception of the work, and in collating relevant press releases and patent literature.

References

1 Global Data, *Global Propylene Capacity and Capital Expenditure Outlook to 2030 – Asia and Middle East to Lead Globally in Terms of Propylene Capacity Additions*, 2021.
2 J. J. H. B. Sattler, J. Ruiz-Martinez, E. Santillan-Jimenez and B. M. Weckhuysen, *Chem. Rev.*, 2014, **114**, 10613–10653.
3 M. A. Atanga, F. Rezaei, A. Jawad, M. Fitch and A. A. Rownaghi, *Appl. Catal., B*, 2018, **220**, 429–445.
4 C. A. Carrero, R. Schloegl, I. E. Wachs and R. Schomaecker, *ACS Catal.*, 2014, **4**, 3357–3380.
5 L. Shi, Y. Wang, B. Yan, W. Song, D. Shao and A. H. Lu, *Chem. Commun.*, 2018, **54**, 10936–10946.
6 A. Akah, J. Williams and M. Ghrami, *Catal. Surv. Asia*, 2019, **23**, 265–276.
7 I. Amghizar, L. A. Vandewalle, K. M. Van Geem and G. B. Marin, *Engineering*, 2017, **3**, 171–178.
8 M. Ghanta, D. Fahey and B. Subramaniam, *Appl. Petrochem. Res.*, 2014, **4**, 167–179.
9 M. O. Xunhua, B. De Graaf and P. Diddams, *HCN emissions in fluid catalytic cracking*, 2013, vol. 18.
10 Global petrochemical trends: H2 2020 | S&P Global Platts.
11 D. F. Rodríguez-Vallejo, G. Guillén-Gosálbez and B. Chachuat, *ACS Sustainable Chem. Eng.*, 2020, **8**, 3072–3081.
12 A. Agarwal, D. Sengupta and M. El-Halwagi, *ACS Sustainable Chem. Eng.*, 2018, **6**, 2407–2421.
13 Formule-verte, Biocarburants: la bioraffinerie de Total à La Mède opérationnelle en 2018, https://www.formule-verte.com/biocarburants-la-bioraffinerie-de-total-a-la-mede-operationnelle-en-2018/.
14 Neste, Neste delivers first batch of 100% renewable propane to European market - Green Car Congress, https://www.neste.com/releases-and-news/renewable-solutions/neste-delivers-first-batch-100-renewable-propane-european-market%0Ahttps://www.greencarcongress.com/2018/03/20180319neste.html, (accessed 3 March 2021).
15 Borealis, Borealis and Neste begin strategic co-operation to accelerate circularity and bioeconomy in plastics, https://www.borealisgroup.com/news/borealis-and-neste-begin-strategic-co-operation-to-accelerate-circularity-and-bioeconomy-in-plastics, (accessed 4 May 2021).
16 UK Dept of Energy & Climate Change, Atlantic Consulting and Menecon Consulting, *RHI Evidence Report : Biopropane for Grid Injection*, 2014.
17 D. Taher, M. E. Thibault, D. Di Mondo, M. Jennings and M. Schlaf, *Chem. – Eur. J.*, 2009, **15**, 10132–10143.
18 N. Menon, A. Pásztor, B. R. K. Menon, P. Kallio, K. Fisher, M. K. Akhtar, D. Leys, P. R. Jones and N. S. Scrutton, *Biotechnol. Biofuels*, 2015, **8**, 61.
19 K. Chen, A. Khodakov, J. Yang, A. T. Bell and E. Iglesia, *J. Catal.*, 1999, **186**, 325–333.
20 A. M. Gaffney and O. M. Mason, *Catal. Today*, 2017, **285**, 159–165.
21 E. Gomez, S. Kattel, B. Yan, S. Yao, P. Liu and J. G. Chen, *Nat. Commun.*, 2018, **9**, 1398.

22 F. T. Zangeneh, A. Taeb, K. Gholivand and S. Sahebdelfar, *Chem. Eng. Commun.*, 2016, **203**, 557–565.
23 M. Aresta, A. Dibenedetto and E. Quaranta, *J. Catal.*, 2016, **343**, 2–45.
24 M. Pretz, B. Fish, L. Luo and B. Tears, Shaping the future of on-purpose propylene production, https://www.hydrocarbonprocessing.com/magazine/2017/april-2017/special-focus-petrochemical-developments/shaping-the-future-of-on-purpose-propylene-production, (accessed 13 May 2021).
25 S. Sarkaer, in *Global Refining and Petrochemicals Congress*, 2019.
26 Clariant, CATOFIN® Propane/Butane Dehydrogenation, http://www.cbi.com/What-We-Do/Technology/Refining/Propane-Butane-Upgrading/Propane-Butane-Dehydrogenation.
27 Clariant, Clariant's breakthrough hgm concept for propane dehydrogenation unit - a proven success in China, https://www.clariant.com/en/Corporate/News/2015/03/Clariants-breakthrough-HGM-concept-for-Propane-dehydrogenation-Unit-a-proven-success-in-China, (accessed 6 May 2021).
28 US Pat., USO09725380B2, 2017.
29 Inside Industry, Ineos selects clariant's catofin® catalysts for europe's largest propane dehydrogenation plan, https://www.insideindustry.com/index.php/news2/chemicals-pharmaceuticals/897-ineos-selects-clariant-s-catofin-catalysts-for-europe-s-largest-propane-dehydrogenation-plant, (accessed 6 May 2021).
30 Hydrocarbon Engineering, KBR signs agreement for propane dehydrogenation project, https://www.hydrocarbonengineering.com/petrochemicals/14042021/kbr-signs-agreement-for-propane-dehydrogenation-project/, (accessed 6 May 2021).
31 E. Araujo-Lopez, B. D. Vandegehuchte, D. Curulla-Ferre, D. I. Sharapa and F. Studt, *J. Phys. Chem. C*, 2020, **124**, 27503–27510.
32 I. Horiuti and M. Polanyi, *Trans. Faraday Soc.*, 1934, **30**, 1164–1172.
33 A. Iglesias-Juez, A. M. Beale, K. Maaijen, T. C. Weng, P. Glatzel and B. M. Weckhuysen, *J. Catal.*, 2010, **276**, 268–279.
34 A. Farjoo, F. Khorasheh, S. Niknaddaf and M. Soltani, *Sci. Iran.*, 2011, **18**, 458–464.
35 Q. Li, Z. Sui, X. Zhou, Y. Zhu, J. Zhou and D. Chen, *Top. Catal.*, 2011, **54**, 888–896.
36 Z. J. Zhao, C. C. Chiu and J. Gong, *Chem. Sci.*, 2015, **6**, 4403–4425.
37 R. M. Rioux, H. Song, J. D. Hoefelmeyer, P. Yang and G. A. Somorjai, *J. Phys. Chem. B*, 2005, **109**, 2192–2202.
38 R. T. Vang, K. Honkala, S. Dahl, E. K. Vestergaard, J. Schnadt, E. Lægsgaard, B. S. Clausen, J. K. Nørskov and F. Besenbacher, *Nat. Mater.*, 2005, **4**, 160–162.
39 M. Santhosh Kumar, D. Chen, J. C. Walmsley and A. Holmen, *Catal. Commun.*, 2008, **9**, 747–750.
40 W. Zhang, H. Wang, J. Jiang, Z. Sui, Y. Zhu, D. Chen and X. Zhou, *ACS Catal.*, 2020, **10**, 12932–12942.
41 S. Chen, X. Chang, G. Sun, T. Zhang, Y. Xu, Y. Wang, C. Pei and J. Gong, *Chem. Soc. Rev.*, 2021, **50**, 3315–3354.
42 S. Chen, C. Pei, G. Sun, Z.-J. Zhao and J. Gong, *Acc. Mater. Res.*, 2020, **1**, 30–40.
43 M.-L. Yang, Y.-A. Zhu, X.-G. Zhou, Z.-J. Sui and D. Chen, *ACS Catal.*, 2012, **2**, 1247–1258.
44 G. J. Siri, J. M. Ramallo-López, M. L. Casella, J. L. G. Fierro, F. G. Requejo and O. A. Ferretti, *Appl. Catal., A*, 2005, **278**, 239–249.
45 O. A. Bariås, A. Holmen and E. A. Blekkan, *J. Catal.*, 1996, **158**, 1–12.
46 S. Rimaz, L. Chen, S. Kawi and A. Borgna, *Appl. Catal., A*, 2019, **588**, 1172663.
47 G. Sun, Z. J. Zhao, R. Mu, S. Zha, L. Li, S. Chen, K. Zang, J. Luo, Z. Li, S. C. Purdy, A. J. Kropf, J. T. Miller, L. Zeng and J. Gong, *Nat. Commun.*, 2018, **9**, 4454.
48 R. M. Mironenko, O. B. Belskaya, V. P. Talsi, T. I. Gulyaeva, M. O. Kazakov, A. I. Nizovskii, A. V. Kalinkin, V. I. Bukhtiyarov, A. V. Lavrenov and V. A. Likholobov, *Appl. Catal., A*, 2014, **469**, 472–482.
49 L. Shi, G. M. Deng, W. C. Li, S. Miao, Q. N. Wang, W. P. Zhang and A. H. Lu, *Angew. Chem., Int. Ed.*, 2015, **54**, 13994–13998.
50 E. J. Jang, J. Lee, H. Y. Jeong and J. H. Kwak, *Appl. Catal., A*, 2019, **572**, 1–8.
51 Q. Yu, T. Yu, H. Chen, G. Fang, X. Pan and X. Bao, *J. Energy Chem.*, 2020, **41**, 93–99.
52 F. Jiang, L. Zeng, S. Li, G. Liu, S. Wang and J. Gong, *ACS Catal.*, 2015, **5**, 438–447.
53 X. Chen, M. Ge, Y. Li, Y. Liu, J. Wang and L. Zhang, *Appl. Surf. Sci.*, 2019, **490**, 611–621.
54 W. Tolek, K. Suriye, P. Praserthdam and J. Panpranot, *Catal. Today*, 2020, **358**, 100–108.
55 L. L. Shen, K. Xia, W. Z. Lang, L. F. Chu, X. Yan and Y. J. Guo, *Chem. Eng. J.*, 2017, **324**, 336–346.
56 X. Wu, Q. Zhang, L. Chen, Q. Liu, X. Zhang, Q. Zhang, L. Ma and C. Wang, *Fuel Process. Technol.*, 2020, **198**, 106222.
57 Y. Zhang, Y. Zhou, M. Tang, X. Liu and Y. Duan, *Chem. Eng. J.*, 2012, **181–182**, 530–537.
58 M. Santhosh Kumar, A. Holmen and D. Chen, *Microporous Mesoporous Mater.*, 2009, **126**, 152–158.
59 W. Wannapakdee, T. Yutthalekha, P. Dugkhuntod, K. Rodponthukwaji, A. Thivasasith, S. Nokbin, T. Witoon, S. Pengpanich and C. Wattanakit, *Catalysts*, 2019, **9**, 174.
60 Z. Guofu and D. Shengxin, *CN Pat.*, CN104607235, 2015.
61 C. Zunzhong and S. Luyang, *CN Pat.*, CN105056990, 2015.
62 S. Barri, *EU Pat.*, EP0212850, 1985.
63 Y. Wang, Z. P. Hu, X. Lv, L. Chen and Z. Y. Yuan, *J. Catal.*, 2020, **385**, 61–69.
64 Z. Xu, Y. Yue, X. Bao, Z. Xie and H. Zhu, *ACS Catal.*, 2020, **10**, 818–828.
65 Z. Wu, B. C. Bukowski, Z. Li, C. Milligan, L. Zhou, T. Ma, Y. Wu, Y. Ren, F. H. Ribeiro, W. N. Delgass, J. Greeley, G. Zhang and J. T. Miller, *J. Am. Chem. Soc.*, 2018, **140**, 14870–14877.

66 L. Deng, T. Shishido, K. Teramura and T. Tanaka, in *Catalysis Today*, 2014, vol. 232, pp. 33–39.
67 L. Deng, H. Miura, T. Shishido, Z. Wang, S. Hosokawa, K. Teramura and T. Tanaka, *J. Catal.*, 2018, **365**, 277–291.
68 L. Deng, H. Miura, T. Shishido, S. Hosokawa, K. Teramura and T. Tanaka, *Chem. Commun.*, 2017, **53**, 6937–6940.
69 Z. Ji, D. Miao, L. Gao, X. Pan and X. Bao, *Chin. J. Catal.*, 2020, **41**, 719–729.
70 L. Wang, Y. Wang, C. W. Zhang, J. Wen, X. Weng and L. Shi, *Catal. Sci. Technol.*, 2020, **10**, 1248–1255.
71 J. Wu, L. Wang, X. Yang, B. Lv and J. Chen, *Ind. Eng. Chem. Res.*, 2018, **57**, 2805–2810.
72 C. Meng, Y. Li, H. Wu, W. Wei, Y. Ning, Y. Cui, Q. Fu and X. Bao, *Phys. Chem. Chem. Phys.*, 2018, **20**, 11013–11020.
73 L. Jie, R. Junfeng, M. Aizeng, D Zhijian, L. Changcheng and X. Jingxin, *CN Pat.*, CN106607017, 2017.
74 T. Fengya, S. Qing, M. Zhangxi, S. Yifan and W. Yangdong, *CN Pat.*, CN107970919, 2018.
75 F. Zhigui, M. Changxi, W. Wenhai, Z. Tieqiang, W. Xing and J. Dongyu, *CN Pat.*, CN110898833, 2020.
76 Q. Botao, G. Yalin, H. Jiahui, Z. Junying and L. Fang, *CN Pat.*, CN110237840, 2019.
77 P. E. Højlund Nielsen, N. Munksgård and L. J. Lemus-Yegres, *Int. Pat.*, WO2017162427A.1, 2017.
78 L. A. Petrov, Y. A. Alhamed, A. A. Al-Zahrani, M. A. Daous, A. A. Khamis and M. H. Al-Hazmi, *Int. Pat.*, WO/2014/181289, 2014.
79 T. Wang, F. Jiang, G. Liu, L. Zeng, Z. J. Zhao and J. Gong, *AIChE J.*, 2016, **62**, 4365–4376.
80 F. E. Frey and W. F. Huppke, *Ind. Eng. Chem.*, 1933, **25**, 54–59.
81 A. Hakuli, A. Kytökivi and A. O. I. Krause, *Appl. Catal., A*, 2000, **190**, 219–232.
82 B. M. Weckhuysen, *J. Catal.*, 2002, **210**, 418–430.
83 A. Hakuli, M. E. Harlin, L. B. Backman and A. O. I. Krause, *J. Catal.*, 1999, **184**, 349–356.
84 P. Michorczyk, J. Ogonowski and K. Zeńczak, *J. Mol. Catal. A: Chem.*, 2011, **349**, 1–12.
85 P. Michorczyk, P. Pietrzyk and J. Ogonowski, *Microporous Mesoporous Mater.*, 2012, **161**, 56–66.
86 B. M. Weckhuysen, *Phys. Chem. Chem. Phys.*, 2003, **5**, 4351–4360.
87 B. M. Weckhuysen, I. E. Wachs and R. A. Schoonheydt, *Chem. Rev.*, 1996, **96**, 3327–3349.
88 P. Michorczyk, J. Ogonowski, P. Kuśtrowski and L. Chmielarz, *Appl. Catal., A*, 2008, **349**, 62–69.
89 M. Santhosh Kumar, N. Hammer, M. Rønning, A. Holmen, D. Chen, J. C. Walmsley and G. Øye, *J. Catal.*, 2009, **261**, 116–128.
90 S. Sokolov, M. Stoyanova, U. Rodemerck, D. Linke and E. V. Kondratenko, *J. Catal.*, 2012, **293**, 67–75.
91 K. Takehira, Y. Ohishi, T. Shishido, T. Kawabata, K. Takaki, Q. Zhang and Y. Wang, *J. Catal.*, 2004, **224**, 404–416.
92 B. M. Weckhuysen and R. A. Schoonheydt, *Catal. Today*, 1999, **51**, 223–232.
93 D. He, Y. Zhang, S. Yang, Y. Mei and Y. Luo, *ChemCatChem*, 2018, **10**, 5434–5440.
94 S. De Rossi, G. Ferraris, S. Fremiotti, E. Garrone, G. Ghiotti, M. C. Campa and V. Indovina, *J. Catal.*, 1994, **148**, 36–46.
95 M. P. Conley, M. F. Delley, F. Núnez-Zarur, A. Comas-Vives and C. Copéret, *Inorg. Chem.*, 2015, **54**, 5065–5078.
96 C. Liu, G. Li, E. J. M. Hensen and E. A. Pidko, *J. Catal.*, 2016, **344**, 570–577.
97 X. Q. Gao, W. D. Lu, S. Z. Hu, W. C. Li and A. H. Lu, *Chin. J. Catal.*, 2019, **40**, 184–191.
98 W. Z. Lang, C. L. Hu, L. F. Chu and Y. J. Guo, *RSC Adv.*, 2014, **4**, 37107–37113.
99 A. WÈ©grzyniak, S. Jarczewski, A. WÈ©grzynowicz, B. Michorczyk, P. Kuśtrowski and P. Michorczyk, *Nanomaterials*, 2017, **7**, 249.
100 Y. Zhang, S. Yang, J. Lu, Y. Mei, D. He and Y. Luo, *Ind. Eng. Chem. Res.*, 2019, **58**, 19818–19824.
101 P. P. Li, W. Z. Lang, K. Xia, L. Luan, X. Yan and Y. J. Guo, *Appl. Catal., A*, 2016, **522**, 172–179.
102 Z. P. Hu, Y. Wang, D. Yang and Z. Y. Yuan, *J. Energy Chem.*, 2020, **47**, 225–233.
103 S. Han, Y. Zhao, T. Otroshchenko, Y. Zhang, D. Zhao, H. Lund, T. H. Vuong, J. Rabeah, U. Bentrup, V. A. Kondratenko, U. Rodemerck, D. Linke, M. Gao, H. Jiao, G. Jiang and E. V. Kondratenko, *ACS Catal.*, 2020, **10**, 1575–1590.
104 S. Han, T. Otroshchenko, D. Zhao, H. Lund, N. Rockstroh, T. H. Vuong, J. Rabeah, U. Rodemerck, D. Linke, M. Gao, G. Jiang and E. V. Kondratenko, *Appl. Catal., A*, 2020, **590**, 117350.
105 K. L. Fujdala and T. D. Tilley, *J. Catal.*, 2003, **218**, 123–134.
106 S. Han, T. Otroshchenko, D. Zhao, H. Lund, U. Rodemerck, D. Linke, M. Gao, G. Jiang and E. V. Kondratenko, *Catal. Commun.*, 2020, **138**, 105956.
107 A. WÈ©grzyniak, A. Rokicińska, E. HÈ©drzak, B. Michorczyk, K. Zeńczak-Tomera, P. Kuśtrowski and P. Michorczyk, *Catal. Sci. Technol.*, 2017, **7**, 6059–6068.
108 J. Liu, Y. Liu, Y. Ni, H. Liu, W. Zhu and Z. Liu, *Catal. Sci. Technol.*, 2020, **10**, 1739–1746.
109 P. C. Doolan and P. R. Pujado, *Hydrocarbon Process.*, 1989, **68**, 72–74.
110 A. Bhan and W. N. Delgass, *Catal. Rev. - Sci. Eng.*, 2008, **50**, 19–151.
111 K. Searles, G. Siddiqi, O. V. Safonova and C. Copéret, *Chem. Sci.*, 2017, **8**, 2661–2666.
112 J. Im and M. Choi, *ACS Catal.*, 2016, **6**, 2819–2826.
113 Y. Ren, J. Wang, W. Hua, Y. Yue and Z. Gao, *J. Ind. Eng. Chem.*, 2012, **18**, 731–736.
114 B. Xu, B. Zheng, W. Hua, Y. Yue and Z. Gao, *J. Catal.*, 2006, **239**, 470–477.
115 B. Xu, T. Li, B. Zheng, W. Hua, Y. Yue and Z. Gao, *Catal. Lett.*, 2007, **119**, 283–288.
116 J. Wang, F. Zhang, W. Hua, Y. Yue and Z. Gao, *Catal. Commun.*, 2012, **18**, 63–67.

117 J. J. H. B. Sattler, I. D. Gonzalez-Jimenez, L. Luo, B. A. Stears, A. Malek, D. G. Barton, B. A. Kilos, M. P. Kaminsky, T. W. G. M. Verhoeven, E. J. Koers, M. Baldus and B. M. Weckhuysen, *Angew. Chemie*, 2014, **126**, 9405–9410.

118 K. Searles, K. W. Chan, J. A. Mendes Burak, D. Zemlyanov, O. Safonova and C. Copéret, *J. Am. Chem. Soc.*, 2018, **140**, 11674–11679.

119 K. C. Szeto, Z. R. Jones, N. Merle, C. Rios, A. Gallo, F. Le Quemener, L. Delevoye, R. M. Gauvin, S. L. Scott and M. Taoufik, *ACS Catal.*, 2018, **8**, 7566–7577.

120 V. J. Cybulskis, S. U. Pradhan, J. J. Lovón-Quintana, A. S. Hock, B. Hu, G. Zhang, W. N. Delgass, F. H. Ribeiro and J. T. Miller, *Catal. Lett.*, 2017, **147**, 1252–1262.

121 C. T. Shao, W. Z. Lang, X. Yan and Y. J. Guo, *RSC Adv.*, 2017, **7**, 4710–4723.

122 W. G. Kim, J. So, S. W. Choi, Y. Liu, R. S. Dixit, C. Sievers, D. S. Sholl, S. Nair and C. W. Jones, *Chem. Mater.*, 2017, **29**, 7213–7222.

123 S. W. Choi, W. G. Kim, J. S. So, J. S. Moore, Y. Liu, R. S. Dixit, J. G. Pendergast, C. Sievers, D. S. Sholl, S. Nair and C. W. Jones, *J. Catal.*, 2017, **345**, 113–123.

124 M. W. Schreiber, C. P. Plaisance, M. Baumgärtl, K. Reuter, A. Jentys, R. Bermejo-Deval and J. A. Lercher, *J. Am. Chem. Soc.*, 2018, **140**, 4849–4859.

125 N. M. Phadke, E. Mansoor, M. Bondil, M. Head-Gordon and A. T. Bell, *J. Am. Chem. Soc.*, 2019, **141**, 1614–1627.

126 N. Raman, S. Maisel, M. Grabau, N. Taccardi, J. Debuschewitz, M. Wolf, H. Wittkämper, T. Bauer, M. Wu, M. Haumann, C. Papp, A. Görling, E. Spiecker, J. Libuda, H. P. Steinrück and P. Wasserscheid, *ACS Catal.*, 2019, **9**, 9499–9507.

127 T. Bauer, S. Maisel, D. Blaumeiser, J. Vecchietti, N. Taccardi, P. Wasserscheid, A. Bonivardi, A. Görling and J. Libuda, *ACS Catal.*, 2019, **9**, 2842–2853.

128 J. Keränen, A. Auroux, S. Ek and L. Niinistö, *Appl. Catal., A*, 2002, **228**, 213–225.

129 F. Roozeboom, M. C. Mittelmeijer-Hazeleger, J. A. Moulijn, J. Medema, V. H. J. De Beer and P. J. Gellings, *J. Phys. Chem.*, 1980, **84**, 2783–2791.

130 V. Murgia, E. M. F. Torres, J. C. Gottifredi and E. L. Sham, *Appl. Catal., A*, 2006, **312**, 134–143.

131 A. Klisińska, S. Loridant, B. Grzybowska, J. Stoch and I. Gressel, *Appl. Catal., A*, 2006, **309**, 17–27.

132 G. Liu, Z. J. Zhao, T. Wu, L. Zeng and J. Gong, *ACS Catal.*, 2016, **6**, 5207–5214.

133 Z. J. Zhao, T. Wu, C. Xiong, G. Sun, R. Mu, L. Zeng and J. Gong, *Angew. Chem., Int. Ed.*, 2018, **57**, 6791–6795.

134 F. Klose, T. Wolff, H. Lorenz, A. Seidel-Morgenstern, Y. Suchorski, M. Piórkowska and H. Weiss, *J. Catal.*, 2007, **247**, 176–193.

135 M. E. Harlin, V. M. Niemi and A. O. I. Krause, *J. Catal.*, 2000, **195**, 67–78.

136 U. Rodemerck, M. Stoyanova, E. V. Kondratenko and D. Linke, *J. Catal.*, 2017, **352**, 256–263.

137 R. R. Langeslay, D. M. Kaphan, C. L. Marshall, P. C. Stair, A. P. Sattelberger and M. Delferro, *Chem. Rev.*, 2019, **119**, 2128–2191.

138 D. E. Keller, S. M. K. Airaksinen, A. O. Krause, B. M. Weckhuysen and D. C. Koningsberger, *J. Am. Chem. Soc.*, 2007, **129**, 3189–3197.

139 S. Sokolov, M. Stoyanova, U. Rodemerck, D. Linke and E. V. Kondratenko, *Catal. Sci. Technol.*, 2014, **4**, 1323–1332.

140 S. Sokolov, V. Y. Bychkov, M. Stoyanova, U. Rodemerck, U. Bentrup, D. Linke, Y. P. Tyulenin, V. N. Korchak and E. V. Kondratenko, *ChemCatChem*, 2015, **7**, 1691–1700.

141 P. Bai, Z. Ma, T. Li, Y. Tian, Z. Zhang, Z. Zhong, W. Xing, P. Wu, X. Liu and Z. Yan, *ACS Appl. Mater. Interfaces*, 2016, **8**, 25979–25990.

142 Y. Gu, H. Liu, M. Yang, Z. Ma, L. Zhao, W. Xing, P. Wu, X. Liu, S. Mintova, P. Bai and Z. Yan, *Appl. Catal., B*, 2020, **274**, 119089.

143 T. Wu, G. Liu, L. Zeng, G. Sun, S. Chen, R. Mu, S. Agbotse Gbonfoun, Z. J. Zhao and J. Gong, *AIChE J.*, 2017, **63**, 4911–4919.

144 O. Ovsitser, R. Schomaecker, E. V. Kondratenko, T. Wolfram and A. Trunschke, *Catal. Today*, 2012, **192**, 16–19.

145 P. Hu, W. Z. Lang, X. Yan, X. F. Chen and Y. J. Guo, *Appl. Catal., A*, 2018, **553**, 65–73.

146 Q. Liu, Z. Yang, M. Luo, Z. Zhao, J. Wang, Z. Xie and L. Guo, *Microporous Mesoporous Mater.*, 2019, **282**, 133–145.

147 P. Hu, W. Z. Lang, X. Yan, L. F. Chu and Y. J. Guo, *J. Catal.*, 2018, **358**, 108–117.

148 C. Chen, M. Sun, Z. Hu, Y. Liu, S. Zhang and Z. Y. Yuan, *Chin. J. Catal.*, 2020, **41**, 276–285.

149 Y. Xie, R. Luo, G. Sun, S. Chen, Z. J. Zhao, R. Mu and J. Gong, *Chem. Sci.*, 2020, **11**, 3845–3851.

150 N. Jeon, H. Choe, B. Jeong and Y. Yun, *Catal. Today*, 2020, **352**, 337–344.

151 Y. Zhang, Y. Zhao, T. Otroshchenko, H. Lund, M.-M. Pohl, U. Rodemerck, D. Linke, H. Jiao, G. Jiang and E. V. Kondratenko, *Nat. Commun.*, 2018, **9**, 3794.

152 Y. Zhang, Y. Zhao, T. Otroshchenko, S. Han, H. Lund, U. Rodemerck, D. Linke, H. Jiao, G. Jiang and E. V. Kondratenko, *J. Catal.*, 2019, **371**, 313–324.

153 N. Jeon, H. Choe, B. Jeong and Y. Yun, *Appl. Catal., A*, 2019, **586**, 117211.

154 Y. N. Sun, C. Gao, L. Tao, G. Wang, D. Han, C. Li and H. Shan, *Catal. Commun.*, 2014, **50**, 73–77.

155 C. Chen, Z. P. Hu, J. T. Ren, S. Zhang, Z. Wang and Z. Y. Yuan, *Mol. Catal.*, 2019, **476**, 110508.

156 D. Zhao, Y. Li, S. Han, Y. Zhang, G. Jiang, Y. Wang, K. Guo, Z. Zhao, C. Xu, R. Li, C. Yu, J. Zhang, B. Ge and E. V. Kondratenko, *iScience*, 2019, **13**, 269–276.

157 S. Han, D. Zhao, T. Otroshchenko, H. Lund, U. Bentrup, V. A. Kondratenko, N. Rockstroh, S. Bartling, D. E. Doronkin, J.-D. Grunwaldt, U. Rodemerck, D. Linke,

M. Gao, G. Jiang and E. V. Kondratenko, *ACS Catal.*, 2020, **10**, 8933–8949.
158 M. Mukherjee, Hydrocarbonprocesssing.com https://www.hydrocarbonprocessing.com/authors/e/exelus-inc/mukherjee-m, (accessed 27 May 2021).
159 M. Mukherjee, V. M. Vadhri, N. Joshi and G. Brock, *US Pat.*, 2020/0101445A1, 2020.
160 Y. Dai, J. Gu, S. Tian, Y. Wu, J. Chen, F. Li, Y. Du, L. Peng, W. Ding and Y. Yang, *J. Catal.*, 2020, **381**, 482–492.
161 X. Li, P. Wang, H. Wang and C. Li, *Appl. Surf. Sci.*, 2018, **441**, 688–693.
162 G. Wang, H. Zhang, H. Wang, Q. Zhu, C. Li and H. Shan, *J. Catal.*, 2016, **344**, 606–608.
163 G. Wang, H. Zhang, Q. Zhu, X. Zhu, X. Li, H. Wang, C. Li and H. Shan, *J. Catal.*, 2017, **351**, 90–94.
164 H. Wang, H. Huang, K. Bashir and C. Li, *Appl. Catal., A*, 2020, **590**, 117291.
165 C. Yang, Z. Wu, G. Zhang, H. Sheng, J. Tian, Z. Duan, H. Sohn, A. J. Kropf, T. Wu, T. R. Krause and J. T. Miller, *Catal. Today*, 2019, **323**, 123–128.
166 Y. He, Y. Song, D. A. Cullen and S. Laursen, *J. Am. Chem. Soc.*, 2018, **140**, 14010–14014.
167 Z. Zhao, G. Ge, W. Li, X. Guo and G. Wang, *Chin. J. Catal.*, 2016, **37**, 644–670.
168 Z. P. Hu, H. Zhao, C. Chen and Z. Y. Yuan, *Catal. Today*, 2018, **316**, 214–222.
169 L. Liu, Q. F. Deng, B. Agula, X. Zhao, T. Z. Ren and Z. Y. Yuan, *Chem. Commun.*, 2011, **47**, 8334–8336.
170 Z. P. Hu, J. T. Ren, D. Yang, Z. Wang and Z. Y. Yuan, *Chin. J. Catal.*, 2019, **40**, 1385–1394.
171 S. F. Pan, J. L. Yin, X. L. Zhu, X. J. Guo, P. Hu, X. Yan, W. Z. Lang and Y. J. Guo, *Carbon*, 2019, **152**, 855–864.
172 M. A. Chaar, D. Patel and H. H. Kung, *J. Catal.*, 1988, **109**, 463–467.
173 D. Siew Hew Sam, V. Soenen and J. C. Volta, *J. Catal.*, 1990, **123**, 417–435.
174 A. Corma, J. M. López-Nieto, N. Paredes, M. Pérez, Y. Shen, H. Cao and S. L. Suib, *Stud. Surf. Sci. Catal.*, 1992, **72**, 213–220.
175 H. H. Kung and M. C. Kung, *Appl. Catal., A*, 1997, **157**, 105–116.
176 T. Blasco and J. M. López Nieto, *Appl. Catal., A*, 1997, **157**, 117–142.
177 A. Khodakov, B. Olthof, A. T. Bell and E. Iglesia, *J. Catal.*, 1999, **181**, 205–216.
178 B. Solsona, T. Blasco, J. M. López Nieto, M. L. Peña, F. Rey and A. Vidal-Moya, *J. Catal.*, 2001, **203**, 443–452.
179 G. Du, S. Lim, M. Pinault, C. Wang, F. Fang, L. Pfefferle and G. L. Haller, *J. Catal.*, 2008, **253**, 74–90.
180 A. Christodoulakis, M. Machli, A. A. Lemonidou and S. Boghosian, *J. Catal.*, 2004, **222**, 293–306.
181 M. D. Argyle, K. Chen, A. T. Bell and E. Iglesia, *J. Catal.*, 2002, **208**, 139–149.
182 J. T. Grant, C. A. Carrero, A. M. Love, R. Verel and I. Hermans, *ACS Catal.*, 2015, **5**, 5787–5793.
183 Y. M. Liu, Y. Cao, N. Yi, W. L. Feng, W. L. Dai, S. R. Yan, H. Y. He and K. N. Fan, *J. Catal.*, 2004, **224**, 417–428.
184 B. Schimmoeller, Y. Jiang, S. E. Pratsinis and A. Baiker, *J. Catal.*, 2010, **274**, 64–75.
185 A. Z. Varzaneh, M. S. Moghaddam and J. T. Darian, *Pet. Chem.*, 2018, **58**, 13–21.
186 T. S. Kharlamova, K. L. Timofeev, M. A. Salaev, V. A. Svetlichnyi and O. V. Vodyankina, *Appl. Catal., A*, 2020, **598**, 117574.
187 S. Zhang and H. Liu, *Appl. Catal., A*, 2019, **573**, 41–48.
188 G. Mitran, R. Ahmed, E. Iro, S. Hajimirzaee, S. Hodgson, A. Urdă, M. Olea and I. C. Marcu, *Catal. Today*, 2018, **306**, 260–267.
189 H. Zhu, S. Ould-Chikh, H. Dong, I. Llorens, Y. Saih, D. H. Anjum, J. L. Hazemann and J. M. Basset, *ChemCatChem*, 2015, **7**, 3332–3339.
190 S. Barman, N. Maity, K. Bhatte, S. Ould-Chikh, O. Dachwald, C. Haeßner, Y. Saih, E. Abou-Hamad, I. Llorens, J. L. Hazemann, K. Köhler, V. D'Elia and J. M. Basset, *ACS Catal.*, 2016, **6**, 5908–5921.
191 Q. X. Luo, X. K. Zhang, B. L. Hou, J. G. Chen, C. Zhu, Z. W. Liu, Z. T. Liu and J. Lu, *Catal. Sci. Technol.*, 2018, **8**, 4864–4876.
192 J. J. Ternero-Hidalgo, J. Torres-Liñán, M. O. Guerrero-Pérez, J. Rodríguez-Mirasol and T. Cordero, *Catal. Today*, 2019, **325**, 131–143.
193 Q. Liu, M. Luo, Z. Zhao and L. Guo, *Catal. Lett.*, 2019, **149**, 1345–1358.
194 J. Guo, X. Li, Y. Tang and J. Zhang, *ChemistrySelect*, 2019, **4**, 13576–13581.
195 Q. Weng, X. Wang, X. Wang, Y. Bando and D. Golberg, *Chem. Soc. Rev.*, 2016, **45**, 3989–4012.
196 J. T. Grant, C. A. Carrero, F. Goeltl, J. Venegas, P. Mueller, S. P. Burt, S. E. Specht, W. P. McDermott, A. Chieregato and I. Hermans, *Science*, 2016, **354**, 1570–1573.
197 L. Shi, D. Wang, W. Song, D. Shao, W. P. Zhang and A. H. Lu, *ChemCatChem*, 2017, **9**, 1788–1793.
198 R. Belgamwar, A. G. M. Rankin, A. Maity, A. K. Mishra, J. S. Gómez, J. Trébosc, C. P. Vinod and O. Lafon, *ACS Sustainable Chem. Eng.*, 2020, **8**, 16124–16135.
199 J. T. Grant, W. P. McDermott, J. M. Venegas, S. P. Burt, J. Micka, S. P. Phivilay, C. A. Carrero and I. Hermans, *ChemCatChem*, 2017, **9**, 3623–3626.
200 J. M. Venegas, W. P. McDermott and I. Hermans, *Acc. Chem. Res.*, 2018, **51**, 2556–2564.
201 B. Yan, W. C. Li and A. H. Lu, *J. Catal.*, 2019, **369**, 296–301.
202 L. Shi, D. Wang and A. H. Lu, *Chin. J. Catal.*, 2018, **39**, 908–913.
203 H. Li, J. Zhang, P. Wu, S. Xun, W. Jiang, M. Zhang, W. Zhu and H. Li, *J. Phys. Chem. C*, 2019, **123**, 2256–2266.
204 X. Zhang, R. You, Z. Wei, X. Jiang, J. Yang, Y. Pan, P. Wu, Q. Jia, Z. Bao, L. Bai, M. Jin, B. Sumpter, V. Fung, W. Huang and Z. Wu, *Angew. Chem., Int. Ed.*, 2020, **59**, 8042–8046.

205 J. Tian, J. Tan, M. Xu, Z. Zhang, S. Wan, S. Wang, J. Lin and Y. Wang, *Sci. Adv.*, 2019, **5**, 1–7.
206 J. M. Venegas, Z. Zhang, T. O. Agbi, W. P. McDermott, A. Alexandrova and I. Hermans, *Angew. Chem., Int. Ed.*, 2020, **59**, 16527–16535.
207 W. D. Lu, D. Wang, Z. Zhao, W. Song, W. C. Li and A. H. Lu, *ACS Catal.*, 2019, **9**, 8263–8270.
208 A. M. Love, B. Thomas, S. E. Specht, M. P. Hanrahan, J. M. Venegas, S. P. Burt, J. T. Grant, M. C. Cendejas, W. P. McDermott, A. J. Rossini and I. Hermans, *J. Am. Chem. Soc.*, 2019, **141**, 182–190.
209 A. M. Love, M. C. Cendejas, B. Thomas, W. P. McDermott, P. Uchupalanun, C. Kruszynski, S. P. Burt, T. Agbi, A. J. Rossini and I. Hermans, *J. Phys. Chem. C*, 2019, **123**, 27000–27011.
210 Y. Wang, W. C. Li, Y. X. Zhou, R. Lu and A. H. Lu, *Catal. Today*, 2020, **339**, 62–66.
211 W. D. Lu, X. Q. Gao, Q. G. Wang, W. C. Li, Z. C. Zhao, D. Q. Wang and A. H. Lu, *Chin. J. Catal.*, 2020, **41**, 1837–1845.
212 H. Chen, Z. Yang, Z. Zhang, Z. Chen, M. Chi, S. Wang, J. Fu and S. Dai, *Angew. Chem., Int. Ed.*, 2019, **58**, 10626–10630.
213 F. Cavani, N. Ballarini and A. Cericola, *Catal. Today*, 2007, **127**, 113–131.
214 Z. Qiao, Z. Wang, C. Zhang, S. Yuan, Y. Zhu and J. Wang, *AIChE J.*, 2012, **59**, 215–228.
215 K. Chen, A. T. Bell and E. Iglesia, *J. Phys. Chem. B*, 2000, **104**, 1292–1299.
216 K. Chen, S. Xie, E. Iglesia and A. T. Bell, *J. Catal.*, 2000, **189**, 421–430.
217 G. Tsilomelekis, A. Christodoulakis and S. Boghosian, *Catal. Today*, 2007, **127**, 139–147.
218 K. Chen, S. Xie, A. T. Bell and E. Iglesia, *J. Catal.*, 2000, **195**, 244–252.
219 M. Høj, T. Kessler, P. Beato, A. D. Jensen and J. D. Grunwaldt, *Appl. Catal., A*, 2014, **472**, 29–38.
220 S. Chen, L. Zeng, R. Mu, C. Xiong, Z. J. Zhao, C. Zhao, C. Pei, L. Peng, J. Luo, L. S. Fan and J. Gong, *J. Am. Chem. Soc.*, 2019, **141**, 18653–18657.
221 S. K. Matam, C. Moffat, P. Hellier, M. Bowker, I. P. Silverwood, C. R. A. Catlow, S. D. Jackson, J. Craswell, P. P. Wells, S. F. Parker and E. K. Gibson, *Catalysts*, 2020, **10**, 1–13.
222 E. Goudarzi, R. Asadi, J. T. Darian and A. Shahbazi Kootenaei, *RSC Adv.*, 2019, **9**, 11797–11809.
223 X. Fan, D. Liu, Z. Zhao, J. Li and J. Liu, *Catal. Today*, 2020, **339**, 67–78.
224 M. Chen, J. L. Wu, Y. M. Liu, Y. Cao, L. Guo, H. Y. He and K. N. Fan, *J. Solid State Chem.*, 2011, **184**, 3357–3363.
225 X. Fan, J. Li, Z. Zhao, Y. Wei, J. Liu, A. Duan and G. Jiang, *J. Energy Chem.*, 2014, **23**, 171–178.
226 D. Delgado, R. Sanchis, B. Solsona, P. Concepción and J. M. López Nieto, *Top. Catal.*, 2020, **63**, 1731–1742.
227 Q. Zhang, C. Cao, T. Xu, M. Sun, J. Zhang, Y. Wang and H. Wan, *Chem. Commun.*, 2009, 2376–2378.
228 K. Du, M. Hao, Z. Li, W. Hong, J. Liu, L. Xiao, S. Zou, H. Kobayashi and J. Fan, *Chin. J. Catal.*, 2019, **40**, 1057–1062.
229 Q. Xie, H. Zhang, J. Kang, J. Cheng, Q. Zhang and Y. Wang, *ACS Catal.*, 2018, **8**, 4902–4916.
230 K. Fang, L. Liu, M. Zhang, L. Zhao, J. Zhou, W. Li, X. Mu and C. Yang, *Catalysts*, 2018, **8**, 19.
231 J. Liu, M. Hao, C. Chen, K. Du, Q. Zhou, S. Zou, L. Xiao and J. Fan, *Appl. Surf. Sci.*, 2020, **528**, 147025.
232 L. Wang, C. Ao, Y. Zhai, B. Feng, J. Duan, S. Qian, W. Zhao, L. Zhang and F. Liu, *Inorg. Chem. Commun.*, 2020, **112**, 107725.
233 S. Tanasoi, G. Mitran, N. Tanchoux, T. Cacciaguerra, F. Fajula, I. Sndulescu, D. Tichit and I. C. Marcu, *Appl. Catal., A*, 2011, **395**, 78–86.
234 F. Ma, S. Chen, Y. Li, H. Zhou, A. Xu and W. Lu, *Appl. Surf. Sci.*, 2014, **313**, 654–659.
235 F. Ma, S. Chen, H. Zhou, Y. Li and W. Lu, *RSC Adv.*, 2014, **4**, 40776–40781.
236 B. Frank, J. Zhang, R. Blume, R. Schlögl and D. S. Su, *Angew. Chem., Int. Ed.*, 2009, **48**, 6913–6917.
237 W. Qi, P. Yan and D. S. Su, *Acc. Chem. Res.*, 2018, **51**, 640–648.
238 L. Cao, P. Dai, L. Zhu, L. Yan, R. Chen, D. Liu, X. Gu, L. Li, Q. Xue and X. Zhao, *Appl. Catal., B*, 2020, **262**, 118277.
239 C. P. Hubbard, K. Otto, H. S. Gandhi and K. Y. S. Ng, *J. Catal.*, 1993, **139**, 268–276.
240 S. Vajda, M. J. Pellin, J. P. Greeley, C. L. Marshall, L. A. Curtiss, G. A. Ballentine, J. W. Elam, S. Catillon-Mucherie, P. C. Redfern, F. Mehmood and P. Zapol, *Nat. Mater.*, 2009, **8**, 213–216.
241 L. Sun, Y. Chai, W. Dai, G. Wu, N. Guan and L. Li, *Catal. Sci. Technol.*, 2018, **8**, 3044–3051.
242 Z. Nawaz and F. Wei, *Ind. Eng. Chem. Res.*, 2013, **52**, 346–352.
243 B. Farin, M. Devillers and E. M. Gaigneaux, *Microporous Mesoporous Mater.*, 2017, **242**, 200–207.
244 R. B. Jackson, J. G. Canadell, C. Le Quéré, R. M. Andrew, J. I. Korsbakken, G. P. Peters and N. Nakicenovic, *Nat. Clim. Change*, 2016, **6**, 7–10.
245 S. Sato, M. Ohhara, T. Sodesawa and F. Nozaki, *Appl. Catal.*, 1988, **37**, 207–215.
246 B. M. Reddy, S. C. Lee, D. S. Han and S. E. Park, *Appl. Catal., B*, 2009, **87**, 230–238.
247 J. Guo, H. Lou, H. Zhao, L. Zheng and X. Zheng, *J. Mol. Catal. A: Chem.*, 2005, **239**, 222–227.
248 I. Takahara and M. Saito, *Chem. Lett.*, 1996, 973–974.
249 K. Nakagawa, C. Kajita, N. Ikenaga, M. Nishitani-Gamo, T. Ando and T. Suzuki, *Catal. Today*, 2003, **84**, 149–157.
250 X. Zhang, Y. Yue and Z. Gao, *Catal. Lett.*, 2002, **83**, 19–25.
251 R. Wu, P. Xie, Y. Cheng, Y. Yue, S. Gu, W. Yang, C. Miao, W. Hua and Z. Gao, *Catal. Commun.*, 2013, **39**, 20–23.
252 Z. Xie, Y. Ren, J. Li, Z. Zhao, X. Fan, B. Liu, W. Song, L. Kong, X. Xiao, J. Liu and G. Jiang, *J. Catal.*, 2019, **372**, 206–216.

253 J. F. S. de Oliveira, D. P. Volanti, J. M. C. Bueno and A. P. Ferreira, *Appl. Catal., A*, 2018, **558**, 55–66.
254 P. Michorczyk and J. Ogonowski, *React. Kinet. Catal. Lett.*, 2005, **87**, 177–183.
255 M. A. Botavina, Y. A. Agafonov, N. A. Gaidai, E. Groppo, V. Cortés Corberán, A. L. Lapidus and G. Martra, *Catal. Sci. Technol.*, 2016, **6**, 840–850.
256 L. Li, W. Zhu, L. Shi, Y. Liu, H. Liu, Y. Ni, S. Liu, H. Zhou and Z. Liu, *Chin. J. Catal.*, 2016, **37**, 359–366.
257 P. Michorczyk, J. Ogonowski and M. Niemczyk, *Appl. Catal., A*, 2010, **374**, 142–149.
258 H. M. Wang, Y. Chen, X. Yan, W. Z. Lang and Y. J. Guo, *Microporous Mesoporous Mater.*, 2019, **284**, 69–77.
259 J. Baek, H. J. Yun, D. Yun, Y. Choi and J. Yi, *ACS Catal.*, 2012, **2**, 1893–1903.
260 P. Kuśtrowski, P. Michorczyk, L. Chmielarz, Z. Piwowarska, B. Dudek, J. Ogonowski and R. Dziembaj, *Thermochim. Acta*, 2008, **471**, 26–32.
261 F. Zhang, R. Wu, Y. Yue, W. Yang, S. Gu, C. Miao, W. Hua and Z. Gao, *Microporous Mesoporous Mater.*, 2011, **145**, 194–199.
262 Q. Zhu, M. Takiguchi, T. Setoyama, T. Yokoi, J. N. Kondo and T. Tatsumi, *Catal. Lett.*, 2011, **141**, 670–677.
263 P. Michorczyk, K. Zeńczak-Tomera, B. Michorczyk, A. WÈ©grzyniak, M. Basta, Y. Millot, L. Valentin and S. Dzwigaj, *J. CO_2 Util.*, 2020, **36**, 54–63.
264 D. Yun, J. Baek, Y. Choi, W. Kim, H. J. Lee and J. Yi, *ChemCatChem*, 2012, **4**, 1952–1959.
265 M. Veronica Ganduglia-Pirovano, J. De, L. Figuera, V. Matolin, J. I. Flege, P. Luches, G. Gasperi, M. Sauerbrey, S. Valeri and J. Falta, *Front. Chem.*, 2019, **7**, 57 http://www.frontiersin.org.
266 R. Jin, J. Easa, D. T. Tran and C. P. O'Brien, *Catal. Sci. Technol.*, 2020, **10**, 1769–1777.
267 X. Du, B. Yao, S. Gonzalez-Cortes, V. L. Kuznetsov, H. Almegren, T. Xiao and P. P. Edwards, *Faraday Discuss.*, 2015, **183**, 161–176.
268 N. S. Gnep, J. Y. Doyement and M. Guisnet, *J. Mol. Catal.*, 1988, **45**, 281–284.
269 K. Nakagawa, M. Okamura, N. Ikenaga, T. Suzuki and T. Kobayashi, *Chem. Commun.*, 1998, 1025–1026.
270 K. Nakagawa, C. Kajita, K. Okumura, N. Ikenaga, T. Suzuki, K. Nakagawa, T. Ando, T. Suzuki, M. Nishitani-Gamo, T. Ando and T. Kobayashi, *J. Catal.*, 2001, **203**, 87–93.
271 B. Zheng, W. Hua, Y. Yue and Z. Gao, *J. Catal.*, 2005, **232**, 143–151.
272 P. Michorczyk, K. Góra-Marek and J. Ogonowski, *Catal. Lett.*, 2006, **109**, 195–198.
273 P. Michorczyk, P. Kuśtrowski, A. Kolak and M. Zimowska, *Catal. Commun.*, 2013, **35**, 95–100.
274 M. Chen, J. Xu, Y. M. Liu, Y. Cao, H. Y. He, J. H. Zhuang and K. N. Fan, *Catal. Lett.*, 2008, **124**, 369–375.
275 M. Chen, J. Xu, F. Z. Su, Y. M. Liu, Y. Cao, H. Y. He and K. N. Fan, *J. Catal.*, 2008, **256**, 293–300.
276 L. Zhang, Z. Y. Wang, J. Song, Y. Lang, J. G. Chen, Q. X. Luo, Z. H. He, K. Wang, Z. W. Liu and Z. T. Liu, *J. CO_2 Util.*, 2020, **38**, 306–313.
277 P. Michorczyk, P. Kuśtrowski, L. Chmielarz and J. Ogonowski, *React. Kinet. Catal. Lett.*, 2004, **82**, 121–130.
278 Y. Ren, F. Zhang, W. Hua, Y. Yue and Z. Gao, *Catal. Today*, 2009, **148**, 316–322.
279 M. Chen, J. Xu, Y. Cao, H. Y. He, K. N. Fan and J. H. Zhuang, *J. Catal.*, 2010, **272**, 101–108.
280 M. Chen, J. Xu, Y. M. Liu, Y. Cao, H. Y. He and J. H. Zhuang, *Appl. Catal., A*, 2010, **377**, 35–41.
281 M. Chen, J. L. Wu, Y. M. Liu, Y. Cao, L. Guo, H. Y. He and K. N. Fan, *Appl. Catal., A*, 2011, **407**, 20–28.
282 H. Tian, J. Liao, F. Zha, X. Guo, X. Tang, Y. Chang and X. Ma, *ChemistrySelect*, 2020, **5**, 3626–3637.
283 K. Srivastava, V. Devra and A. Rani, *Fuel Process. Technol.*, 2014, **121**, 1–8.
284 E. V. Danilevich, G. Y. Popova, T. V. Andrushkevich, V. V. Kaichev, I. G. Danilova, Y. A. Chesalov, V. A. Rogov, V. I. Bukhtiyarov and V. N. Parmon, *Appl. Catal., A*, 2014, **475**, 98–108.
285 J. Kang, A. D. Czaja and V. V. Guliants, *Eur. J. Inorg. Chem.*, 2017, **2017**, 4757–4762.
286 Z. F. Han, X. L. Xue, J. M. Wu, W. Z. Lang and Y. J. Guo, *Chin. J. Catal.*, 2018, **39**, 1099–1109.
287 H. Wang and G. Tsilomelekis, *Catal. Sci. Technol.*, 2020, **10**, 4362–4372.
288 J. H. Carter, X. Liu, Q. He, S. Althahban, E. Nowicka, S. J. Freakley, L. Niu, D. J. Morgan, Y. Li, J. W. H. Niemantsverdriet, S. Golunski, C. J. Kiely and G. J. Hutchings, *Angew. Chem., Int. Ed.*, 2017, **56**, 16037–16041.
289 T. Hayashi, K. Tanaka and M. Haruta, *J. Catal.*, 1998, **178**, 566–575.
290 E. Gomez, Z. Xie and J. G. Chen, *AIChE J.*, 2019, DOI: 10.1002/aic.16670.
291 E. Nowicka, C. Reece, S. M. Althahban, K. M. H. Mohammed, S. A. Kondrat, D. J. Morgan, Q. He, D. J. Willock, S. Golunski, C. J. Kiely and G. J. Hutchings, *ACS Catal.*, 2018, **8**, 3454–3468.
292 R. Hou, K. Chang, J. G. Chen and T. Wang, *Top. Catal.*, 2015, **58**, 240–246.
293 A. C. Lausche, J. A. Schaidle, N. Schweitzer and L. T. Thompson, in *Comprehensive Inorganic Chemistry II (Second Edition): From Elements to Applications*, Elsevier Ltd, 2013, vol. 7, pp. 371–404.
294 T. H. Nguyen, T. V. Nguyen, C. G. Cooper, A. A. Adesina, A. C. Lausche, J. A. Schaidle, N. Schweitzer and L. T. Thompson, in *New Developments and Application in Chemical Reaction Engineering*, ed. H.-K. Rhee, I.-S. Nam and J. M. B. Park, Elsevier, 2006, vol. 159, pp. 781–784.
295 M. M. Sullivan and A. Bhan, *J. Catal.*, 2018, **357**, 195–205.
296 B. Frank, T. P. Cotter, M. E. Schuster, R. Schlögl and A. Trunschke, *Chem. – Eur. J.*, 2013, **19**, 16938–16945.
297 J. C. Védrine, *Catalysts*, 2016, **6**, 22.
298 M. Konsolakis, *ACS Catal.*, 2015, **5**, 6397–6421.

299 S. Roy, M. S. Hegde and G. Madras, *Appl. Energy*, 2009, **86**, 2283–2297.
300 X. Rozanska, E. V. Kondratenko and J. Sauer, *J. Catal.*, 2008, **256**, 84–94.
301 G. I. Panov, A. K. Uriarte, M. A. Rodkin and V. I. Sobolev, *Catal. Today*, 1998, **41**, 365–385.
302 K. Nowińska, A. Wącław and A. Izbińska, *Appl. Catal., A*, 2003, **243**, 225–236.
303 J. Pérez-Ramírez and A. Gallardo-Llamas, *J. Catal.*, 2004, **223**, 382–388.
304 P. Sazama, N. K. Sathu, E. Tabor, B. Wichterlová, Š. Sklenák and Z. Sobalík, *J. Catal.*, 2013, **299**, 188–203.
305 J. C. Groen, A. Brückner, E. Berrier, L. Maldonado, J. A. Moulijn and J. Pérez-Ramírez, *J. Catal.*, 2006, **243**, 212–216.
306 I. Melián-Cabrera, S. Espinosa, J. C. Groen, B. V. D. Linden, F. Kapteijn and J. A. Moulijn, *J. Catal.*, 2006, **238**, 250–259.
307 J. Pérez-Ramírez and E. V. Kondratenko, *Chem. Commun.*, 2003, **3**, 2152–2153.
308 J. Pérez-Ramírez and A. Gallardo-Llamas, *Appl. Catal., A*, 2005, **279**, 117–123.
309 R. Bulánek, B. Wichterlová, K. Novoveská and V. Kreibich, *Appl. Catal., A*, 2004, **264**, 13–22.
310 J. Kowalska-Kuś, A. Held and K. Nowińska, *Catal. Lett.*, 2010, **136**, 199–208.
311 A. Ates, C. Hardacre and A. Goguet, *Appl. Catal., A*, 2012, **441442**, 30–41.
312 E. V. Kondratenko and M. Baerns, *Appl. Catal., A*, 2001, **222**, 133–143.
313 E. V. Kondratenko, M. Cherian, M. Baerns, D. Su, R. Schlögl, X. Wang and I. E. Wachs, *J. Catal.*, 2005, **234**, 131–142.
314 E. V. Kondratenko, M. Cherian and M. Baerns, in *Catalysis Today*, Elsevier, 2006, vol. 112, pp. 60–63.
315 O. Ovsitser, M. Cherian and E. V. Kondratenko, *J. Phys. Chem. C*, 2007, **111**, 8594–8602.
316 M. Chen, J. L. Wu, Y. M. Liu, Y. Cao and K. N. Fan, *Catal. Commun.*, 2011, **12**, 1063–1066.
317 C. Rongguo, G. Juan, L. Yin, H. Dieter and L. Maren, *Supply and Demand of Lithium and Gallium*, 2016.
318 U.S. Geological Survey, *Mineral commodity summaries 2020*, 2020.
319 J. D. Burton, F. Culkin and J. P. Riley, *Geochim. Cosmochim. Acta*, 1959, **16**, 151–180.
320 N. E. T. Laboratory, Doe invests 17 million dollars to advance carbon utilization projects, https://netl.doe.gov/node/9789#:~:text=DOEInvests%2417Millionto,Projects%7Cnetl.doe.gov&text=TheU.S.DepartmentofEnergy's, developmentprojectsforcarbonutilization, (accessed 14 May 2021).